SHEAR BEHAVIOUR OF OSB WOOD COMPOSITE I-BEAMS WITH WEB OPENINGS

1995

Sammy Wang and J.J. Roger Cheng
Department of Civil Engnineering
University of Alberta
Edmonton, Alberta
T6G 2G7

This is a joint publication of Canadian Forest Service and Land and Forest Service pursuant to the Canada-Alberta Partnership Agreement in Forestry.

A5021-123

DISCLAIMER

The study on which this report is based was funded in part under the Canada-Alberta Partnership Agreement in Forestry.

The views, conclusions and recommendations are those of the authors. The exclusion of certain manufactured products does not necessarily imply disapproval nor does the mention of other products necessarily imply endorsement by the Canadian Forest Service or Land and Forest Service.

Catalogue No.: Fo42-91/123-1995E
ISBN: 0-662-23080-9

Additional copies of this publication are available at no charge from:

Canadian Forest Service
Natural Resources Canada
Northern Forestry Centre
5320 - 122nd Street
Edmonton, Alberta
T6H 3S5
Telephone: (403) 435 - 7210

or

Land and Forest Service
Alberta Environmental Protection
10th Floor, Bramalea Building
9920 - 108th Street
Edmonton, Alberta
T5K 2M4
Telephone: (403) 427 - 3551

ABSTRACT

In North America, oriented strandboard (OSB) is used as a major web material in prefabricated wood I-beams (joists). Web openings are often required in the web of the beam for the passage of electrical conduits, plumbing lines, and ventilation systems. Current standards consider the effects of web openings on the shear strength of the beam empirically, but not analytically. The purpose of this research is to investigate the effects of web openings on the shear strength of OSB web I-beams, identify possible failure mechanisms and recommend analytical design criteria. The experimental program consisted of testing 610 mm, 406 mm, and 241 mm deep simply supported beams under a single point load. Test parameters included the hole width, hole height, shear span length, and corner radius of the hole. Failure occurred in one or a combination of four modes. Specimens with a hole depth equal to the full height of the web exhibited failure with the web pulling out of the flange. The second mode exhibited Vierendeel truss action causing failure at the corners of the hole. The third mode was due to a cross section shear failure and the last mode exhibited buckling of the web. The shear strength of a beam with an opening was reduced by as much as 79% when compared to a reference beam without holes. The square corner reduced the shear capacity by 6% when compared to the 25 mm radius corner. The longer shear span resulted in increased shear strength of the beam. By using a design procedure based on a Vierendeel analysis and a cross section strength check, the shear capacity of the OSB I-joist can be predicted analytically with reasonable accuracy given the material properties of the web and flange.

ACKNOWLEDGEMENTS

The research was funded by the Canada-Alberta Partnership Agreement in Forestry. The supervision from Dr. J.J. Cheng is greatly appreciated. The assistance from the technicians L. Burden and R. Helfrich at the I.F. Morrison Structural Laboratory in the University of Alberta is greatly appreciated. The assistance from the technicians of the Forest Products Testing Laboratory at the Alberta Research Council is acknowledged.

TABLE OF CONTENTS

LIST OF FIGURES

LIST OF TABLES

1. Introduction

1.1 General

Composite wood members are becoming more prevalent in structural systems as long and large lumber members needed for light frame and commercial construction systems are becoming less available and more expensive. Researchers (Nelson 1975; Tang and Leichti 1984) have estimated that 50% of wood fiber can be saved using wood composite structural shapes. Prefabricated wood composite I-beams represent one such alternative to traditional sawn lumber, as shown in Figure 1.1.

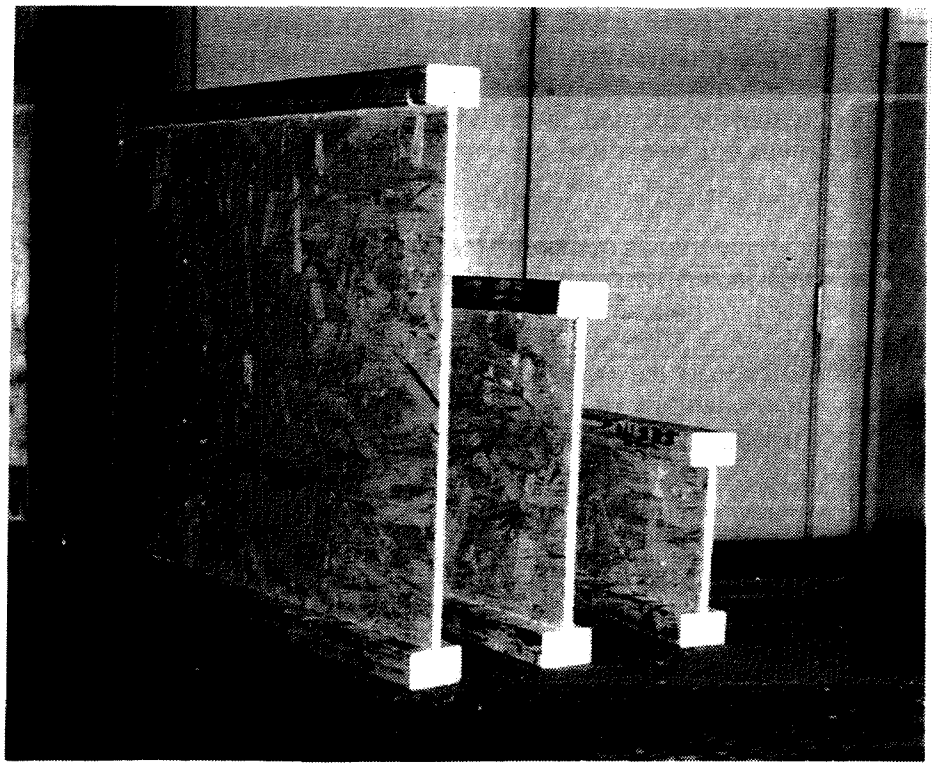

Figure 1.1. Prefabricated OSB Web I-beams

In an industry survey by Leichti, Falk, and Laufenberg (1990a), modern mass production of wood I-joists in North America was initiated in the late 1960's by Trus Joist Corporation. During the late 1970's, two more manufacturers entered the marketplace and six more in the 1980's. In the seven year period between 1980 to 1987, total I-joist production more than doubled and may have tripled by the end of 1989. In 1989, the total I-joist production was estimated at 150 million lineal feet in North America. The present trend in I-joist manufacturing indicates that production is still increasing at a fast pace.

The I-beams are structural members that are manufactured using sawn or structural composite lumber flanges and structural panel webs. The flanges and webs are bonded together using an exterior type adhesive forming the cross-sectional shape of an "I" (ASTM D 5055 1990). In Alberta, the web material used is oriented strandboard (OSB). OSB is made from aspen trees grown in Alberta.

OSB is a panel product which is becoming more widespread and popular. The panels are made exclusively by processing small diameter, fast growing trees into strands of wafers which are bonded under heat and pressure with a waterproof resin. OSB was first commercially produced in the early 1980's, but is now well established in the building industry and is recognized in the 1990 National Building Code of Canada (Structural Board Association 1993).

1.2 Statement of the Problem

Web openings are required for the passage of electrical conduits, plumbing lines, and ventilation ducts so that headroom can be maximized in buildings. The acceptance of prefabricated wood I-beams (joists) is presently based on a standard under the American Society for Testing and Materials (ASTM) D-7 Committee on Wood. The standard, ASTM D 5055 (1990), gives procedures for establishing, monitoring, and evaluating structural capacities such as shear, moment, and stiffness. Concerning web openings, the standard states that shear strength reduction due to the hole must be determined empirically from numerous performance tests representing the whole product range with different hole geometries. Manufacturers use this data to specify where maximum size holes can be located in the web. Typically, shear strength reduction data are proprietary. This leaves engineers and other practitioners relying on the manufacturers product manuals.

OSB is a relatively new material as compared to plywood and its behaviour is not fully understood. The behaviour of OSB is further complicated when it is used as a structural component of an I-beam. The introduction of holes in OSB webs is complicated and attempts to quantify the effects of holes such as in ASTM D 5055 are empirical and not analytical. Therefore, the way I-beams carry shear and moment across the hole has not been determined. The mode in which I-beams fail is also not known. Understanding of failure modes is important so that engineers can avoid them and have confidence using prefabricated wood I-beams with web openings.

1.3 Objectives and Scope

The purpose of this research is to experimentally investigate the behaviour of OSB webbed I-beams with rectangular openings. Rectangular openings were chosen instead of circular openings because the former adversely affects the strength of the beam more than the latter. The objectives of this research are as follows:

- Investigate the effects of rectangular web openings on the shear strength of prefabricated OSB I-beams.
- Identify possible failure mechanisms.
- Develop shear design criteria for OSB I-beams with rectangular holes.
- Add research data to the limited literature devoted to the behaviour of wood composite I-beams with web openings.

The scope of this project is to focus research efforts on the "generic aspects" of OSB I-beams. In this way, research findings will be applicable to different prefabricated OSB I-beams. Therefore, any proprietary constructions such as web splices or web/flange connections will not be investigated since these constructions vary greatly between manufacturers.

2. LITERATURE REVIEW

2.1 Previous Research

In an extensive literature review on wood composite I-beams by Leichti, Falk, and Laufenberg (1990b), the authors reviewed research on the effects of web openings. Maley (1987) found that large openings can reduce the shear capacity, decrease the stiffness of the beam, and develop stress concentrations at the flange-web joint. Leichti et al. also reviewed design information for round openings in hardboard webbed I-beams by Hilson and Rodd (1984). They found that the ratio of beam height to distance between web stiffeners and the web slenderness interacted with the size of the web openings.

Johannesson (1977) performed tests on plywood webbed I-beams with rectangular openings. He reported that all the plywood beams with holes near the support failed in a similar manner with a brittle tension failure at two opposite corners of the hole. The cracks developed roughly at an angle of 45°. Johannesson also observed compression buckles at the other two diagonal corners in some cases. He speculated that the buckling could have initiated the failure.

Fergus (1979) studied the effect of circular web openings on the structural performance of wood composite I-beams. Two different web materials, 9.5 mm structural I douglas-fir plywood and 9.5 mm unsanded oriented strand particleboard (OSP) made from douglas-fir strands, were used in the construction of the I-beam. The OSP was a cross-aligned three layered composite panel made from strands bonded together with an exterior type adhesive. The density of the plywood and OSP was 2490 kg/m^3 and 3502 kg/m^3, respectively, and is based on oven dry weight and test volume. Two different size wood I-beams, moment critical and shear critical, were constructed. The moment critical beams were 7.32 m long and 254 mm deep. The shear critical beams were 2.44 m long and 559 mm deep. Both sizes of beams were subjected to two load conditions. One load condition used a single concentrated load at mid span and the other load condition used a two point concentrated load. Circular holes, with a diameter of 70% of the web depth for moment critical beams and 54% for shear critical beams, were cut into the web. Fergus then conducted extensive material tests to determine the physical properties required for a finite element method (FEM) analysis using SAP IV, a structural analysis program. Fergus compared the deflections and stresses determined from the FEM analysis with experimental results. Some of his results and conclusions are listed below.

- The SAP IV FEM analysis gave good results for both displacement and stress analysis for moment critical beams. Beam deflections in shear critical beams were adequately predicted using the FEM analysis.

- For moment critical beams, no significant performance differences were discovered between plywood and OSP beams. A circular hole, 70% of the depth of the web, did not alter any significant performance criteria.

- For shear critical beams, web buckling was observed near hole locations in plywood web beams. No buckling was observed in OSP web beams.

- OSP with an average edgewise shear modulus of 1664 MPa provided for significantly improved shear beam performance over plywood with an edgewise shear modulus of 630 MPa.

- A sensitivity analysis of the FEM showed that for the moment critical beams, performance was primarily dependent on the flange stiffness. For the shear critical beams, the edgewise

shear modulus of the web, the flange modulus of elasticity (M.O.E.) and the transverse M.O.E. of the web were all significant factors controlling the model.

Fergus also recommended investigating the effect of rectangular holes in Vierendeel beam geometries.

Although limited literature is devoted to analyzing the effect of openings in the webs of wood I-beams, much more research can be found on the effects of round and rectangular openings in steel I-sections such as Bower's (1966) research on wide flange beams with holes. Bower applied the "Vierendeel Method" of analysis to steel wide flange beams with rectangular holes and compared the predicted stresses with the experimental stresses. The author concluded that for rectangular holes not exceeding half the web depth, the Vierendeel analysis predicted the bending stresses on transverse cross sections with reasonable accuracy and predicted the octahedral shear stress conservatively, but did not predict the stress concentrations around the corner. The octahedral shear stress was used as the criterion for yielding under combined stresses.

Bower (1968) later investigated the ultimate strength of steel I-beams with rectangular holes. He noted that the significant relative deflection from one end of a hole to the other end of the hole did not increase rapidly until the web was completely yielded. Yielding first occurred at a corner of a hole and was significantly affected by the stress concentration at the corner. In proposing an ultimate strength solution for wide-flange beams with a rectangular hole, Bower first stated that in beams without holes, a lower bound solution was often derived by assuming that the center part of the web was yielded in shear due to the applied shear force and that the remaining web and flanges were yielded in bending due to the external bending moment. Since the beam is fully yielded, the shear stress distribution in the web is constant. He then applied this solution to beams with a rectangular hole by using a constant shear stress distribution in the remaining area of the web. The hole was regarded as simply reducing the web area that was yielded in shear. Von Mises yield criteria was used to determine yielding in shear. This solution, however, neglected the local bending moment caused by the Vierendeel action. Therefore, this solution would be expected to predict an ultimate strength that is greater than the actual ultimate load for a beam with a hole. Bower then introduced a lower bound solution by assuming rectangular shear and bending stress distributions which would account for the Vierendeel action.

2.2 Vierendeel Analysis

Based on a description by Bower (1966), the basic features of the Vierendeel analysis are described in Figure 2.1.

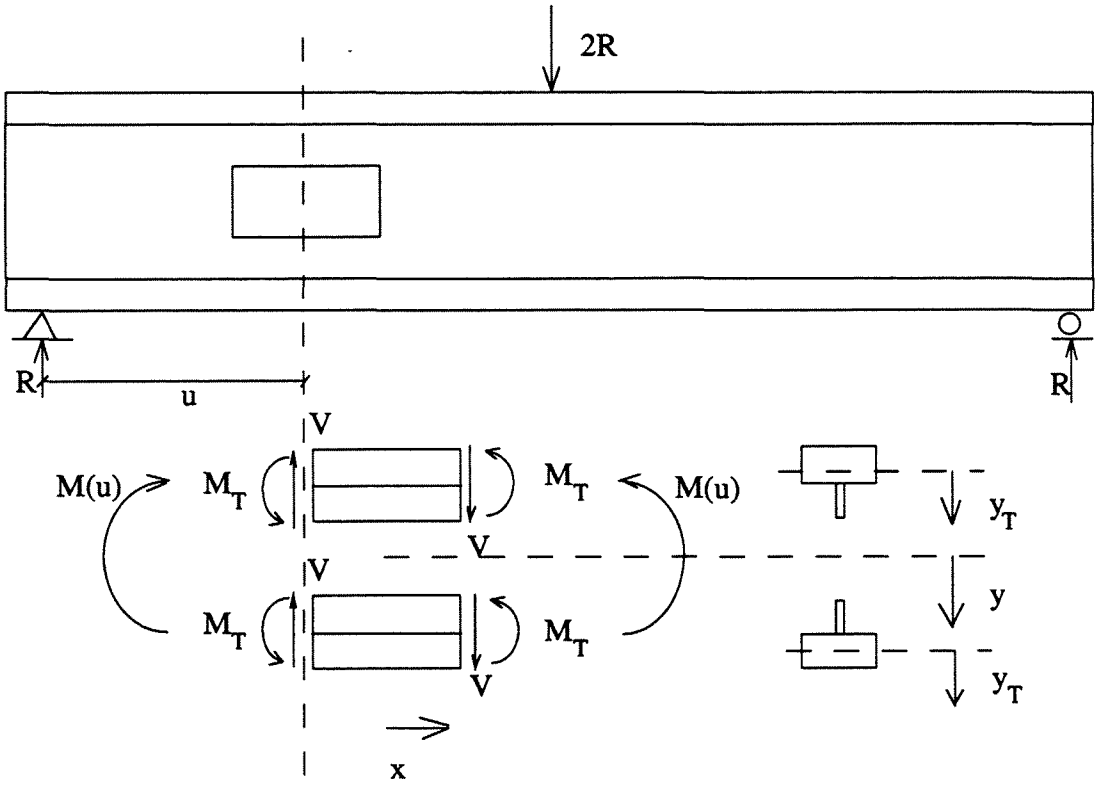

Figure 2.1. Vierendeel analysis

Figure 2.1 shows a simply supported beam under a single point load applied at mid span. A rectangular hole is centered on the centroidal axis of the beam. A free body diagram is drawn at the portion of the beam formed by cutting the beam at the ends of the hole. The shear force is assumed to be carried equally by the "T" sections above and below the hole.

$$V = 0.5R \qquad [1]$$

Assuming that a point of contraflexure occurs at the centre of the hole, the secondary moment M_T can be determined by

$$M_T = V \cdot x \qquad [2]$$

Positive moment causes compression at the top of a beam. The secondary bending stresses, caused by M_T are given by

$$\sigma_{XT} = \frac{V \cdot x \cdot y_T}{I_T} \qquad [3]$$

in which I_T = the moment of inertia of one T-section and y_T = the transverse distance from the centroid of the T-section. From statics, the primary bending moment is given by

$$M(u) = R \cdot u = 2V \cdot u \qquad [4]$$

The primary bending stress, σ_P, is given by

$$\sigma_P = \frac{M(u) \cdot y}{I_n} \qquad [5]$$

in which I_n = the moment of inertia of the net cross section of the beam about its centroidal axis and y = the transverse distance from the centroid of the beam. Equations [3] and [5] are added to obtain the total bending stresses

$$\sigma_x = \frac{V \cdot x \cdot y_T}{I_T} + \frac{M(u) \cdot y}{I_n} \qquad [6]$$

A positive value of σ_x means that the bending stress is in tension.

2.3 Vierendeel Analysis Applied to Steel Wide Flange Beams

The Vierendeel analysis used by Bower (1966) was applied to steel wide flange beams with holes. Structural steel behaves like a linear, elastic material up to yielding of the steel. Steel is an isotropic and homogeneous material. In other words, the material properties of steel are such that the M.O.E. is independent of the orientation of the applied stresses and the material is of uniform quality throughout the beam. In the Vierendeel analysis, the elastic flexure formula ($\sigma_x = My/I$) was applied to the steel beam. The familiar elastic flexure formula is based on the assumptions that

- plane sections remain plane,
- the material is linear,
- the material is elastic.

For plane sections to remain plane when steel beams are transversely loaded, the shear deformations must be small. In other words, the shear modulus must be stiff enough. Structural steel has a shear modulus of 77 000 MPa, over a third of the elastic modulus of 200 000 MPa. Shear deformations in steel I-beams are usually insignificant when compared to the bending deformations.

The application of the Vierendeel analysis to wood I-beams will be discussed in Chapter 6, Analysis and Discussion.

3. EXPERIMENTAL PROGRAM

3.1 General

The experimental program consisted of three phases of testing. Each phase corresponded to a depth of beam. Therefore, three depths were used: 241 mm, 406 mm, and 610 mm. After each phase of testing, results were closely examined so the following tests would be designed to answer questions which arose from earlier test results. The deepest beams were tested first followed by the smallest beams. The last phase included tests to confirm findings in the first two phases. After the beam tests were completed, material tests were performed to determine web and flange material properties.

3.2 Test Specimens

Wood I-joists are made from a variety of wood or wood composite materials. The chords (flanges) can be made from solid sawn lumber such as No.1/No.2 visually graded lumber or machine stress rated (MSR) lumber or wood composite lumber such as laminated veneer lumber (LVL) or parallel strand lumber (PSL). OSB, plywood, or hardboard can be used as web material. The wood I-joists used in testing were prefabricated by an Alberta manufacturer.

The chord material used was No.1/No.2 Spruce-Pine-Fir (S-P-F) visually graded lumber and the web was OSB grade O-2 made from aspen trees in Alberta. The OSB grade O-2 indicates that the strands are oriented in two directions. OSB-grade O-2 has three layers of strands. The two face layer strands are oriented parallel to the long axis of the panel and the core layer strands are oriented perpendicular to the long axis of the panel. OSB panels typically come in 2440 mm x 1220 mm dimensions.

The test specimens were manufactured by splicing the panels approximately every 2440 mm and gluing the chord to the web. Both the web splice and the web/flange connection are proprietary. Figure 3.1 shows the nominal cross section dimensions.

3.3 Test Set-Up

The beams were tested as simply supported beams loaded with a point load applied to the top flange, as shown in Figures 3.2 and 3.3. At each reaction point, bearing plates were made large enough to prevent local crushing of the chord fibers. Below the plate in order were the knife edge, load cell, roller support, and a rigid leveled distributing beam. The point load was applied through a hydraulic jack pumped manually from a hydraulic hand pump. Lateral bracing was provided by placing hollow steel sections or 38 mm x 89 mm lumber against the flanges of the beam and fastening the steel sections or 38 mm x 89 mm lumber to a rigid frame which ran parallel to the length of the test specimen.

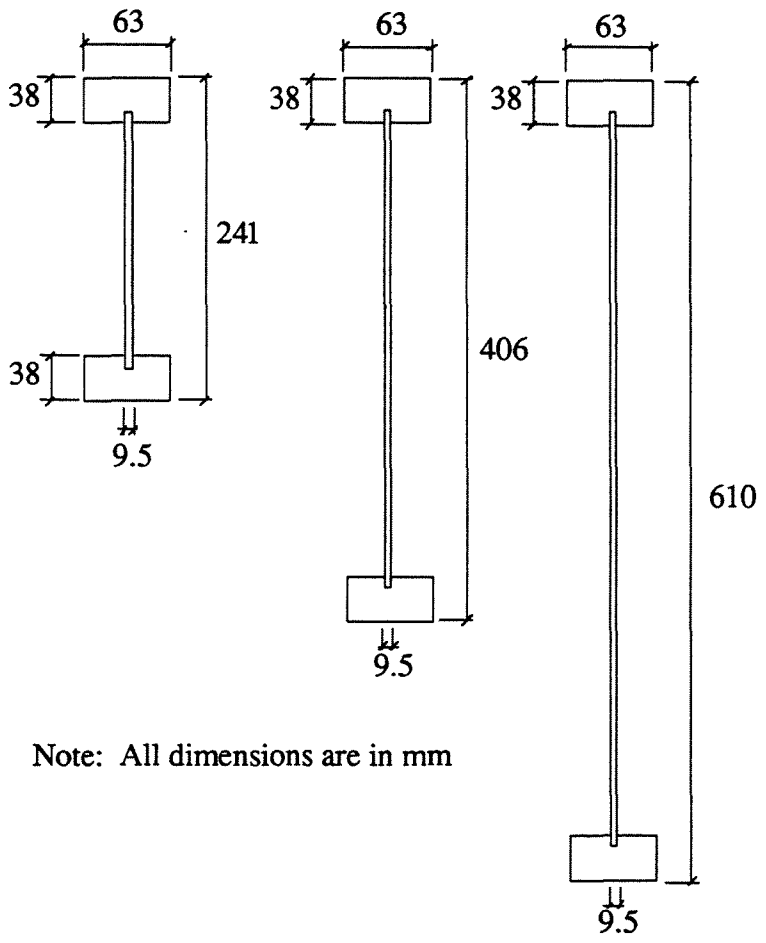

Figure 3.1. Nominal dimensions of OSB I-beam specimens

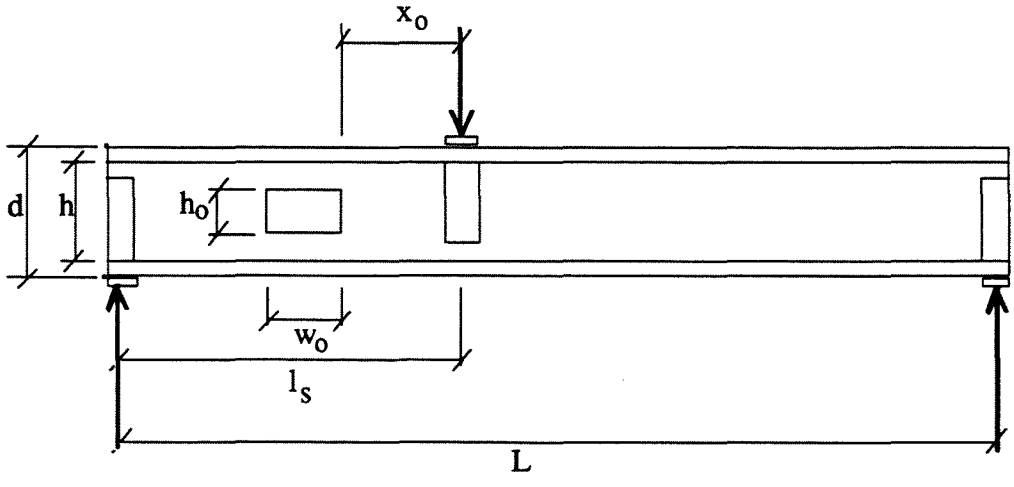

Figure 3.2. Schematic test set-up

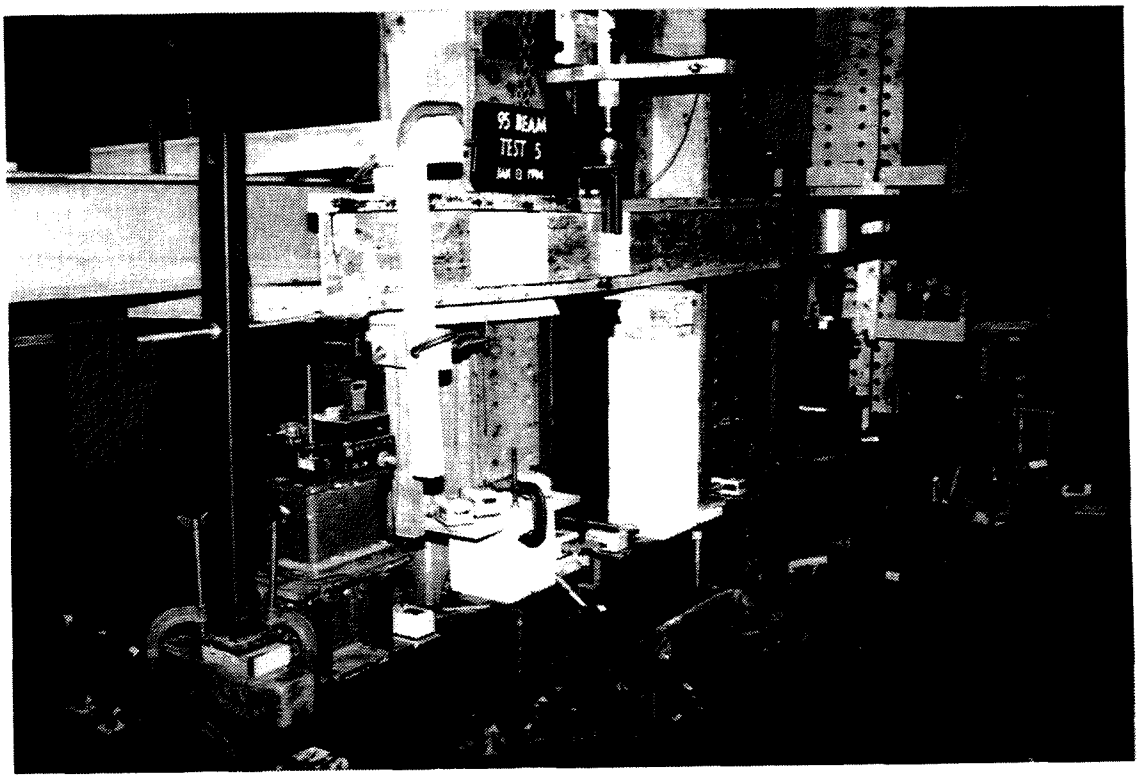

Figure 3.3. Actual test apparatus

3.4 Instrumentation

To observe the deformations around the hole, demec points with a gauge length of 50.8 mm were placed at the corners of the hole at 45° to the horizontal axis. The corner demec points detected cracking or crushing of the OSB fibers. Demec points were also placed horizontally in rows starting from the top flange and ending on the bottom flange (Figure 3.4). These demec points were used to determine longitudinal deformations through the depth of the beam. A profile of the longitudinal deformations above and below the left and right corners of the hole can then be drawn. Demec gage rosettes were also placed at the corners of the hole and at intact sections of the web without any holes. The location of these rosettes can be found in Appendix A. To determine the deflected shape of the beam near the region of the hole, six or seven cable transducers were attached to the bottom of the lower chord of the beam. For specimen 24dT4 which exhibited web buckling, a column of four Linear Variable Differential Transformers (LVDT) were placed on the vertical side of the web to record the buckled shape of the web. A fuller description of this set-up can be found in Appendix B.

The load cells and cable transducers were linked to a Fluke data acquisition system. A personal computer recorded the load and deflection readings of the test specimen. Demec readings were recorded manually at each load step. A plotter displaying the applied load versus the load point deflection was used to monitor the overall behaviour of the beam.

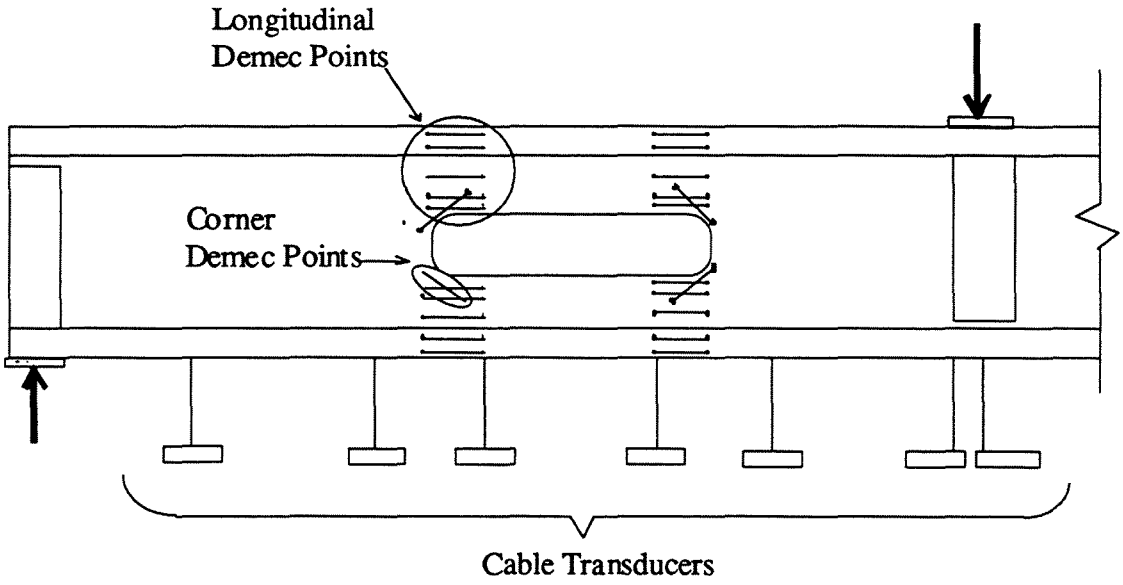

Figure 3.4. Instrumentation

3.5 Test Parameters

Determination of the behaviour of the web with a hole required sufficient number of beams to be tested so that the effect of each parameter could be determined. The test parameters used for all beams were the hole width, hole height, shear span length, and the corner radius of the hole. Table 3.1, shows the specimen parameters used and the order of the specimens tested with the exception of specimen 24dT7 which was tested after specimen 16dT3. The shear span needed to be short enough to ensure the beam failed in shear and not in bending. However, the shear span needed to be long enough to position the hole away from the load points so that the local bearing effects of the load would be small. Also, the shear span needed to be long enough to minimize arching action between the load point and the reaction. The edge of the hole was placed at a distance "d", depth of beam, away from the edge of the nearest web stiffener (note "x_o" in Table 3.1 and Figure 3.2 is a distance between the edge of the hole and the line of the point load.

3.6 Test Method

The beams were loaded manually with a hydraulic jack. Approximately ten load steps were used in each test to describe the beam behaviour throughout the test. After each load increment, the beam was given two minutes to reach equilibrium. Instrument readings were then taken. Another load increment was applied and the process was repeated until the beam could no longer sustain another increment of load. The test was terminated when a sudden drop in load occurred.

Table 3.1. Description of test specimens

specimen	depth of beam, d, mm	position of hole, x_o, mm	height of web, h, mm	height of hole, h_o, % of h	width of hole, w_o, mm	shear span, l_s, mm	length of beam, L, mm
24dT1	610	675	534	67	152	1808	3616
24dT2	610	675	534	33	152	1808	3616
24dT3	610	675	534	33	152	1808	3616
24dT4	610	no hole	534	no hole	no hole	1808	3616
24dT5	610	675	534	33	457	1808	3616
24dT6	610	675	534	100	152	1808	3616
24dT7	610	no hole	534	no hole	no hole	1808	3616
9.5dT1	241	286	165	33	152	1000	3000
9.5dT2	241	no hole	165	no hole	no hole	1000	3000
9.5dT3	241	286	165	33	305	1000	3000
9.5dT4	241	286	165	67	305	1000	3000
9.5dT5	241	286	165	100	305	1000	3000
9.5dT6	241	286	165	33	305	1500	3000
9.5dT7	241	286	165	33	305	1000	3000
9.5dT8	241	286	165	33	305	1000	3000
16dT1	406	450	340	33	305	1250	2750
16dT2	406	450	340	67	305	1250	2750
16dT3	406	no hole	340	no hole	no hole	1250	2750

Note:
- specimen 24dT2 was repeated in 24dT3 due to a bearing failure.
- specimen 24dT4 was repeated in 24dT7 due to a lateral torsional buckling failure.
- all specimens have a corner radius of 25 mm except specimens 9.5dT7 and 9.5dT8 which have a square and 12 mm radius corner, respectively.

4. MATERIAL TESTS

4.1 General

In order to analyze the behaviour of OSB I-beams, material property information was required from standard material tests on the web panel and flange. OSB compression tests were done in two directions, parallel and perpendicular to the length of the beam. The face strands in OSB are oriented parallel to the length of the beam. Similarly, tension tests were conducted in two directions, parallel and perpendicular to the face strands. The edgewise shear strength and plate shear modulus were also obtained for OSB. Tension and compression tests were also conducted on the flange material.

4.2 OSB Compression Tests

OSB compression coupons were cut from the three depth sizes of test specimens. Each test specimen was made by gluing three coupons back to back using a construction adhesive called Ultragrip 9000. The dimensions of the test specimen were approximately 177 mm x 46 mm x 30 mm. Coupons of OSB needed to be glued together so that buckling would not occur before crushing of the fibers. Two sets of compression specimens were made. One set of specimens was loaded parallel to the orientation of the face strands and the other set was loaded perpendicular to the face strands. Each set was tested twice. This was done to determine whether the strain readings from instrumentation on the face strand side of the specimen would be different from the strain readings from instrumentation on the edge side of the specimen. The instrumentation consisted of a 50.8 mm extensometer on one side and a 50.8 mm demec gage on the opposite side. Demec readings and extensometer readings were taken simultaneously. In the first test run, the instrumentation was placed on the edge sides of the specimen. In Figure 4.1, the edge side is shown with demec points mounted on the edge of the middle coupon. The specimen was then loaded to obtain the elastic modulus and then unloaded. In the second test run, the instrumentation was placed on the face strand sides of the specimen. The specimen was loaded until failure to determine the elastic modulus and maximum compression strength. This procedure was repeated for all specimens in both sets of coupons.

The material testing system MTS 1000 at the I.F. Morrison Laboratory at the University of Alberta was used to test the specimen at a rate of 0.5 mm/min. OSB compression testing followed guidelines outlined in ASTM standard D 3501 (1976) with the exception that three coupons were glued together to prevent buckling.

4.3 OSB Tension Tests

Two sets of tension tests, face strands parallel and perpendicular to load, were performed on OSB coupons to determine directional properties of OSB in tension. ASTM standard D 3500 (1990) was used as a rough guide in both sets of tension tests. The coupons with face strands parallel to load were rectangular with dimensions 127 mm wide and at least 1220 mm long. The length between grips was 305 mm. This set of coupons was tested on the Metriguard 412 test proof tester at the Forest Products Laboratory at the Alberta Research Council. The rate of testing was such that failure occurred between two to four minutes. Deformations were recorded using a 229 mm LVDT.

The coupons with face strands perpendicular to the load were cut according to a necked down shape shown in Figure 4.2. The extreme necking was thought necessary because slippage at the grips was a problem in earlier tests with the Metriguard tester. However, in this set of tests, the MTS 1000 was used to test these coupons at a rate of 0.175 mm/min., which caused failure in

three to six minutes, and no slippage was encountered. A 50.8 mm extensometer was used to record the deformation in the coupon. Due to insufficient length, only the webs from 610 mm deep beams were tested.

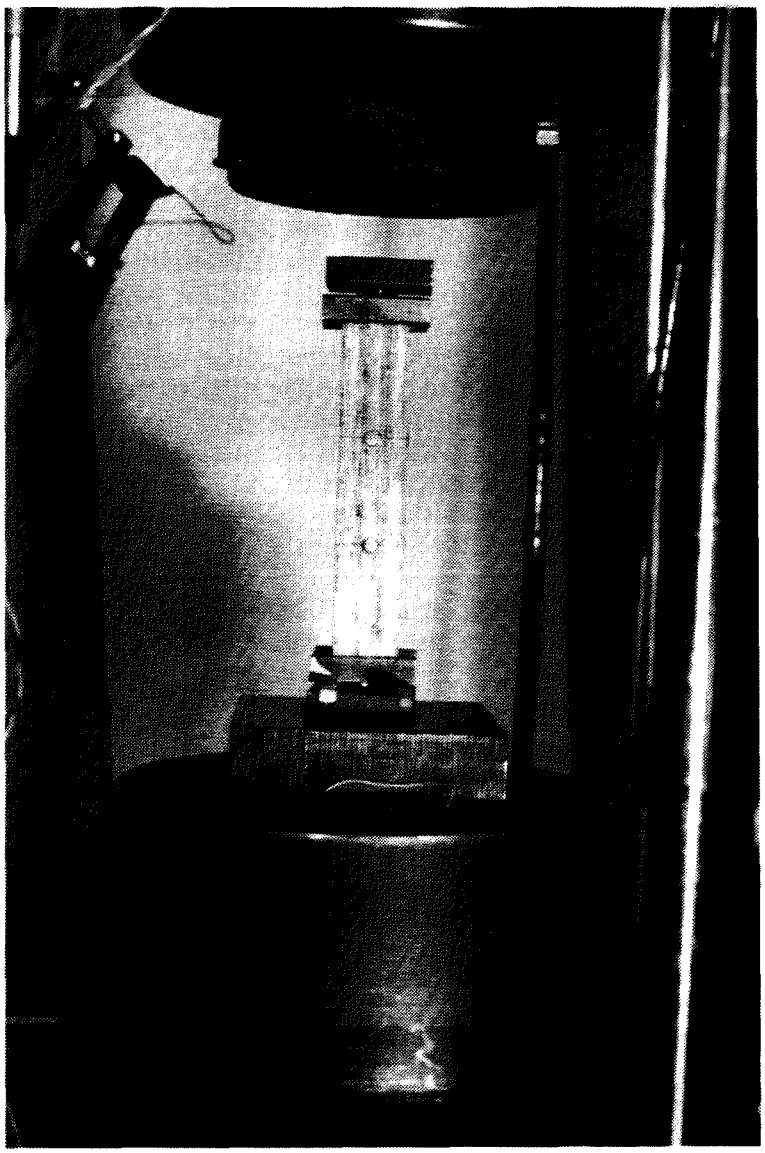

Figure 4.1. Edge side of OSB compression specimen

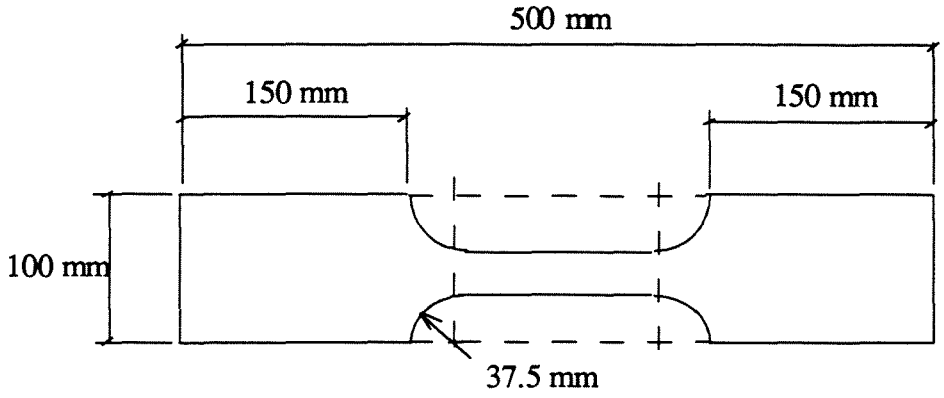

Figure 4.2. OSB tension coupon with face strands perpendicular to load

4.4 OSB Shear Tests

Edgewise shear strength tests were conducted according to ASTM standard D 2719 (1989). This two rail shear test required a specimen 610 mm x 457 mm. Due to the large size of the specimen required, only the webs of the 610 mm depth beams could be tested. The two rails were made of aluminum with bolt holes spaced every 102 mm along the rail so that bolts could clamp the specimen and prevent it from slipping under load as shown in Table 4.4. The Metriguard tester loaded the specimen at a rate such that failure occurred between three to five minutes.

Table 4.4. OSB shear test results

Plate shear modulus tests				Two-rail shear test				
specimen	shear modulus MPA	moisture content %	specific gravity	specimen	shear modulus* MPA	max. shear MPA	moisture content %	specific gravity
24dT1	1836	3.5	0.667	24dT1	1790	7.88	3.73	0.634
24dT3	1683	3.1	0.647	24dT6	1850	8.21	3.94	0.696
24dT5	1450	3.3	0.624					
24dT6A	1478	---	---	average	1820	8.04	3.83	0.665
24dT6B	1509	3.3	0.641					
24dT7	1702	3.2	0.647					
16dT2	1777	3.1	0.661					
16dT3	1662	3.2	0.657					
average	1637	3.26	0.649					
std. dev.	142.9	0.143	0.0143					
c.o.v.	8.73	4.4	2.20					

* value has been increased by a factor of 1.19 recommended by the standard

Plate shear modulus tests for OSB were conducted using ASTM standard D 3044 (1976). These were non-destructive tests which determined the edgewise or in-plane shear modulus of the OSB web. The nominal dimensions of the specimen were 300 mm x 300 mm x 10 mm. Figure 4.3 shows that the test consisted of putting the plate into pure twisting by transversely loading two diagonal corners while the other two corners had roller supports. The relative transverse deflection between the centre of the plate and the corner of a square drawn on the plate was required to determine the shear modulus of OSB. The instrumentation shown in Figure 4.3 consisted of a four legged mechanism which sat on the corners of the drawn square. The instrumentation recorded twice the deflection between the centre of the plate and the corner of the drawn square. Each leg of the specimen was 75 mm measured from the centre of the plate. The MTS 1000 loaded the specimen at a rate of 3.6 mm/min. Deflection readings were taken with a 5 mm LVDT.

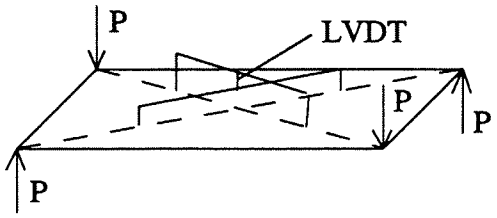

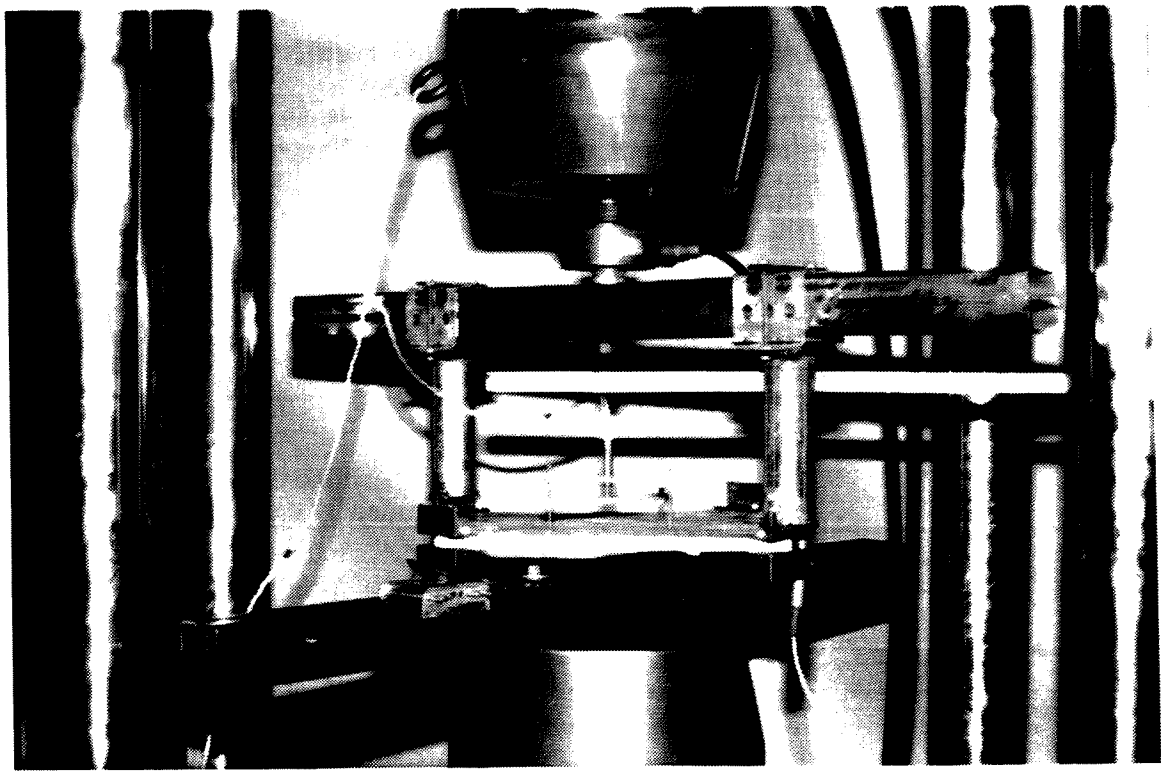

Figure 4.3. Plate shear modulus tests for OSB

4.5 Chord Compression Tests

ASTM standard D 198 (1984) was used to test the chords of the beam as a short column. The specimens length was 178 mm. Instrumentation used for this test was identical to that used in the OSB compression tests. Figure 4.4 shows the extensometer attached to the narrow side of the specimen with elastic bands while demec points are placed on the opposite side. Both extensometer and demec readings were taken simultaneously. The MTS 1000 loaded the specimens at a rate of 0.178 mm which corresponded to failure occurring between eight to twelve minutes.

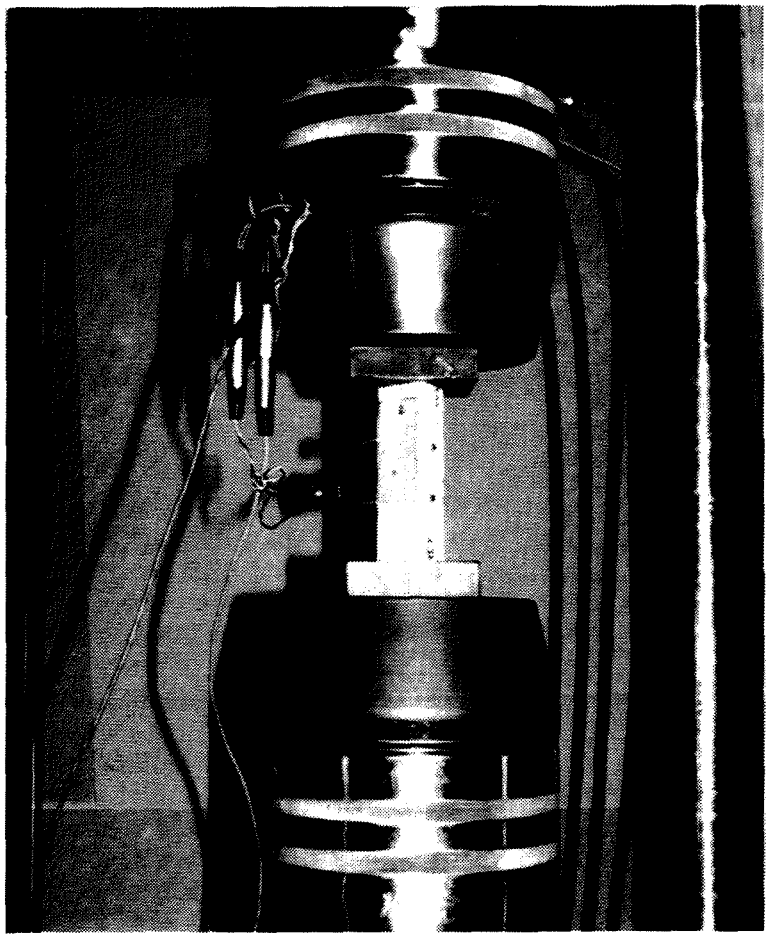

Figure 4.4. Chord compression test

4.6 Chord Tension Tests

ASTM standard D 198 (1984) was used to test the chords of the beam in tension. The Metriguard 412 tension proof tester failed the specimens in three to eleven minutes. The length of the specimen between grips was 610 mm. A 229 mm LVDT was used to measure the deformation.

4.7 Material Test Results

4.7.1 OSB Compression Tests

Tables 4.1 and 4.2 show the M.O.E., maximum stress, moisture content, and specific gravity of the OSB compression specimens with face strands perpendicular and parallel to the applied load, respectively. The slope of the load versus deformation curve is shown so that the edge readings can be compared with the face strand readings. In both tables, the average slopes based on extensometer and demec edge readings are very close to each other as they should be if only axial loads are present. However, the average slopes based on extensometer and demec face strand readings are not as close. The cross section of the specimen is rectangular and therefore has a different moment of inertia about two orthogonal axes. The axis with a smaller moment of inertia is more susceptible to bending about that axis. Due to imperfect alignment, there will always be bending stresses developed in the specimen. The larger difference between the slopes determined from extensometer and demec face strand readings is due to eccentric axial loads which cause bending stresses. Therefore, the M.O.E. based on edge readings was more reliable to use as a material property.

The M.O.E. for specimens with face strands parallel to the axial load (parallel specimens) were 32% greater that the M.O.E. for specimens with face strands perpendicular to the axial load (perpendicular specimens). Also, the maximum stress for parallel specimens was 26% greater than the maximum stress for perpendicular specimens. The specific gravity and moisture content of both parallel and perpendicular compression specimens were very similar.

4.7.2 OSB Tension Test Results

Table 4.3 shows the M.O.E., maximum stress, moisture content, and specific gravity for the OSB tension tests with face strands parallel to load (parallel specimens). The M.O.E. and maximum tension stress of the parallel specimens were 21% and 43% greater than the M.O.E. and the maximum stress of the perpendicular specimens, respectively. The parallel specimens performed differently than the perpendicular specimens because the load was applied in a different direction and the specimens were not the same size. The cross section of the perpendicular specimens were smaller than the parallel specimens. The M.O.E. and the maximum stress values were expected to increase as the cross section area increased because the larger area specimens or parallel specimens would benefit from strands interlocking across the larger width of the specimen. Thus, if a comparison of the material properties is made between the parallel and perpendicular specimens where the sizes of the two sets of specimens are the same, the M.O.E. and the maximum stress of the parallel and perpendicular specimens should be closer than the test results shown. The moisture content and specific gravity for both sets of specimens were similar.

The parallel specimens had a very high coefficient of variation for the M.O.E. This was unexpected because the cross section area was five times as large as the area in the perpendicular specimens and should have resulted in less varying results. An explanation is that slipping occurred at the grips around the parallel specimens. The loading rate was then changed and increased to compensate for the slipping. The erratic loading rate caused more variation in the M.O.E. values. The loading rate for the perpendicular specimens was well controlled and no slipping occurred. The coefficient of variation for the M.O.E. was smaller for the perpendicular specimens than for the parallel specimens.

Table 4.1 OSB compression test results with face strands perpendicular to axial load

M.O.E. is based on edge readings					M.O.E. is based on face strand readings						
	slope* N/microstrain				slope* N/microstrain					max.	
specimen	extens.	demec	average slope	M.O.E. MPa	extens.	demec	average slope	M.O.E. MPa	M.C. %	stress MPa	specific gravity
16dT2	5.483	5.218	5.351	3703	6.288	4.815	5.551	3841	3.5	13.80	0.668
16dT3	5.979	5.458	5.719	4047	6.997	5.481	6.239	4415	3.5	15.52	0.627
24dT1	4.419	5.380	4.900	3470	3.625	6.644	5.135	3637	3.4	12.95	0.635
24dT3	6.672	3.800	5.236	3859	6.160	4.240	5.200	3832	3.4	15.29	0.647
24dT5	5.315	5.446	5.381	3872	5.358	6.267	5.812	4183	3.4	15.67	0.662
24dT6	5.572	4.916	5.244	3809	5.768	5.169	5.468	3972	3.5	15.92	0.674
24dT7	3.481	5.611	4.546	3126	5.629	4.200	4.914	3379	3.5	12.52	0.618
9.5dT2	4.825	6.720	5.772	4214	6.587	5.771	6.179	4511	3.4	18.89	0.662
9.5dT3	4.872	6.284	5.578	4199	5.625	5.321	5.473	4119	3.3	16.23	0.618
9.5dT4	6.973	6.682	6.828	4760	7.771	8.229	8.000	5577	3.3	17.40	0.639
9.5dT5	4.442	6.376	5.409	3831	7.060	4.820	5.940	4208	3.3	12.57	0.626
9.5dT6	4.339	4.985	4.662	3381	4.775	6.530	5.653	4099	3.3	14.08	0.623
9.5dT7	6.958	4.552	5.755	4241	6.680	5.545	6.112	4504	3.2	17.35	0.623
9.5dT8	6.615	4.627	5.621	4223	12.094	3.075	7.584	5698	3.3	11.42	0.594
average	5.425	5.433	5.429	3910	6.458	5.436	5.947	4284	3.4	14.97	0.637
std. dev.	1.098	0.8536	0.5583	418	1.926	1.260	0.880	656	0.109	2.165	0.0229
c.o.v.	20.2	15.7	10.3	10.7	29.8	23.2	14.8	15.3	3.2	14.5	3.60

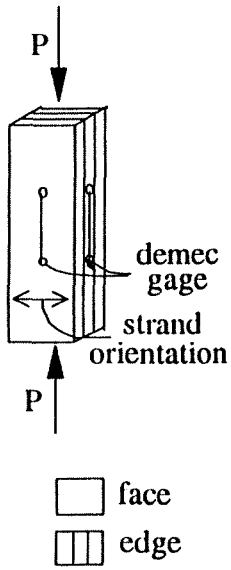

* "Slope" is determined from the load vs. deformation curve.

Table 4.2 OSB compression test results with face strands parallel to axial load

M.O.E. is based on edge readings					M.O.E. is based on face strand readings						
	slope*				slope*					max.	
specimen	N/microstrain extens.	N/microstrain demec	average slope	M.O.E. MPa	N/microstrain extens.	N/microstrain demec	average slope	M.O.E. MPa	M.C. %	stress MPa	specific gravity
16dT2	6.414	8.978	7.696	5332	6.329	8.177	7.253	5025	3.5	15.61	0.655
16dT3	8.884	10.200	9.542	6776	8.407	9.826	9.117	6474	3.3	19.50	0.676
24dT1	6.629	7.848	7.238	4983	4.858	12.95	8.905	6130	3.4	19.52	0.651
24dT3	9.613	6.917	8.265	6006	8.832	8.912	8.872	6447	3.4	20.24	0.652
24dT5	5.520	5.719	5.619	4076	9.688	5.084	7.386	5357	3.4	17.68	0.640
24dT6	6.082	6.519	6.301	4579	8.624	8.074	8.349	6068	3.4	19.15	0.646
24dT7	10.058	7.566	8.812	6071	5.040	10.24	7.640	5264	3.4	17.98	0.642
9.5dT2	8.078	6.720	7.399	5417	7.662	7.771	7.717	5650	3.5	19.17	0.650
9.5dT3	7.230	5.138	6.184	4624	8.989	5.223	7.106	5313	3.4	19.32	0.638
9.5dT4	5.745	6.498	6.122	4264	7.249	10.26	8.756	6099	3.3	16.98	0.644
9.5dT5	7.002	7.422	7.212	5360	8.315	8.696	8.506	6321	3.3	19.66	0.690
9.5dT6	7.011	9.017	8.014	5771	6.853	7.040	6.946	5002	3.3	19.90	0.675
9.5dT7	6.736	7.322	7.029	5220	8.450	12.13	10.290	7642	3.4	21.69	0.684
9.5dT8	5.598	4.751	5.174	3851	6.913	4.707	5.810	4324	3.4	16.95	0.664
average	7.186	7.187	7.186	5166	7.586	8.507	8.047	5794	3.4	18.81	0.658
std. dev.	1.457	1.514	1.234	833	1.457	2.494	1.138	831	0.088	1.587	0.0170
c.o.v.	20.3	21.1	17.2	16.1	19.2	29.3	14.1	14.3	2.6	8.4	2.58

* "Slope" is determined from the load vs. deformation curve.

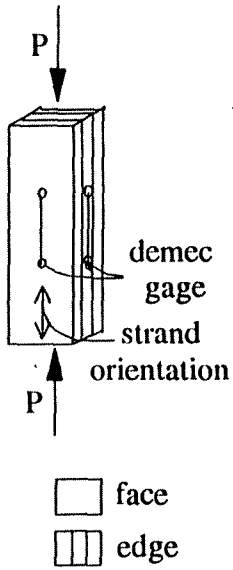

Table 4.3 OSB tension test results

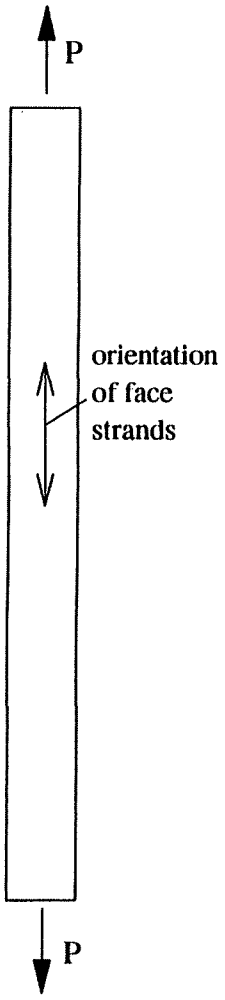

OSB tension tests with face strands parallel to load.

specimen	M.O.E. MPa	max. stress MPa	M.C. %	specific gravity
9.5dT2	4356	11.79	3.0	0.689
9.5dT3	8090	10.73	3.3	0.639
9.5dT6	4359	13.15	3.1	0.636
24dT2A	4909	16.21	3.2	0.665
24dT2B	4792	13.12	3.4	0.641
24dT2C	5995	5.32	3.5	0.563
24dT7A	5251	17.56	3.4	0.646
24dT7B	3954	18.08	3.4	0.642
24dT7C	4468	15.63	3.6	0.563
16dT2A	2941	13.13	3.4	0.641
16dT2B	6846	13.46	3.6	0.634
16dT3A	4308	13.70	3.5	0.608
16dT3B	2721	12.47	3.3	0.663
average	4845	14.09	3.4	0.633
std. dev.	1468	2.282	0.18	0.0365
c.o.v.	30.3	16.2	5.3	5.76

OSB tension tests with face strands perpendicular to load.

Specimen	M.O.E. MPa	max. stress MPa	M.C. %	specific gravity
24dT1A	4423	12.52	3.5	0.608
24dT1B	3713	10.72	3.5	0.615
24dT2	3817	11.99	3.7	0.558
24dT3A	2666	7.66	3.5	0.640
24dT3B	2980	10.14	3.4	0.601
24dT3C	4912	5.89	3.4	0.630
24dT5A	5204	6.58	3.4	0.623
24dT5B	5605	12.72	3.4	0.628
24dT5C	4471	8.30	3.2	0.668
24dT6A	4146	13.01	3.3	0.659
24dT6B	3511	11.01	3.2	0.682
24dT6C	3345	9.64	3.3	0.622
24dT7A	3343	8.83	3.4	0.662
24dT7B	4193	7.99	3.4	0.658
24dT7C	3889	10.62	3.4	0.635
average	4014	9.841	3.4	0.633
std. dev.	817.7	2.250	0.131	0.0311
c.o.v.	20.4	22.9	3.9	4.92

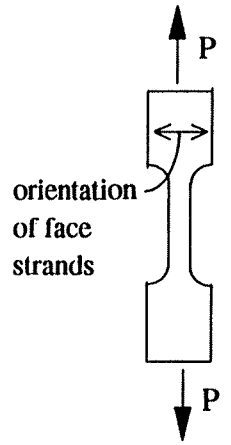

4.7.3 OSB Shear Test Results

Table 4.4 shows the edgewise shear modulus and edgewise maximum shear strength determined from the plate shear modulus and the two-rail shear tests, respectively. The two-rail shear tests yielded a shear modulus 11% greater than the shear modulus determined from the plate shear test. The average shear modulus determined from the plate shear modulus tests was more reliable to use as a material property. This value was preferred over the two-rail shear test because more specimens were tested as plate shear tests, thus, giving a better average and the factor 1.19 used in the two-rail shear test was a stress distribution correction factor which may or may not be used depending on the researcher. Since only two two-rail shear tests were performed, the two-rail shear tests acted as a check to determine if the plate shear modulus tests gave reasonable results.

4.7.4 I-beam Chord Test Results

Table 4.5 shows the M.O.E. and maximum stress obtained from compression and tension tests. The chord tension tests were performed on the same apparatus as the parallel OSB tension tests. However, little slippage occurred at the grips holding the chord specimens. The tension M.O.E. is slightly greater than the compression M.O.E. as expected from wood.

Table 4.4 OSB shear test results

Plate shear modulus tests			
specimen	shear modulus MPa	moisture content %	specific gravity
24dT1	1836	3.5	0.667
24dT3	1683	3.1	0.647
24dT5	1450	3.3	0.624
24dT6A	1478	---	---
24dT6B	1509	3.3	0.641
24dT7	1702	3.2	0.647
16dT2	1777	3.1	0.661
16dT3	1662	3.2	0.657
average	1637	3.26	0.649
std. dev.	142.9	0.143	0.0143
c.o.v.	8.73	4.4	2.20

Two-rail shear test				
specimen	shear modulus* MPa	max. shear MPa	moisture content %	specific gravity
24dT1	1790	7.88	3.73	0.634
24dT6	1850	8.21	3.94	0.696
average	1820	8.04	3.83	0.665

* value has been increased by a factor of 1.19 recommended by the standard

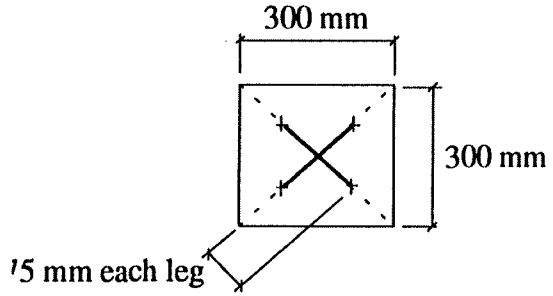

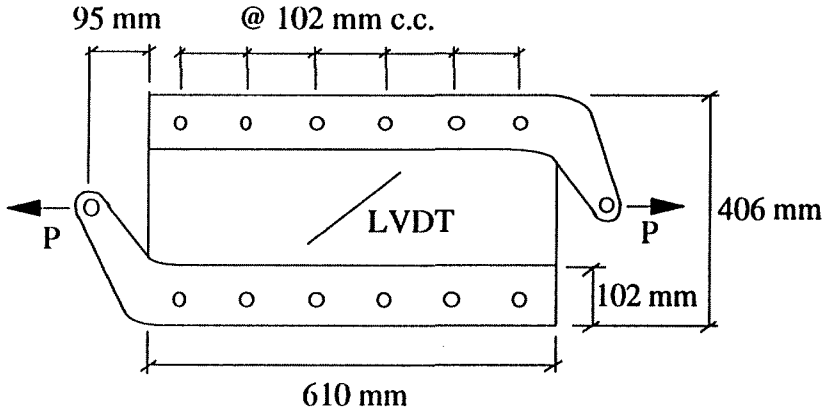

Table 4.5 I-beam chord test results

Tension tests of I-beam chords				
specimen	M.O.E. MPa	max. stress MPa	moisture content %	specific gravity
16dT1A	14532	40.5	5.3	0.515
16dT1B	12165	36.5	5.1	0.473
24dT6A	16631	24.2	4.5	0.470
24dT6B	12607	36.8	4.7	0.493
24dT7A	14150	37.8	5.2	0.499
24dT7B	12149	33.4	5.0	0.462
9.5dT1	15013	30.7	4.9	0.461
9.5dT3	11042	23.9	5.1	0.474
9.5dT6	14468	61.7	4.8	0.513
9.5dT7	13416	49.6	5.0	0.491
average	13617	37.5	4.97	0.485
std. dev.	1661	11.4	0.227	0.0200
c.o.v.	12.2	30.4	4.56	4.13

Compression tests of I-beam chords				
specimen	M.O.E. MPa	max. stress MPa	moisture content %	specific gravity
9.5dT1	12873	63.1	5.2	0.517
9.5dT2	12586	58.6	6.0	0.486
9.5dT3	7610	37.2	4.9	0.497
9.5dT4	17048	63.1	5.0	0.500
9.5dT5	8589	43.5	5.3	0.501
9.5dT6	19785	70.0	5.2	0.596
9.5dT7	10666	51.2	5.9	0.469
9.5dT8	13455	56.4	5.9	0.474
16dT2	13136	53.8	5.0	0.500
16dT3	12210	50.6	5.9	0.474
24dT1	11460	42.3	5.2	0.444
24dT3	12582	56.3	5.4	0.490
24dT5	11265	43.2	5.4	0.446
24dT6	7128	35.9	4.9	0.474
24dT7	11638	54.6	4.9	0.504
average	12135	52.0	5.3	0.492
std. dev.	3252	9.94	0.40	0.0357
c.o.v.	26.8	19.1	7.4	7.26

5. I-BEAM TEST RESULTS

5.1 General

All beams were tested indoors during the winter months. The temperature remained fairly constant between 22°C to 25°C. The relative humidity varied between 20% to 60%, but remained between 20% to 30% for most of the testing program. The shear versus deflection curves for all the beams tested are shown in Figures 5.1 to 5.4. The shear was measured directly at the left load cell and the deflection was measured by a cable transducer attached to the bottom chord (flange) of the beam beneath the load point. Figures 5.5 to 5.8 show the effects of hole size, corner detail, and shear span on the shear strength. As the size of the hole increased, the shear strength of the beam decreased. Also, the hole reduced the stiffness of the beam. Therefore, the beam deflected more when a larger hole was cut into the web. All load versus deflection curves exhibit the fact that OSB web I-beams with holes behaved linearly at the beginning of each test. At each load step at the beginning of the test, the beam sustained an increment of load without relaxing. Relaxation was indicated by a drop in load at a constant deflection. However, near the end of the test, most specimens showed increased relaxation after an increment of load was applied. The relaxation was due to wood fibers breaking in the beam. The OSB web fibers broke in two different regions which were at the corners of the hole and at the web/flange connection. Figures 5.9 to 5.30 show the longitudinal strain distribution through the depth of the beam and at the corners of the hole. These figures record all of the longitudinal strains for the 241 mm, 406 mm and the 610 mm deep beams at each load step up to failure. Most beam failures were characterized by a sudden drop in load and loud cracking sounds. The rosette gage readings and the out-of-plane web deflections can be found in Appendices A and B, respectively.

5.2 Effect of Hole Size

Figure 5.5 shows the shear strength reduction for different size holes compared to the shear strength of a reference beam with no holes. Specimen 24dT3 had a hole size of 152 mm x 178 mm (33% of h) shown in Figure 5.5 while specimens 24dT1 and 24dT6 had the same width dimension, but the hole height varied 356 mm (67% of h) and 533 mm (100% of h) respectively. The hole in specimen 24dT6 reduced the shear strength by 79% of the reference beam strength. The hole height in specimen 24dT5 is the same as 24dT3 but the hole width was increased by 3 times to 457 mm resulting in a strength reduction of 53% of the reference beam strength.

Specimens 16dT1 and 16dT2 in Figure 5.6 had the same width dimension of 305 mm, but the hole height varied 110 mm (33% of h) and 220 mm (67% of h), respectively. The shear strength in specimen 16dT2 was reduced by 61% of the reference beam strength.

Similarly, specimens 9.5dT3, 4 and 5 in Figure 5.7 had the same width dimension of 305 mm, but the hole height varied 55 mm (33% of h), 110 mm (67% of h), and 165 mm (100% of h), respectively. The maximum reduction in shear strength was 73% of the reference beam strength. Specimen 9.5dT1 had a hole 152 mm x 55 mm (33% of h) resulting in a 26% shear strength reduction.

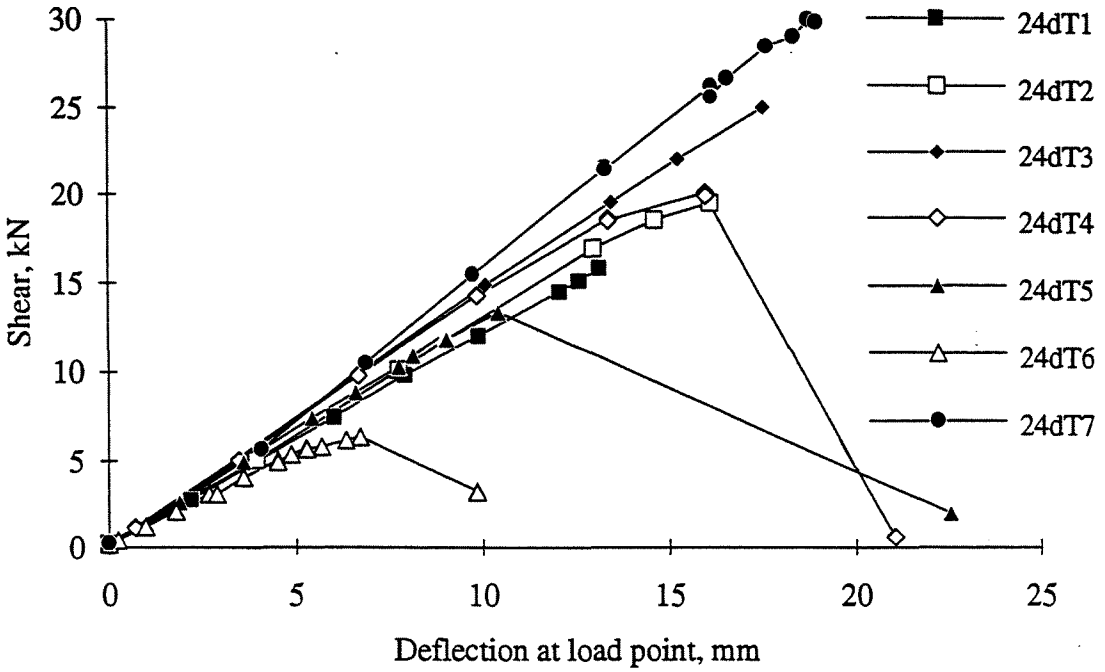

Figure 5.1. Shear vs. deflection of beam during test, 610 mm specimens

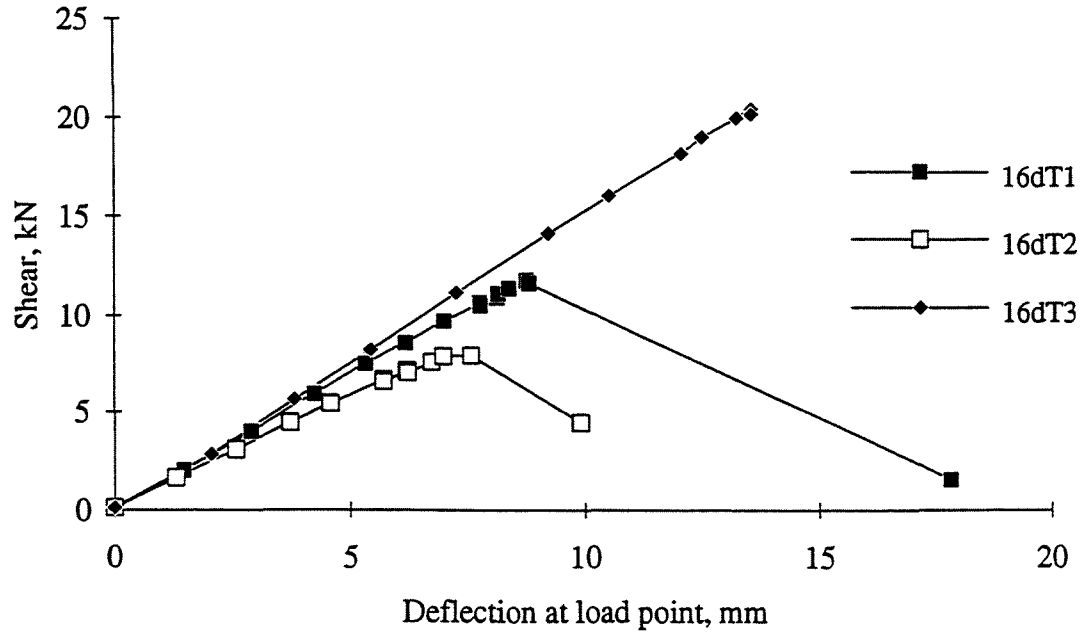

Figure 5.2. Shear vs. deflection of beam during test, 406 mm specimens

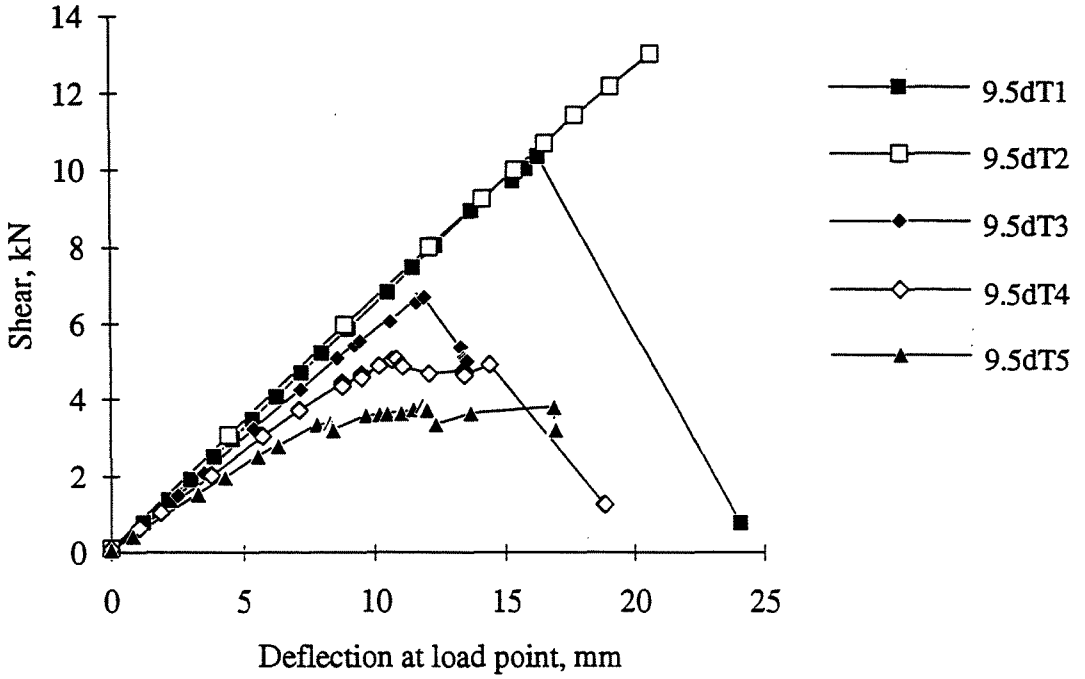

Figure 5.3. Shear vs. deflection of beam during test, specimens 9.5dT1 to 9.5dT5

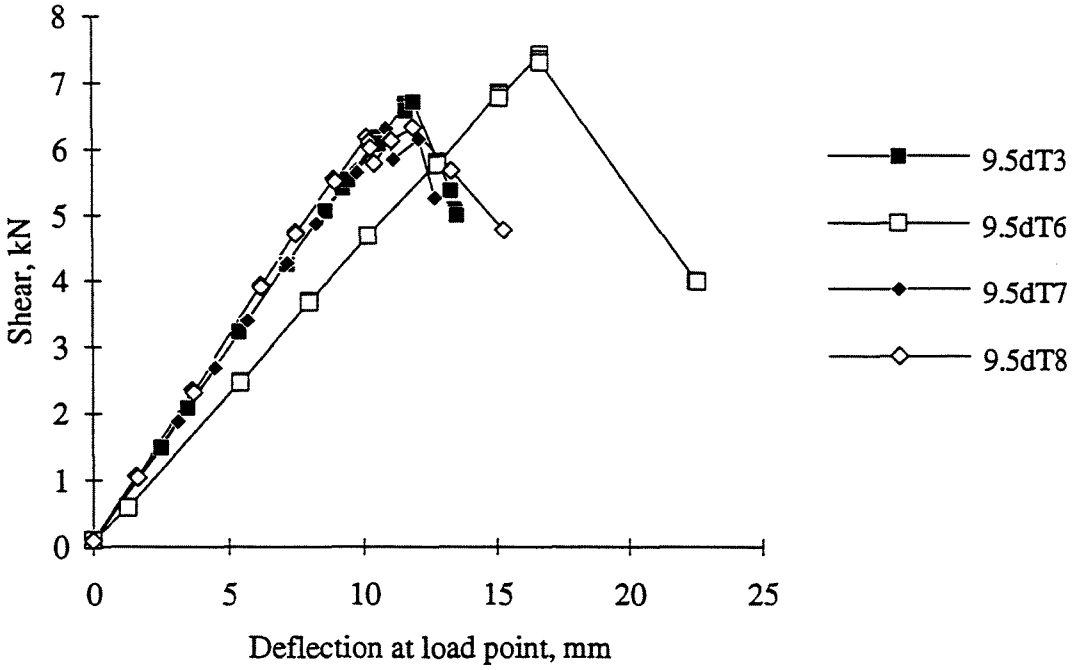

Figure 5.4. Shear vs. deflection of beam during test, specimens 9.5dT3,6,7, and 8

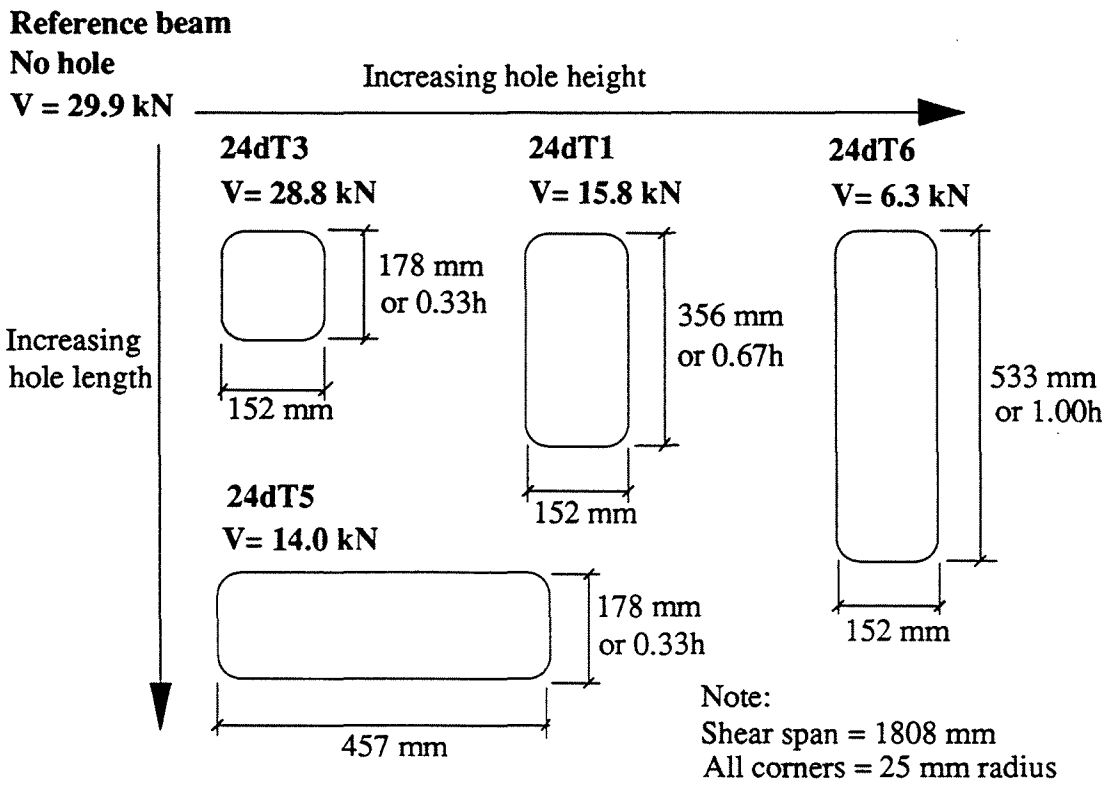

Figure 5.5 Effect of hole size in 610 mm deep beams

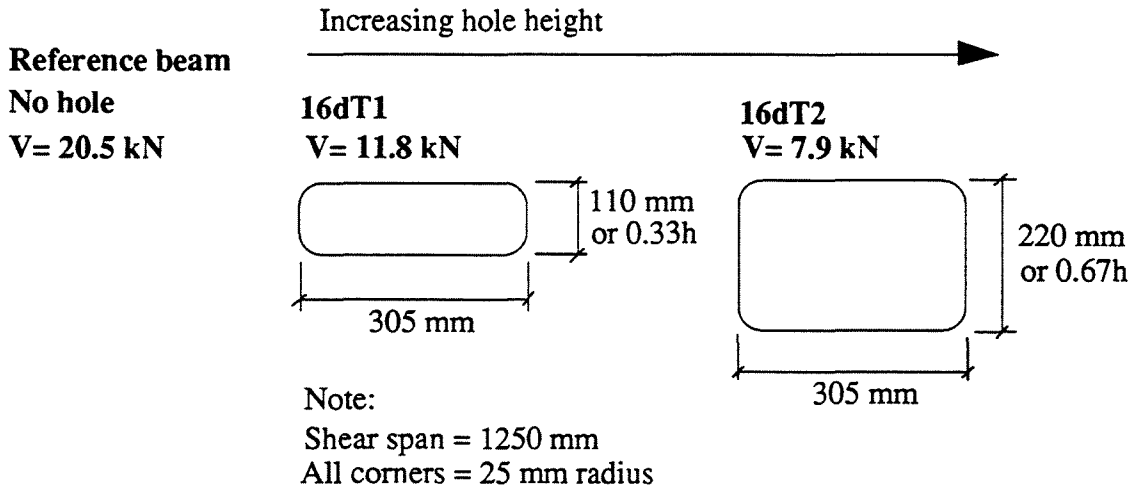

Figure 5.6 Effect of hole size in 406 mm deep beams

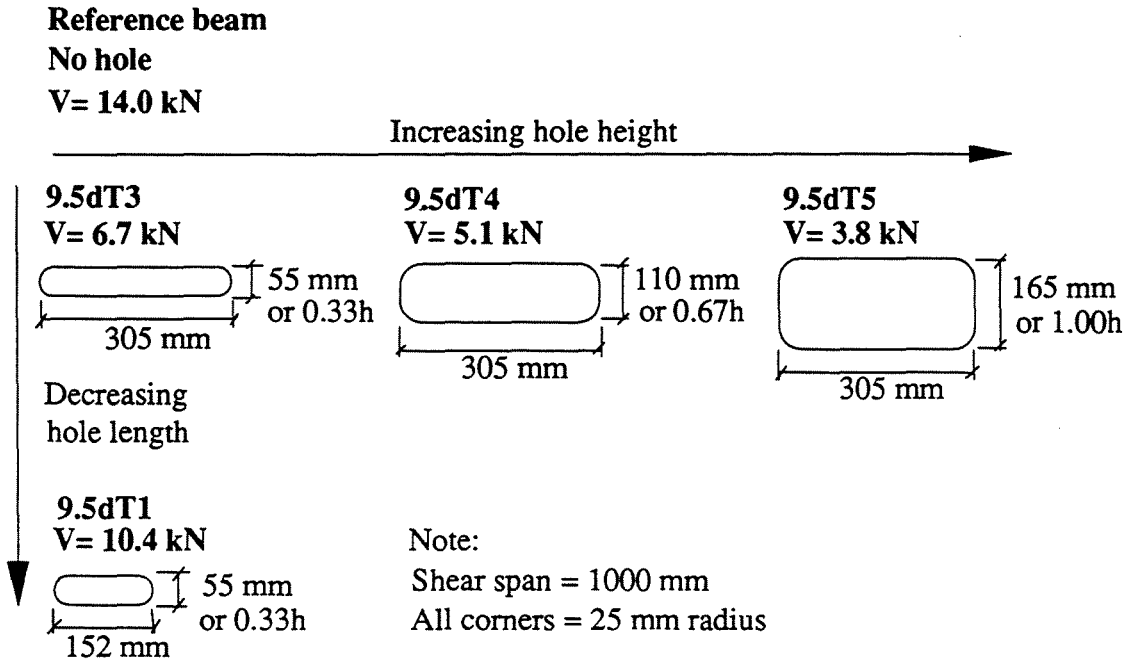

Figure 5.7 Effect of hole size in 241 mm deep beams

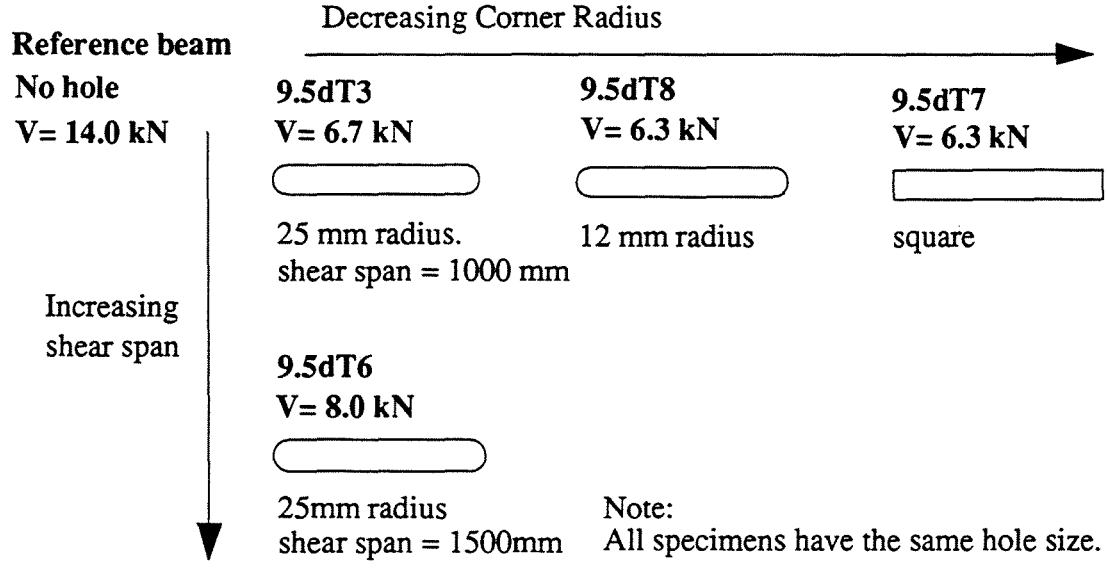

Figure 5.8 Effect of corner radius and shear span in 241 mm deep beams

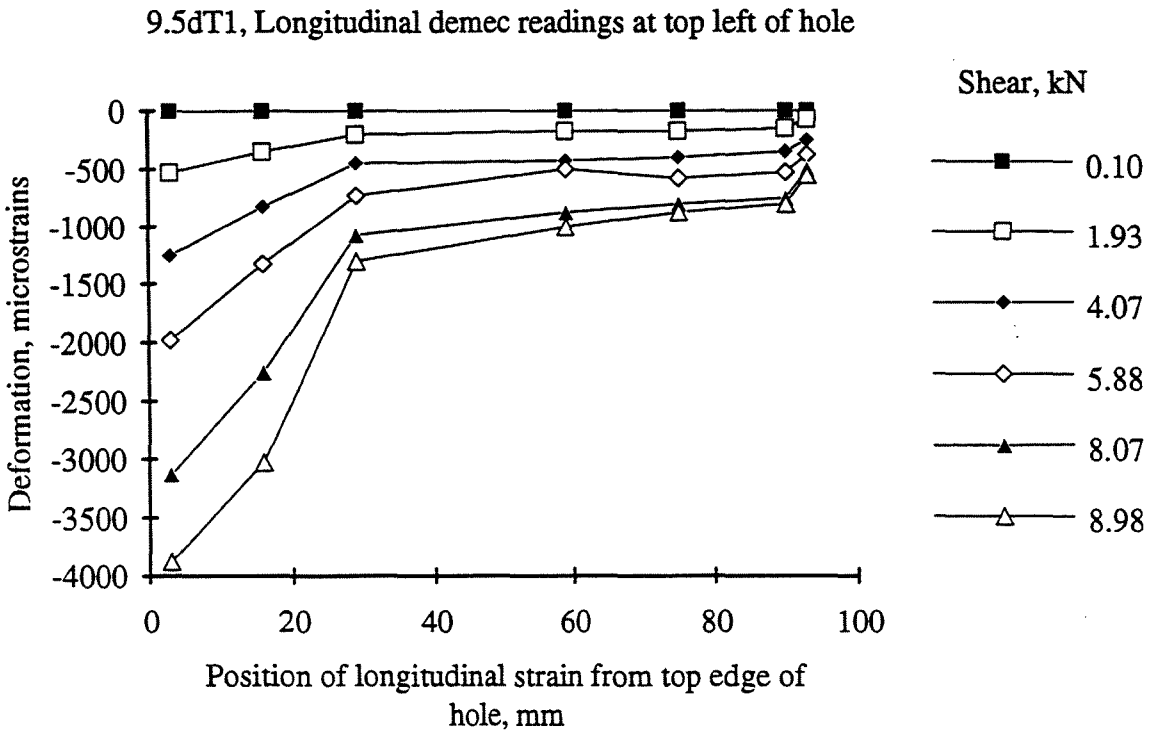

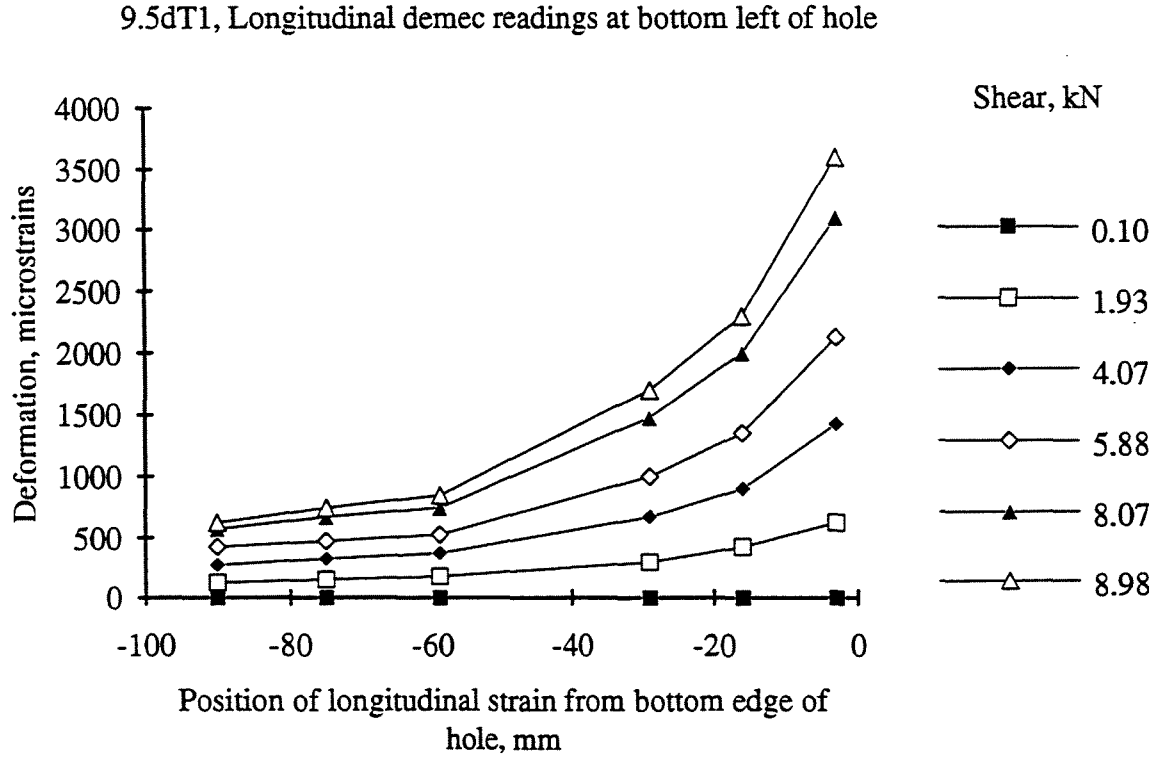

Figure 5.9. Longitudinal strain at the left section of the hole in specimen 9.5dT1

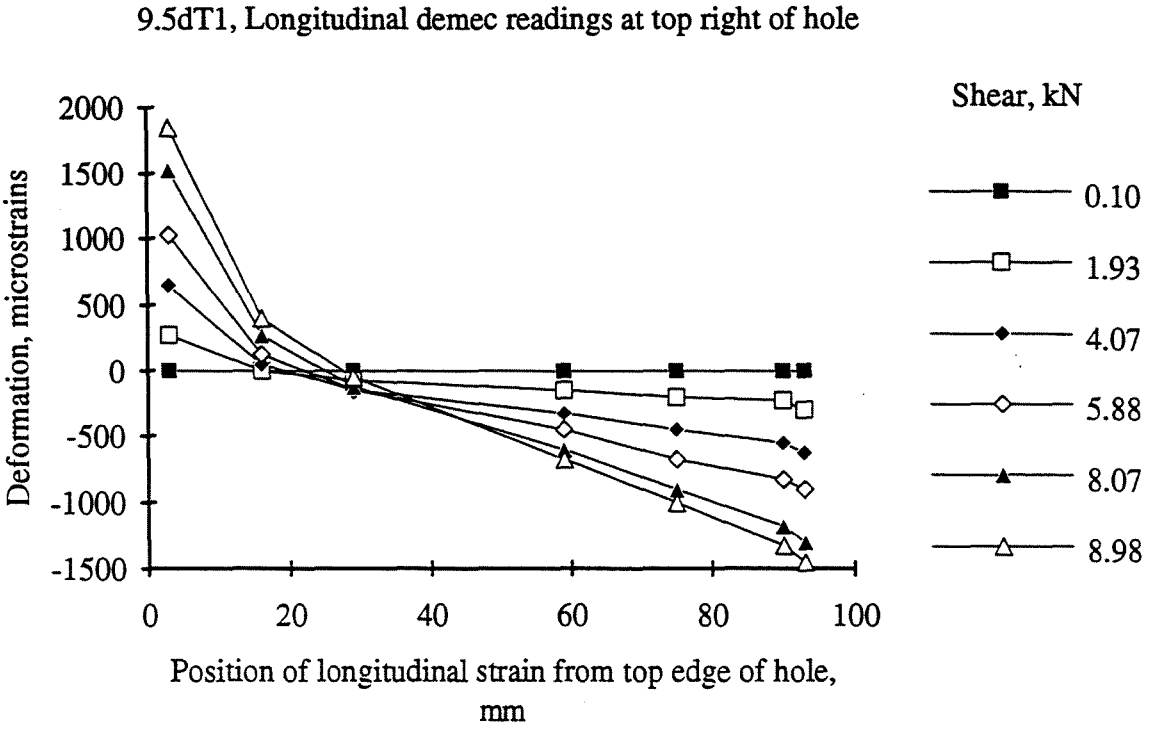

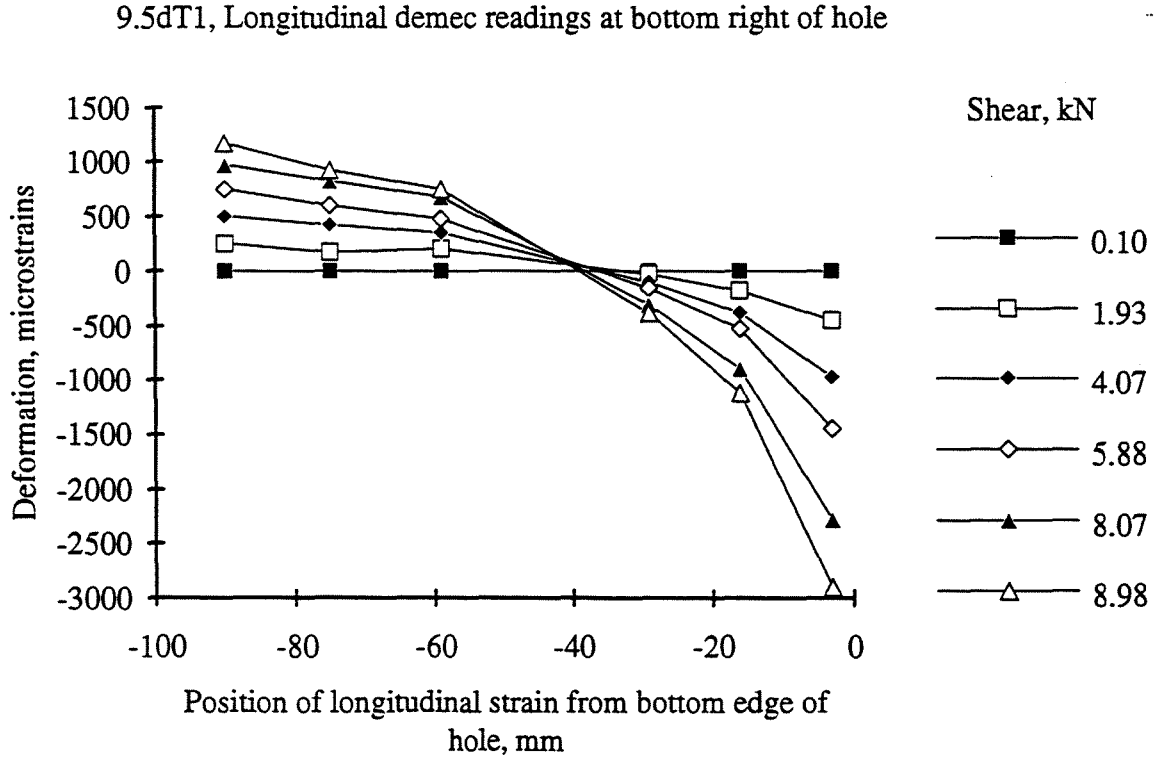

Figure 5.10. Longitudinal strain at the right section of the hole in specimen 9.5dT1

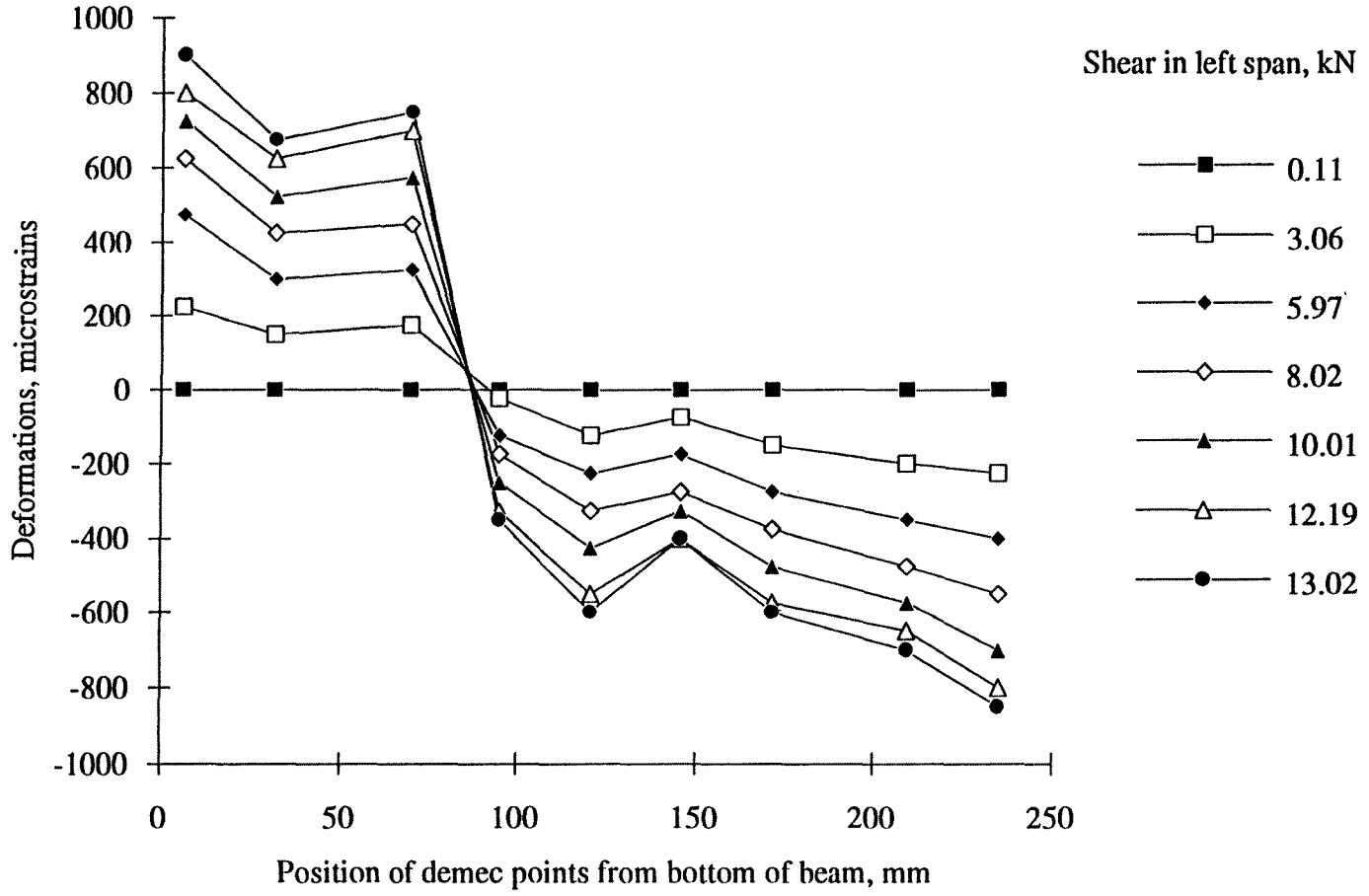

Figure 5.11. Longitudinal strain distribution of specimen 9.5dT2 at 435 mm from left reaction

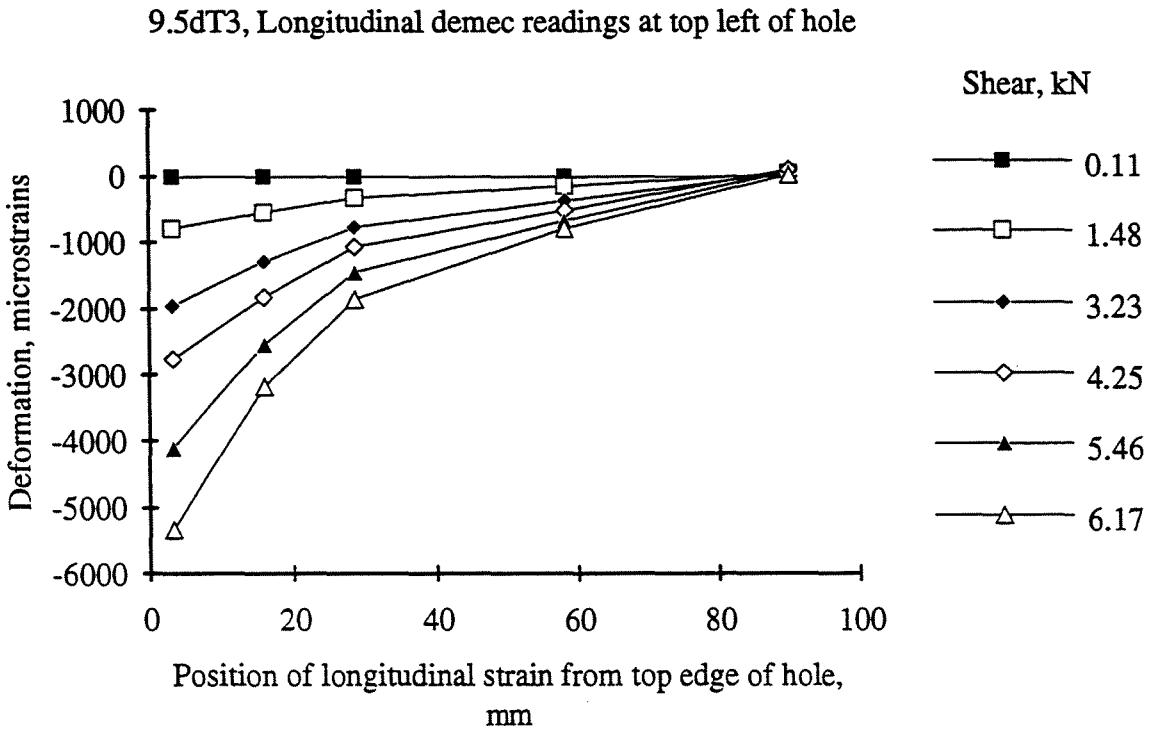

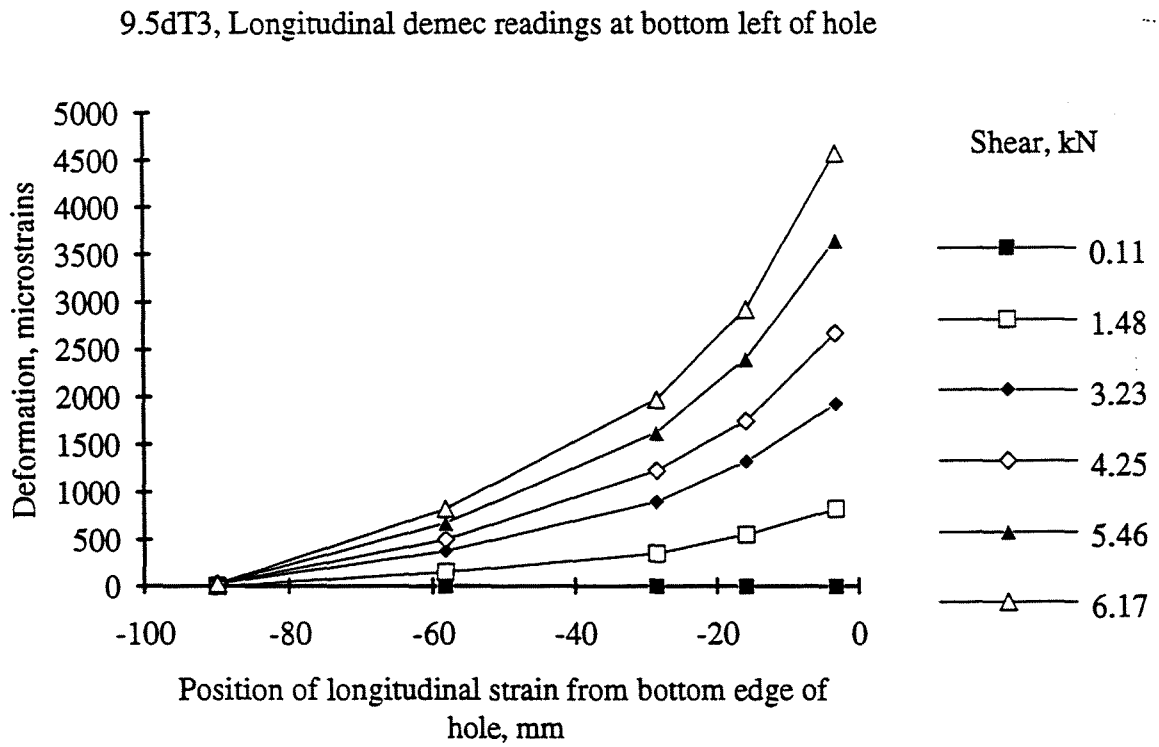

Figure 5.12. Longitudinal strain at the left section of the hole in specimen 9.5dT3

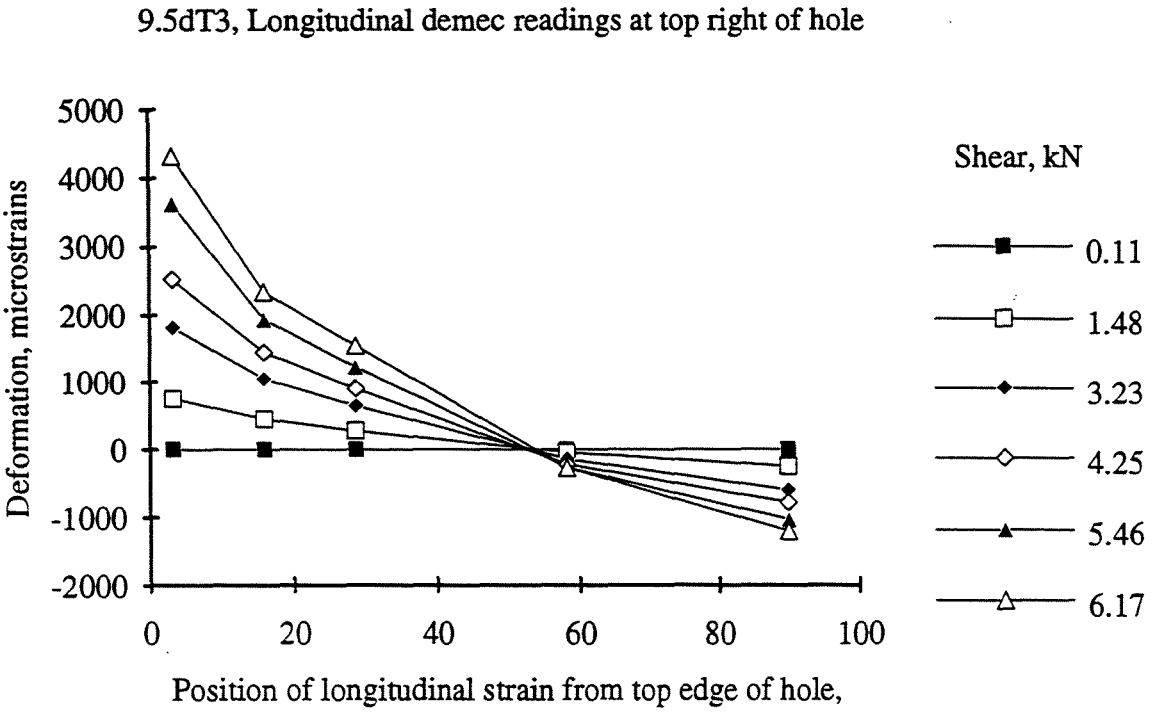

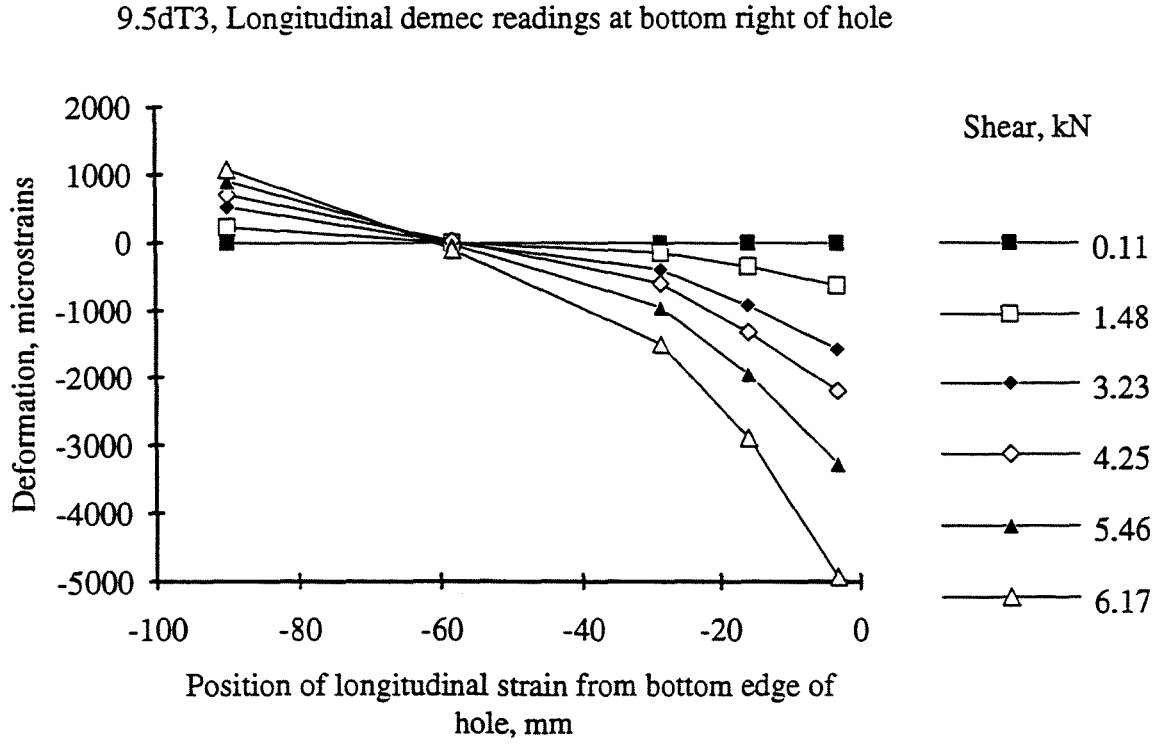

Figure 5.13. Longitudinal strain at the right section of the hole in specimen 9.5dT3

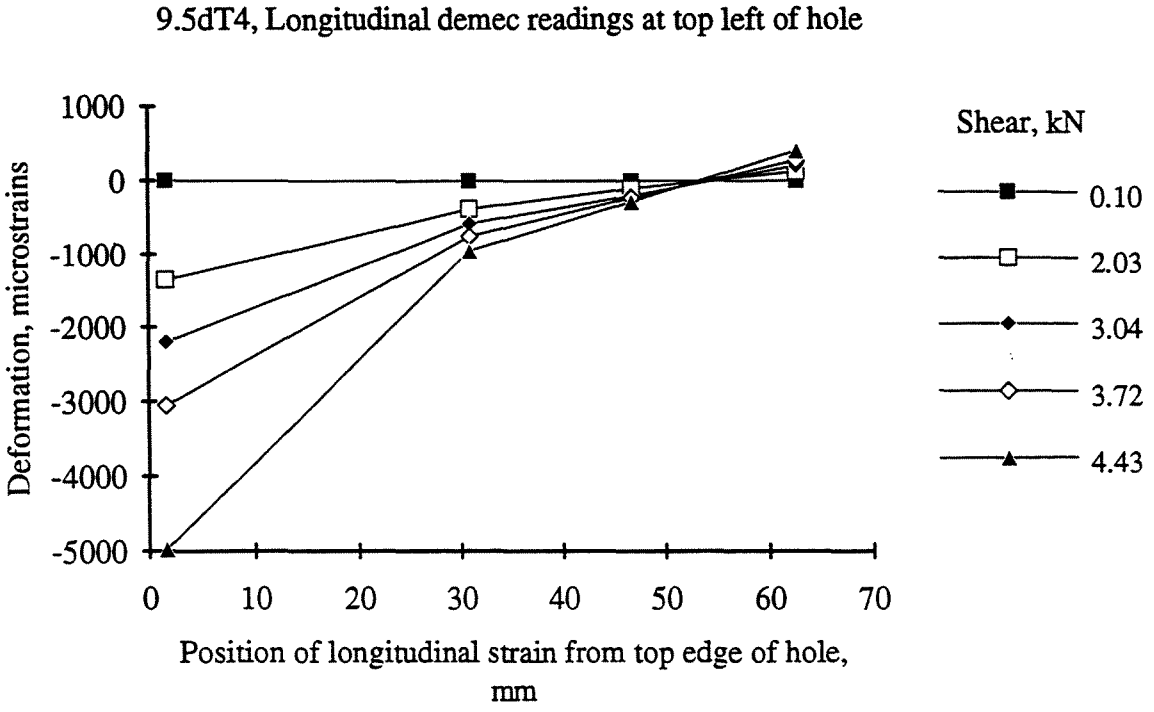

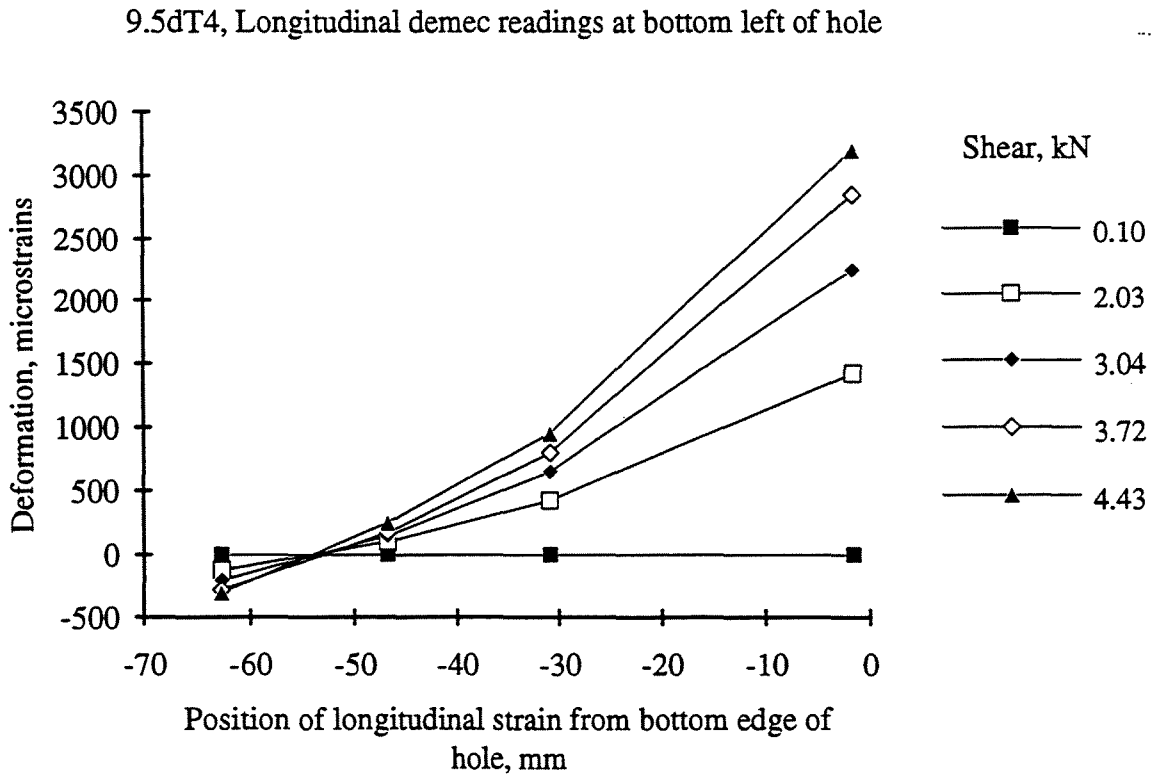

Figure 5.14. Longitudinal strain at the left section of the hole in specimen 9.5dT4

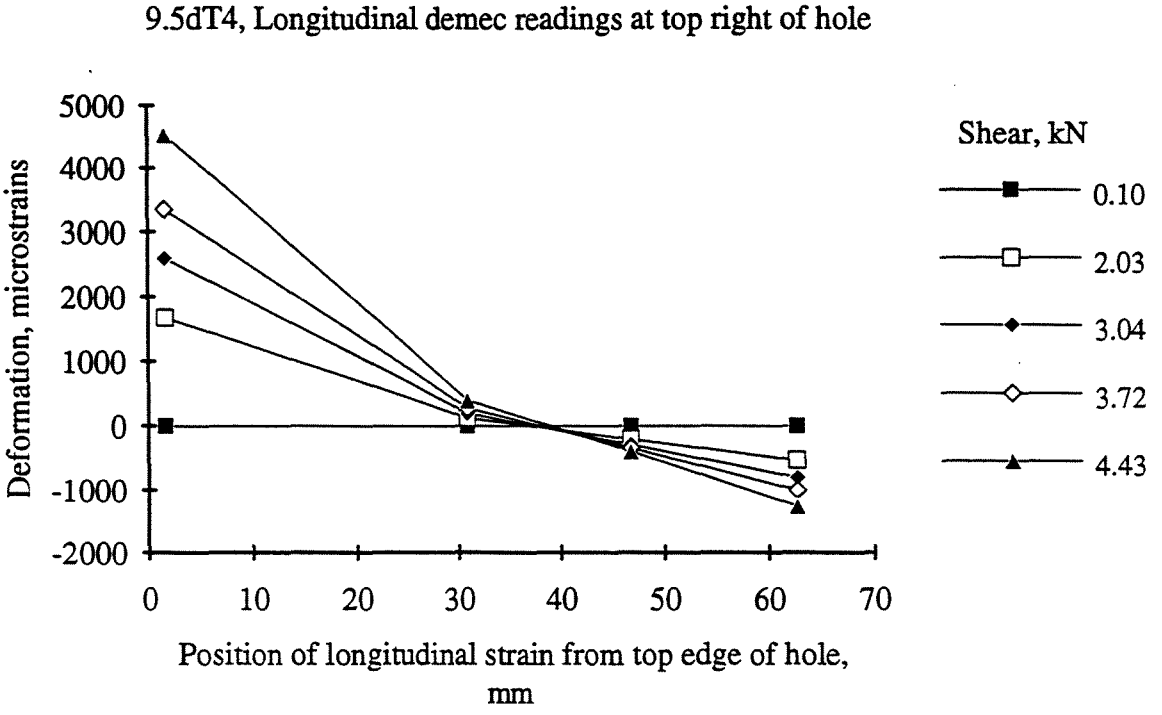

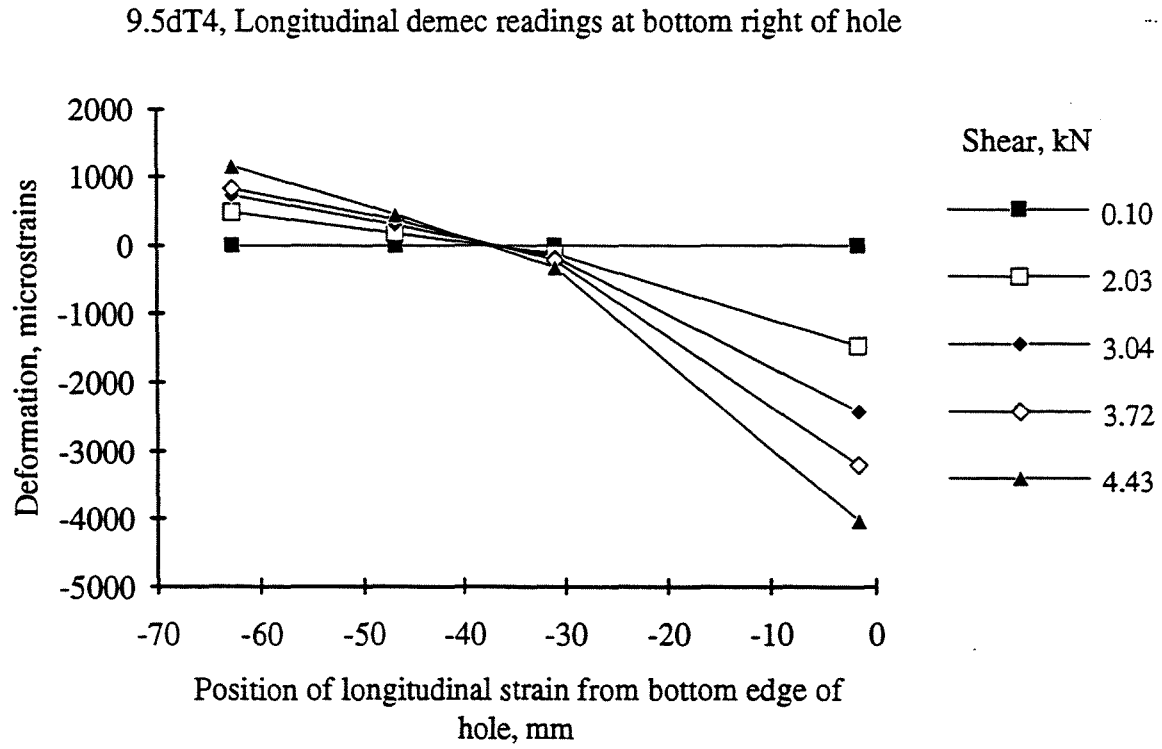

Figure 5.15. Longitudinal strain at the right section of the hole in specimen 9.5dT4

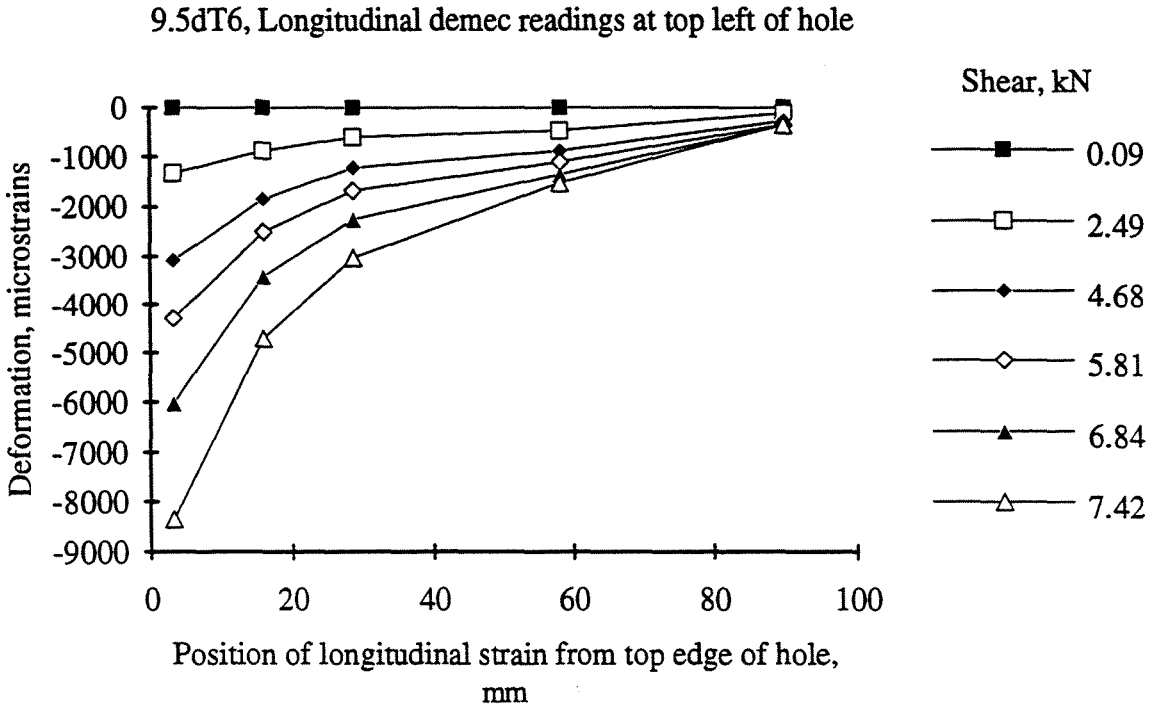

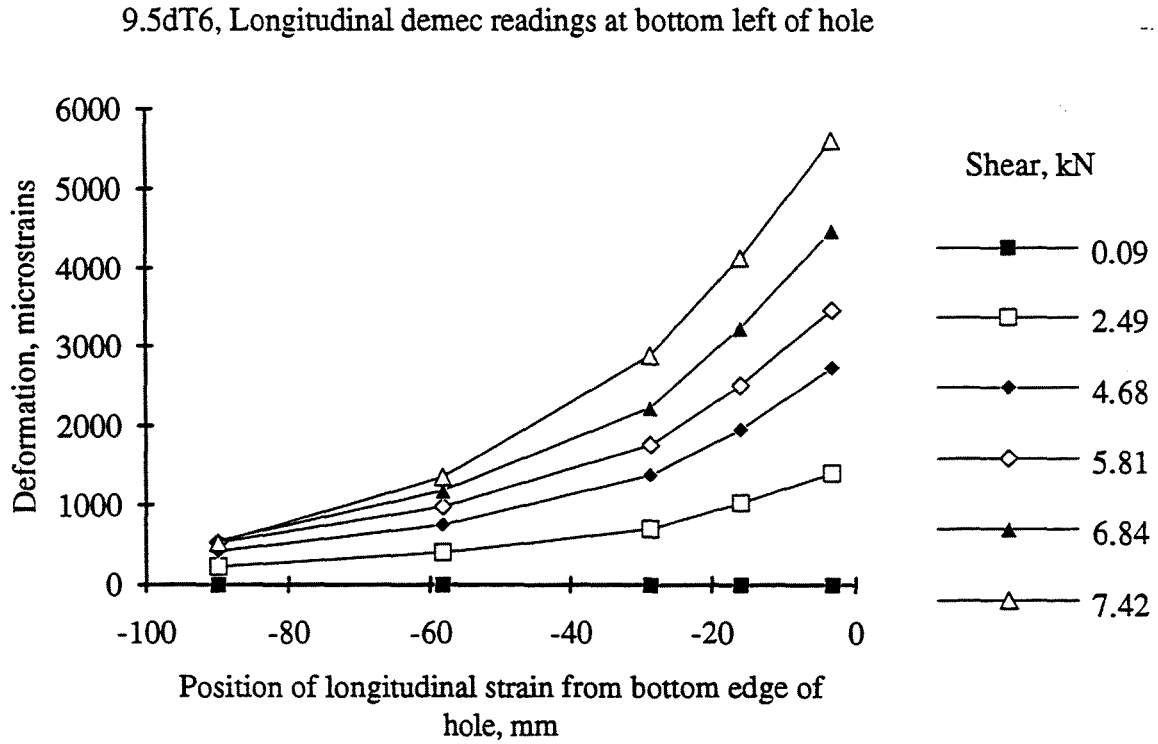

Figure 5.16. Longitudinal strain at the left section of the hole in specimen 9.5dT6

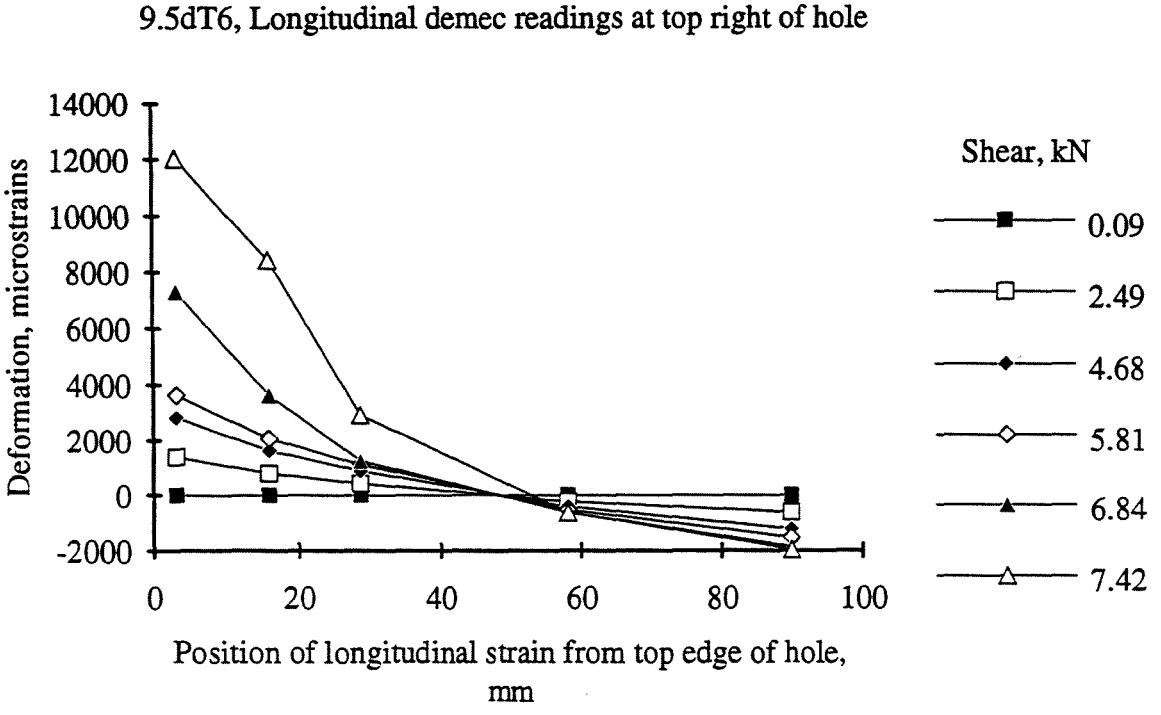

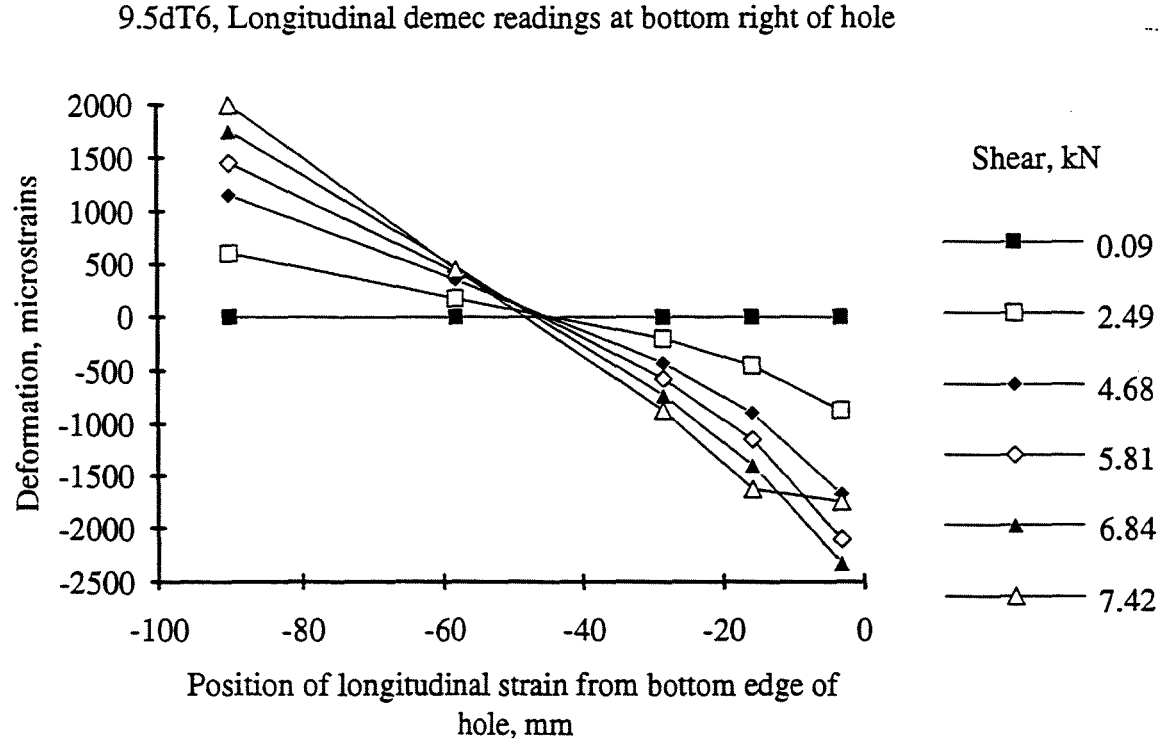

Figure 5.17. Longitudinal strain at the right section of the hole in specimen 9.5dT6

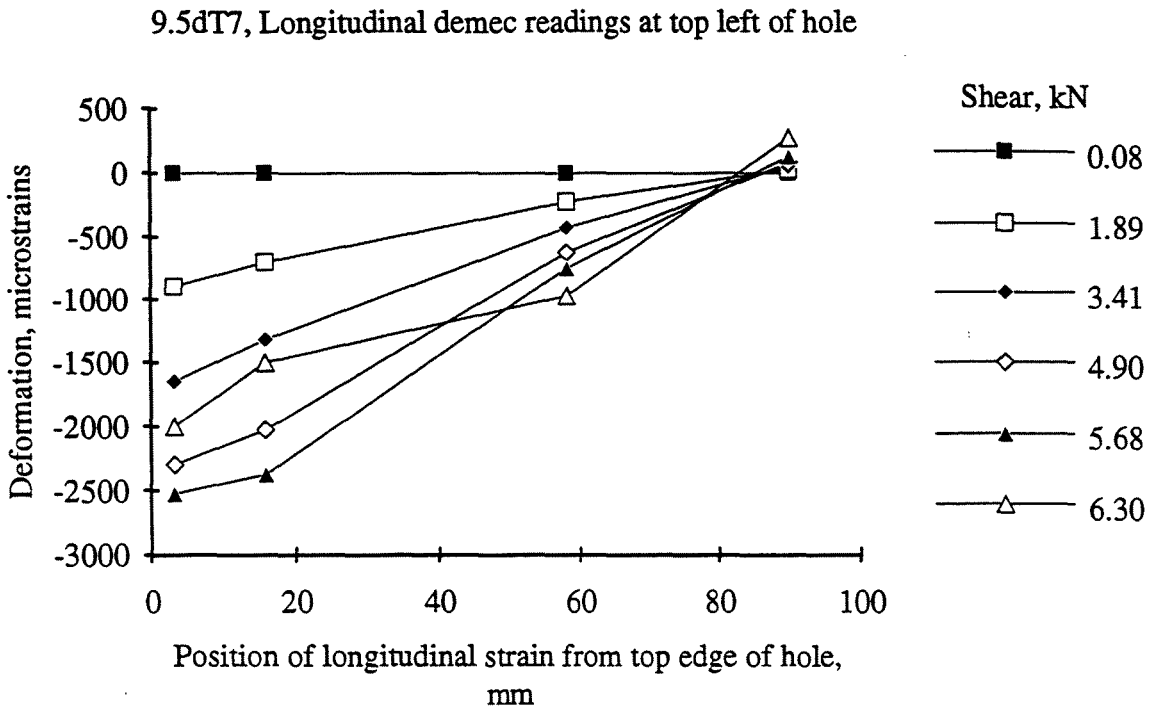

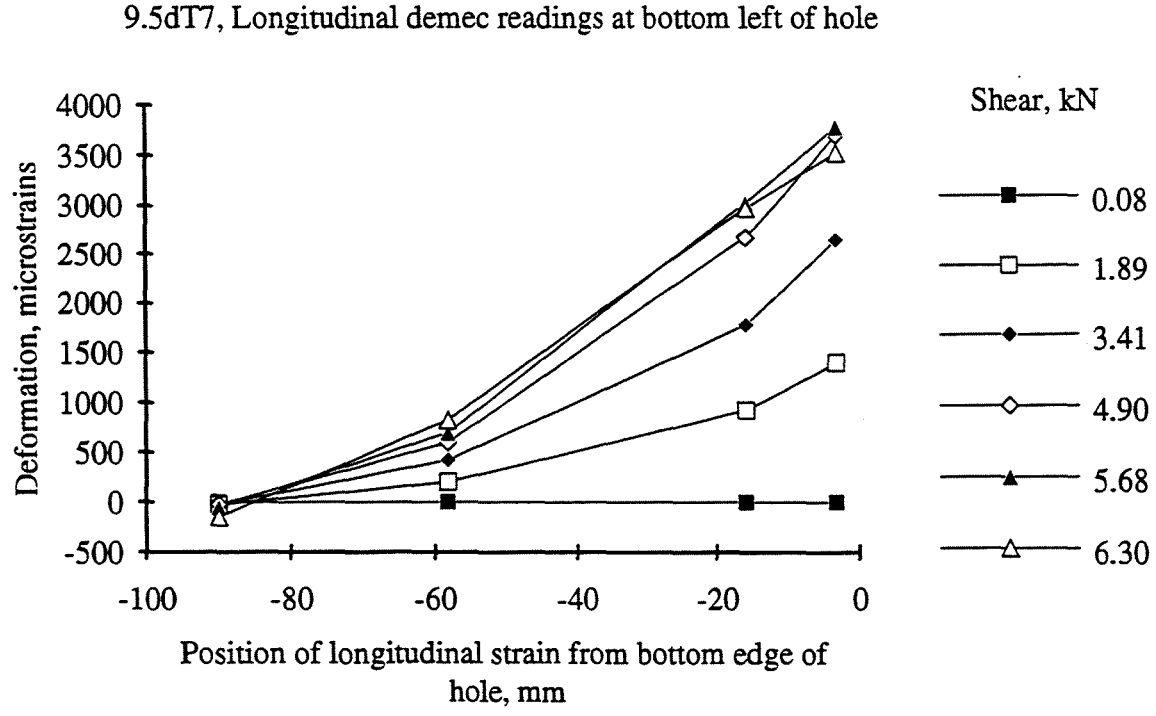

Figure 5.18. Longitudinal strain at the left section of the hole in specimen 9.5dT7

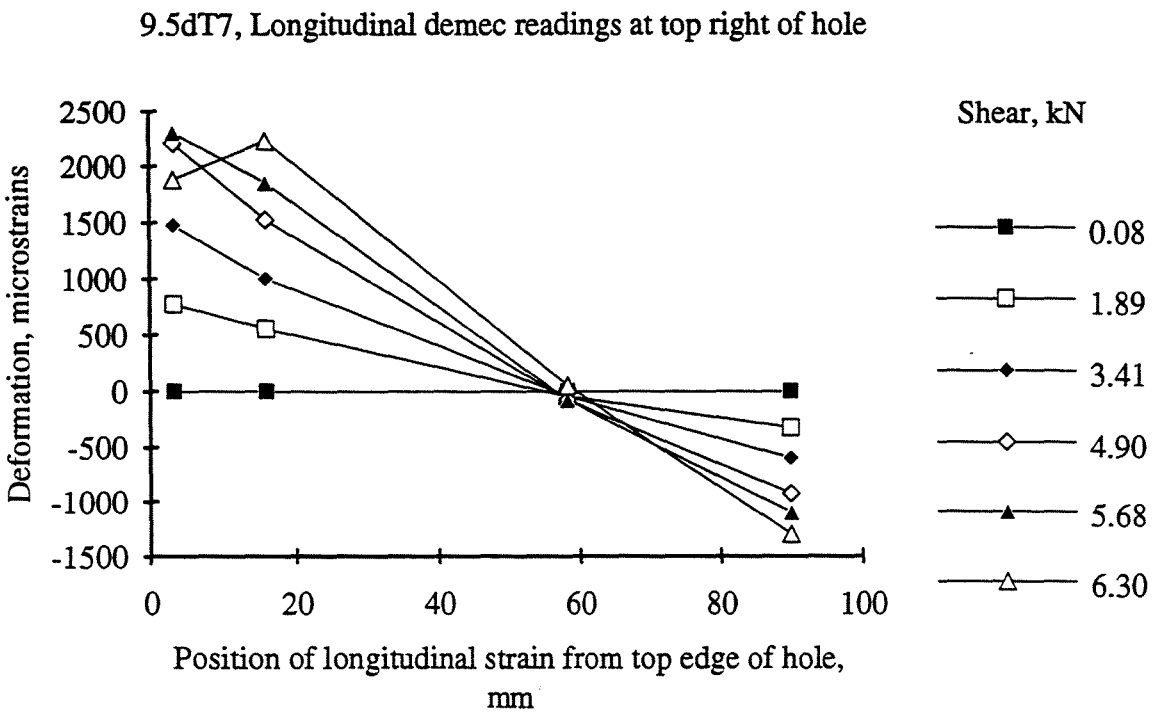

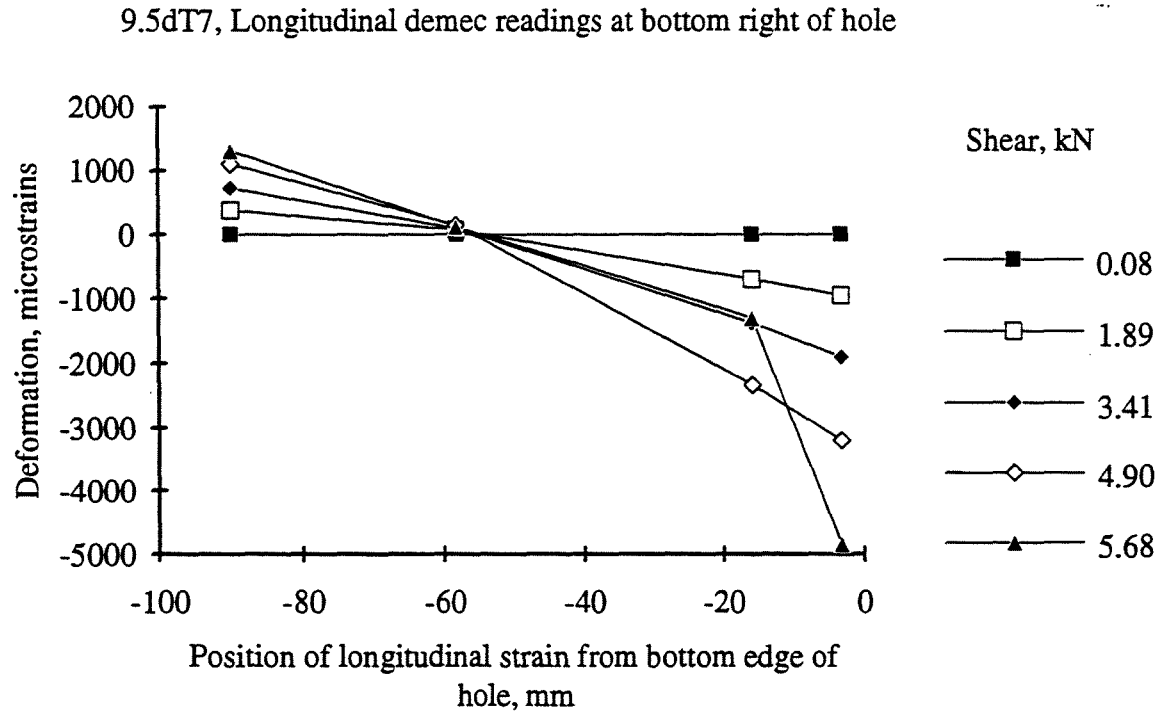

Figure 5.19. Longitudinal strain at the right section of the hole in specimen 9.5dT7

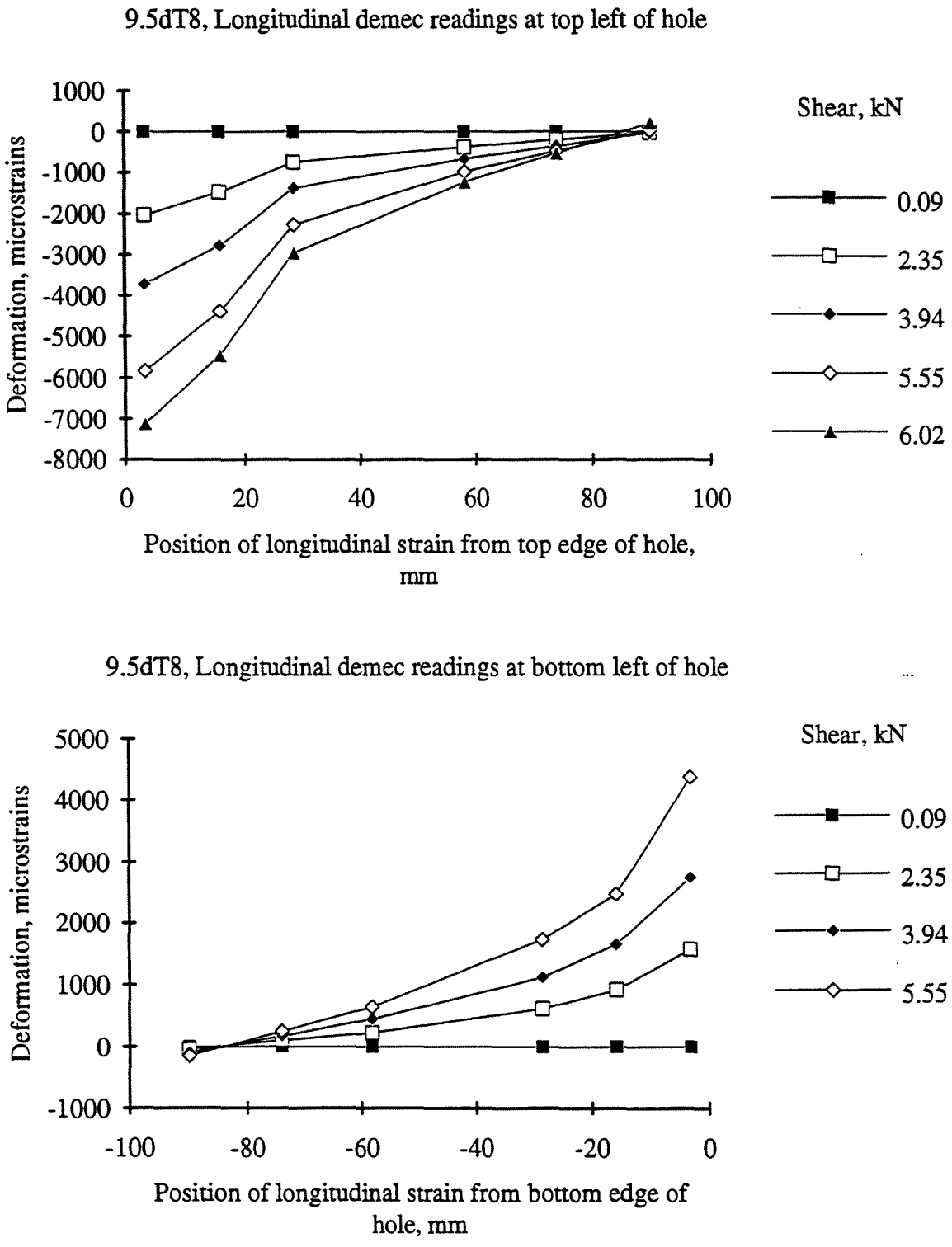

Figure 5.20. Longitudinal strain at the left section of the hole in specimen 9.5dT8

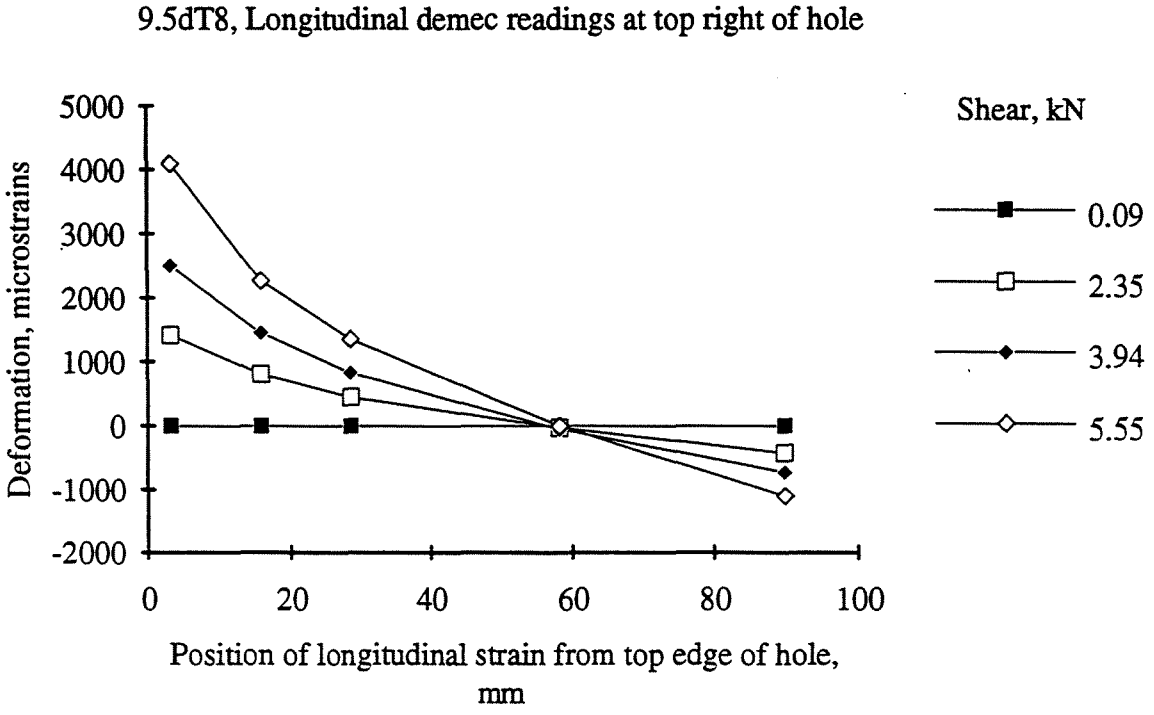

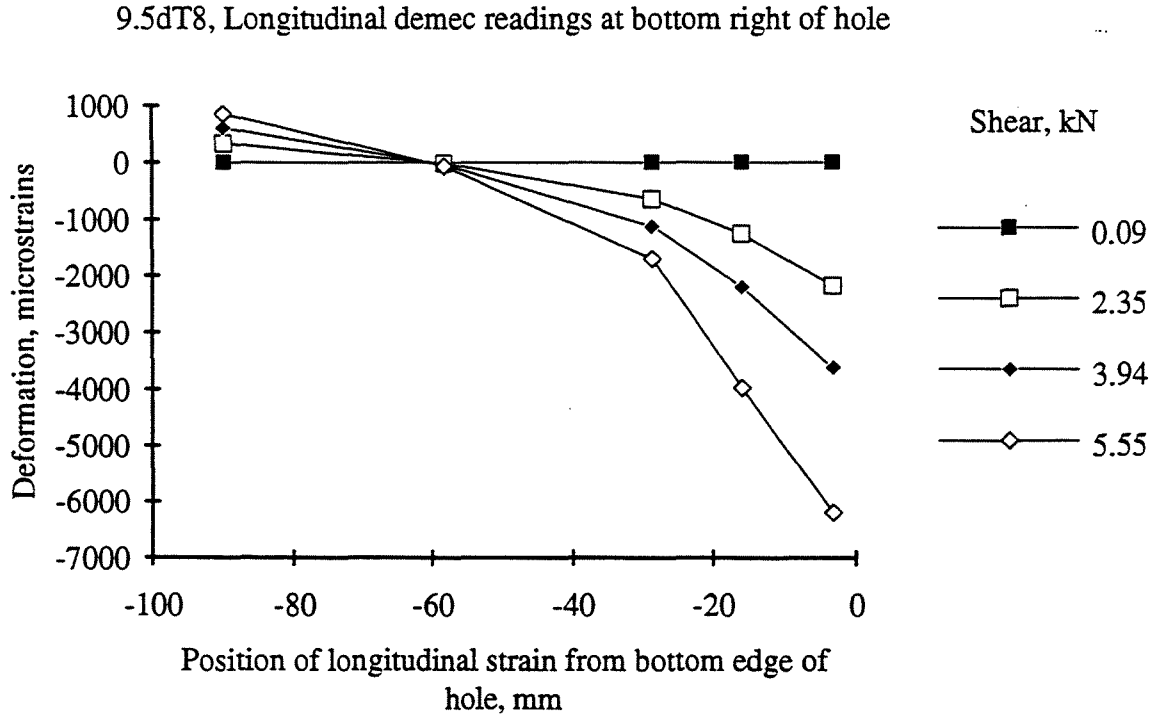

Figure 5.21. Longitudinal strain at the right section of the hole in specimen 9.5dT8

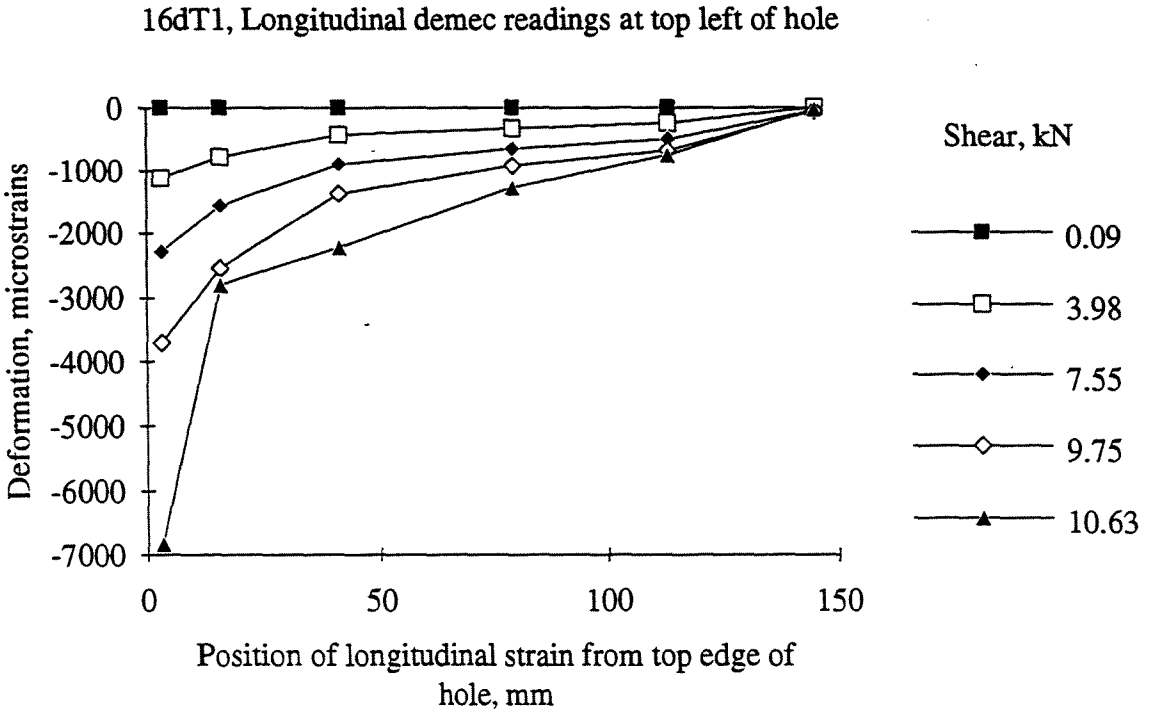

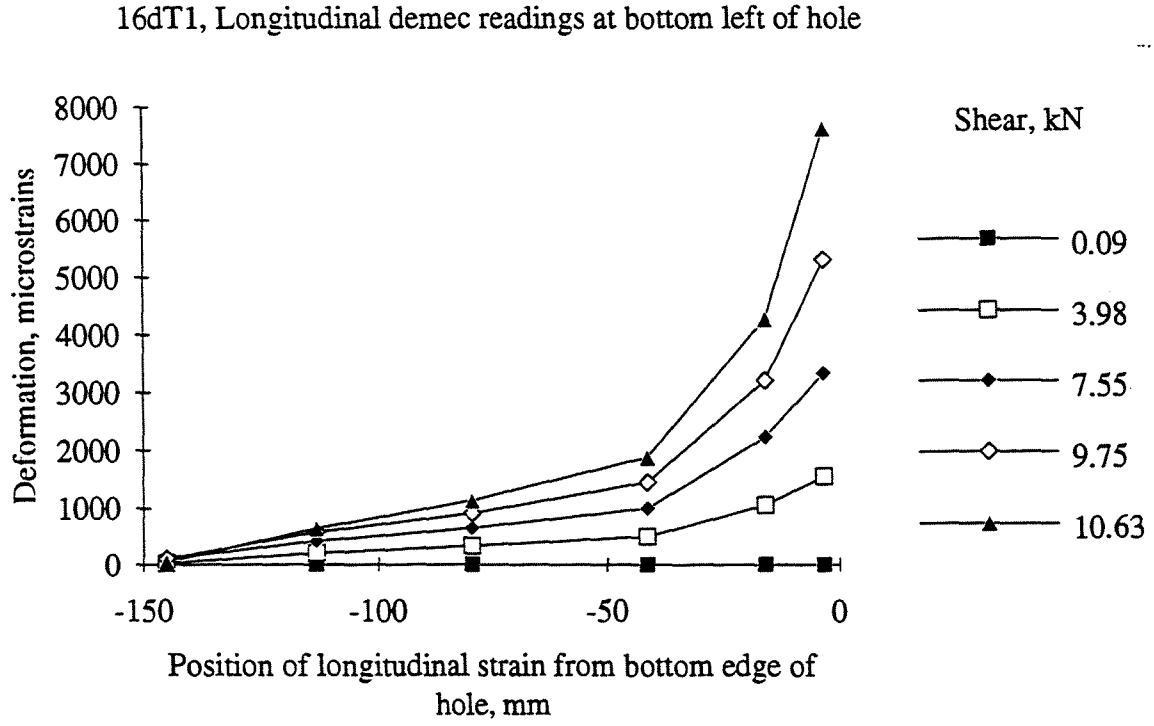

Figure 5.22. Longitudinal strain at the left section of the hole in specimen 16dT1

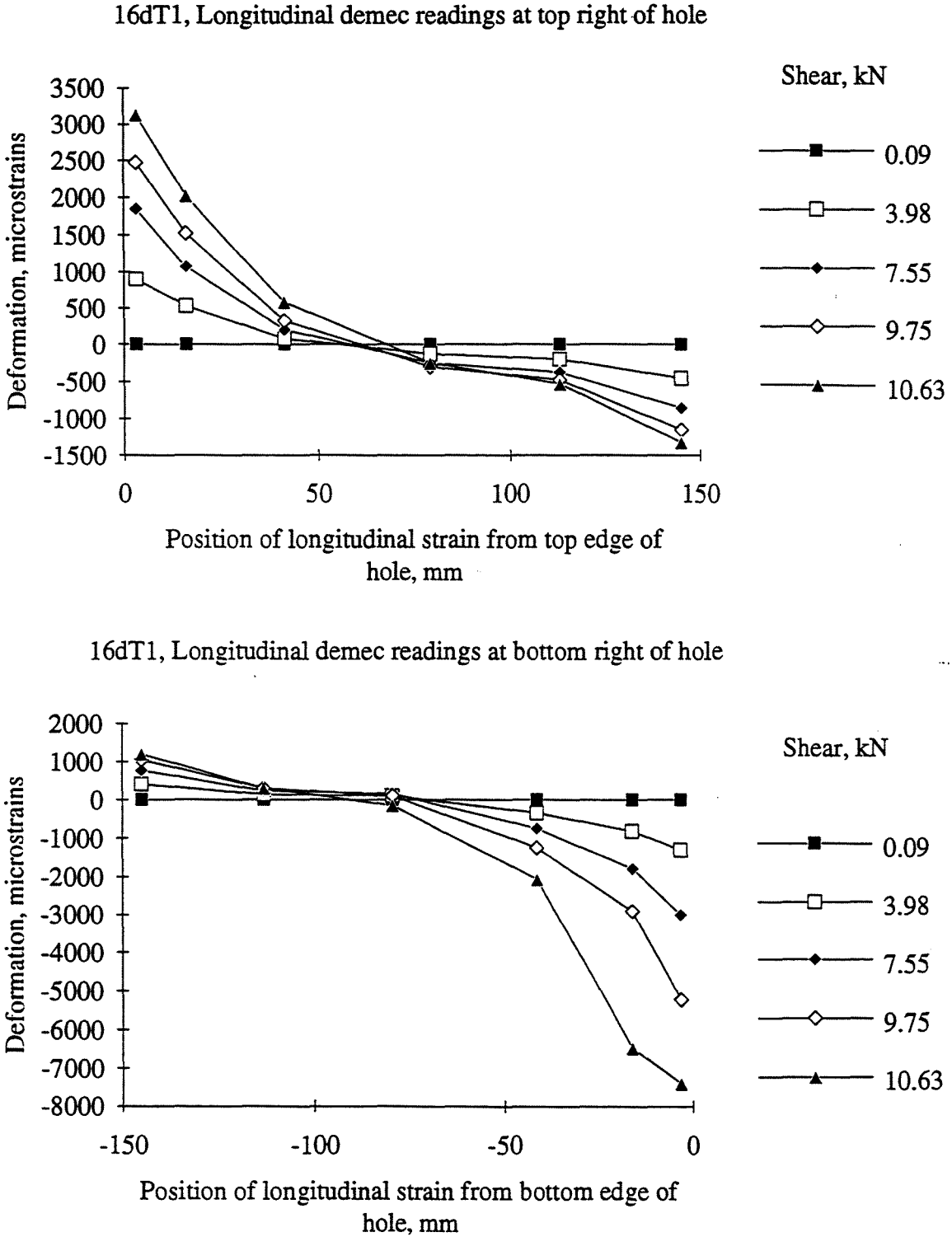

Figure 5.23. Longitudinal strain at the right section of the hole in specimen 16dT1

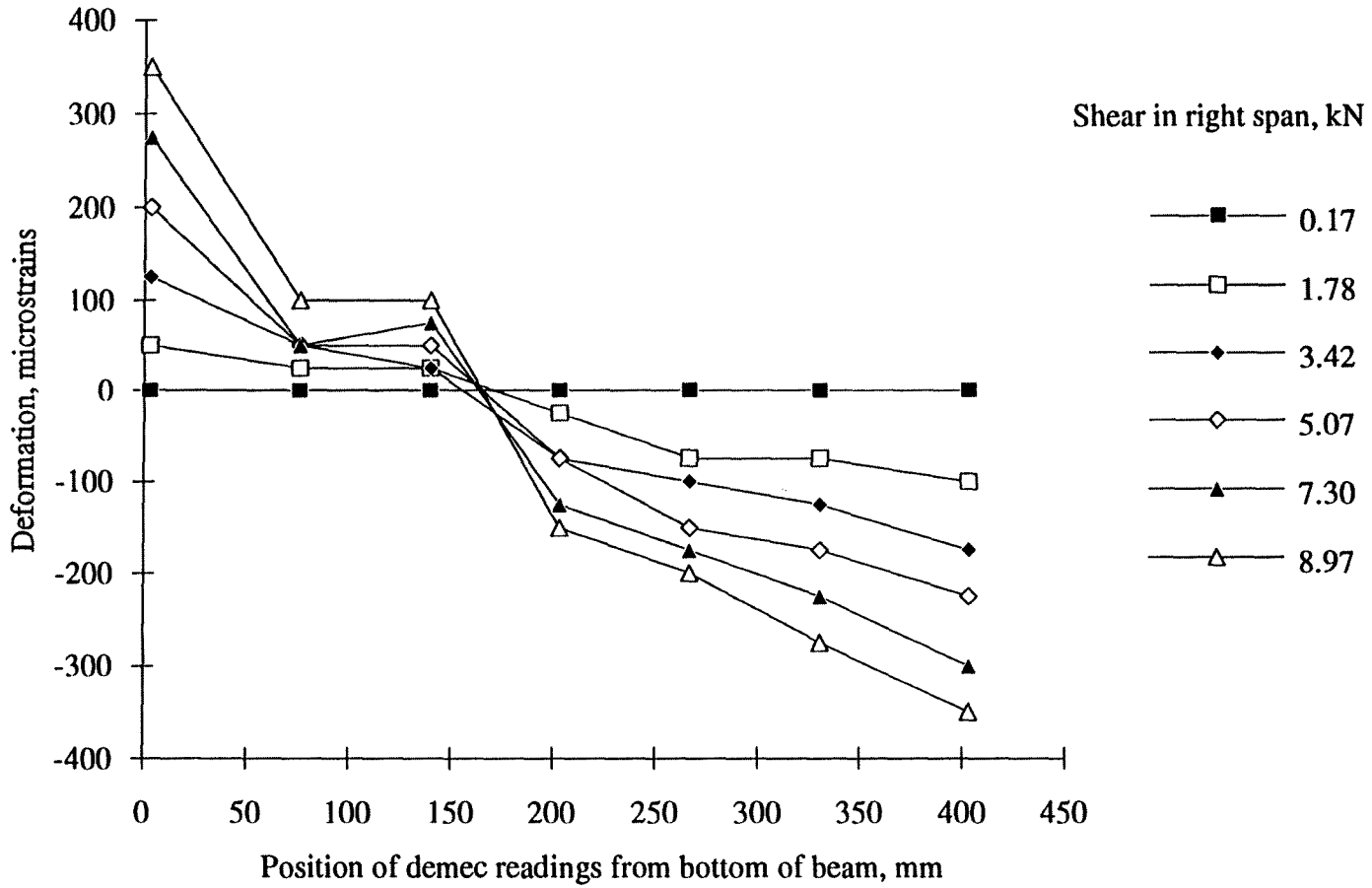

Figure 5.24. Longitudinal strain distribution of specimen 16dT1 at 520 mm from right reaction

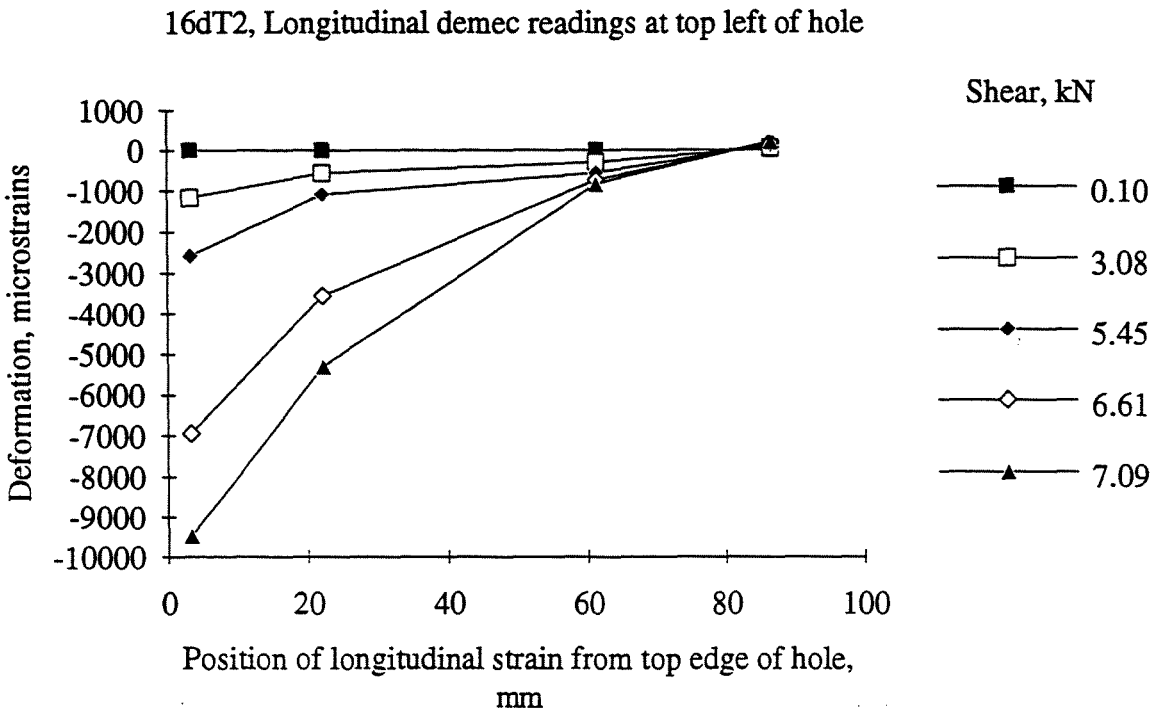

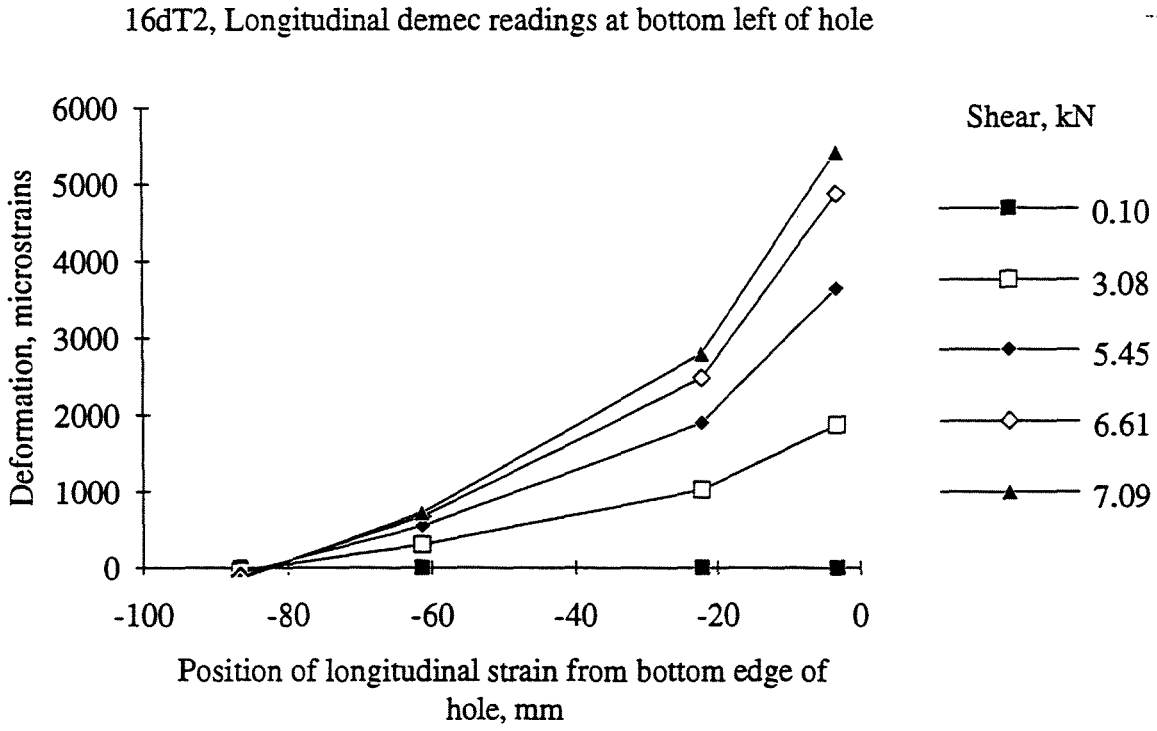

Figure 5.25. Longitudinal strain at the left section of the hole in specimen 16dT2

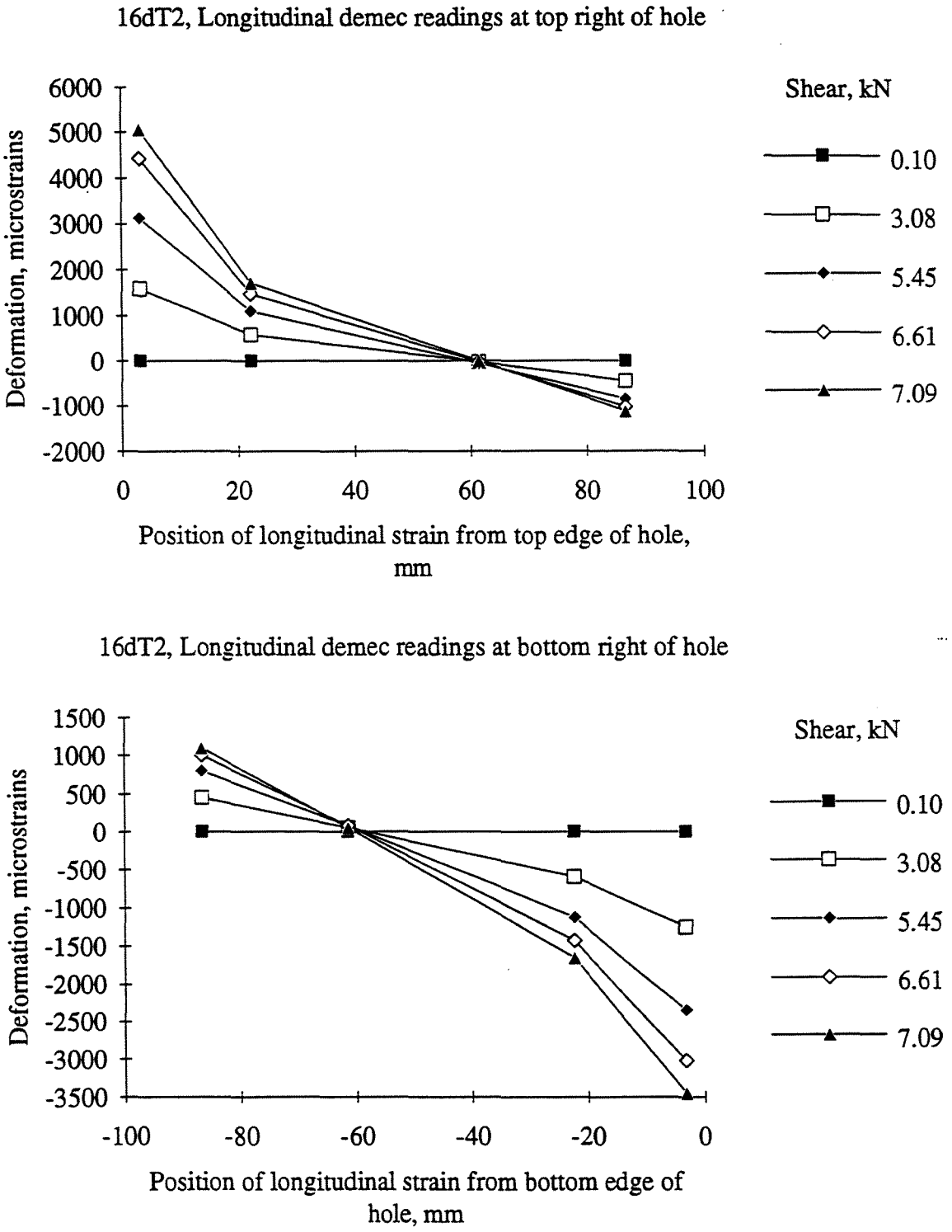

Figure 5.26. Longitudinal strain at the right section of the hole in specimen 16dT2

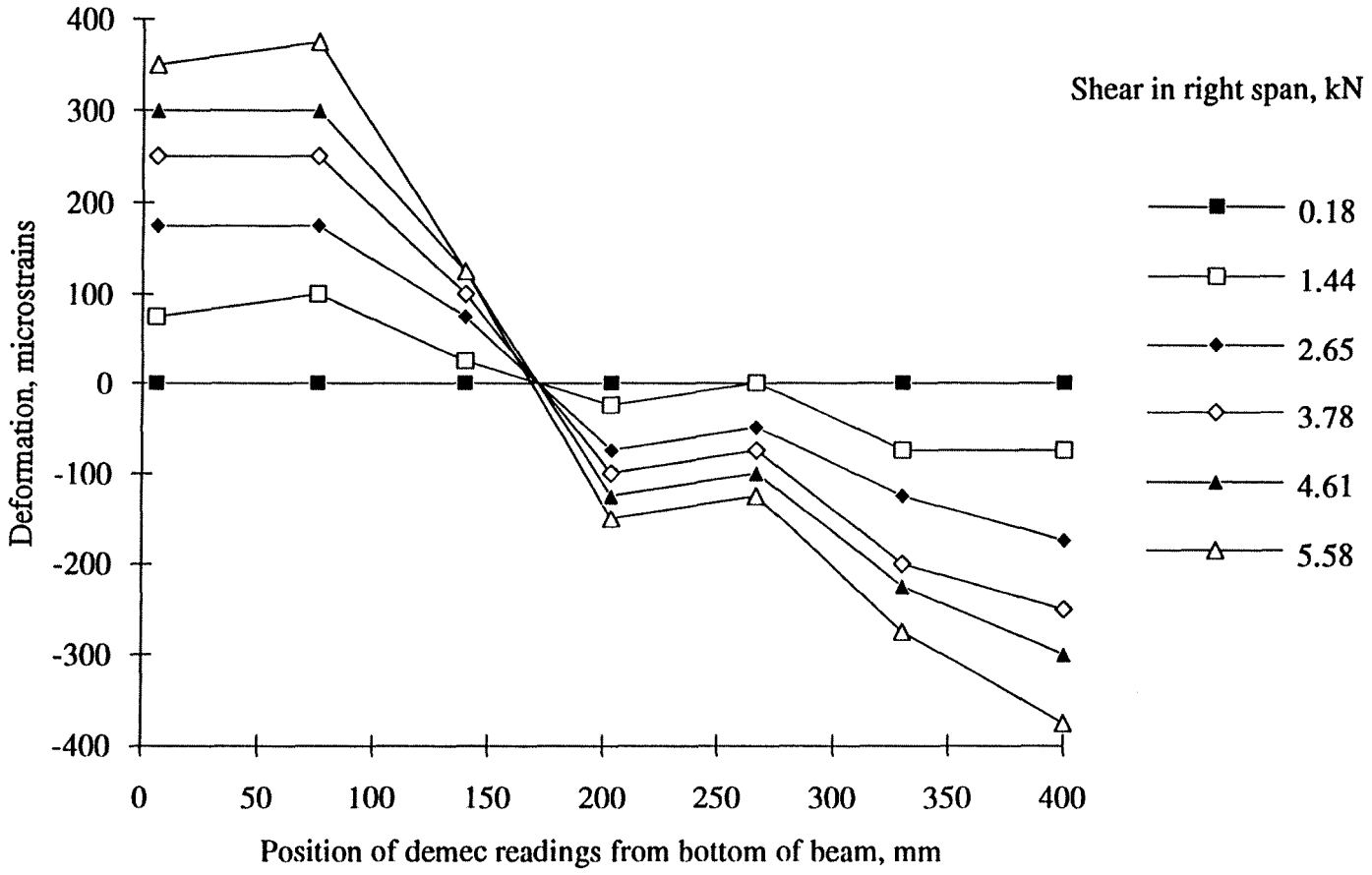

Figure 5.27. Longitudinal strain distribution of specimen 16dT2 at 725 mm from right reaction

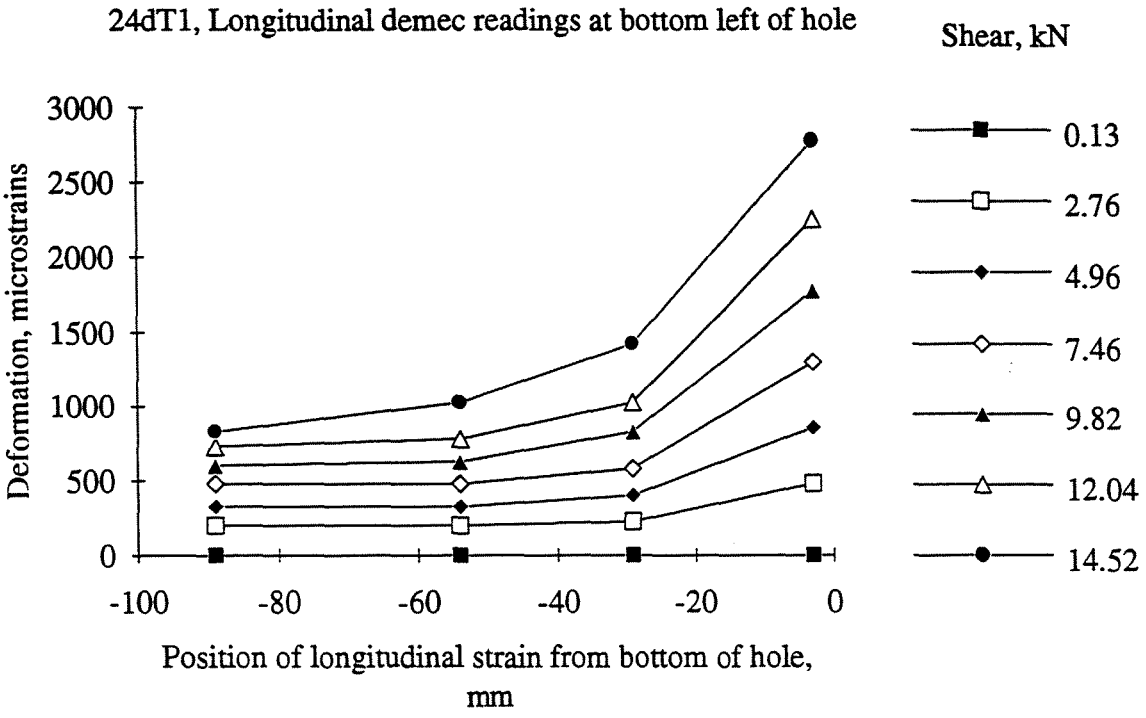

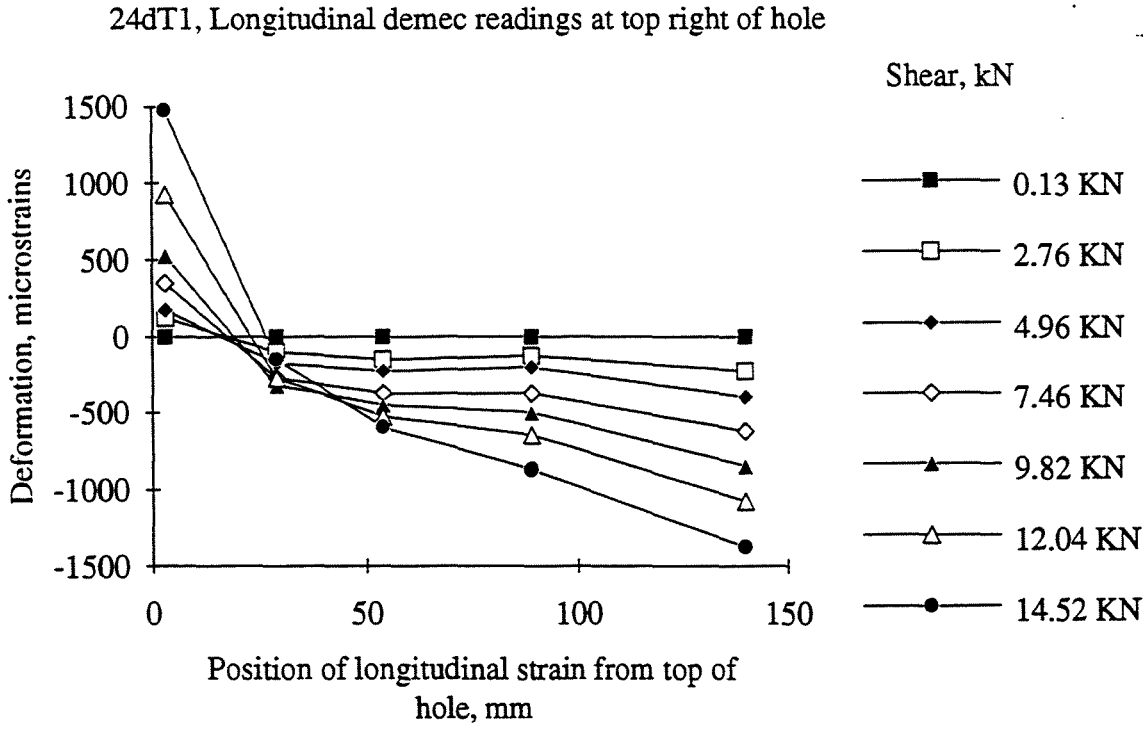

Figure 5.28. Longitudinal strains at the corners of specimen 24dT1

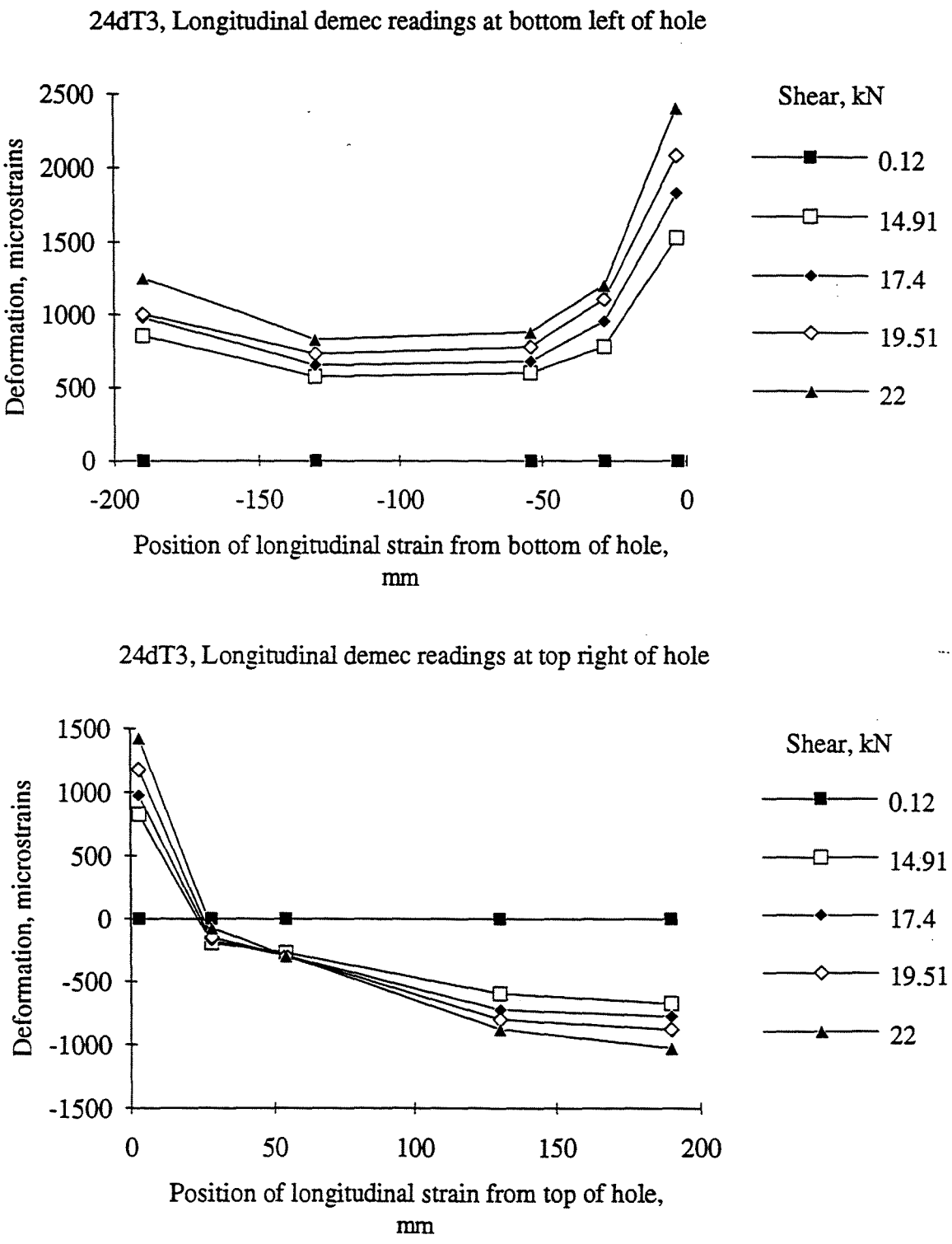

Figure 5.29. Longitudinal strains at the corners of specimen 24dT3

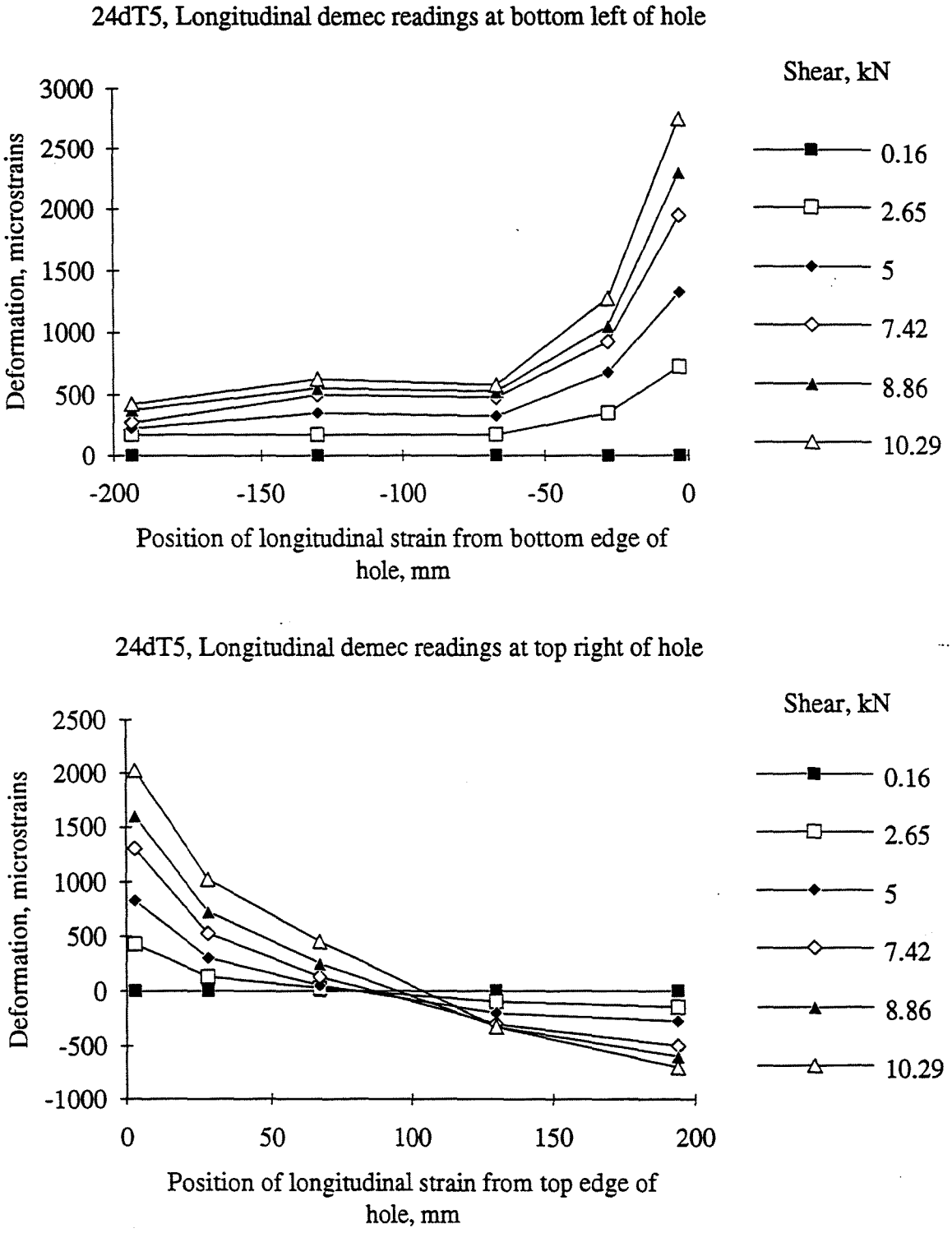

Figure 5.30. Longitudinal strains at thecorners of specimen 24dT5

5.3 Effect of Corner Radius and Shear Span

Rectangular holes with rounded corners are rare in construction practice so the effect of a sharp corner was investigated. The results showed that the corner radius had little effect on the overall behaviour and shear strength of the beams. Figure 5.8 shows that the square corner detail had a 6% shear strength reduction compared to the 25 mm radius corner detail. The slope of the shear versus deflection curves in Figure 5.4 show that all three beams had approximately the same stiffness. The effect of the corner radius can be seen by comparing the longitudinal strain distributions for specimens 9.5dT3 and 9.5dT8 in Figures 5.12, 5.13, 5.20, and 5.21. Specimens 9.5dT3 and 9.5dT8 had the same hole size, but the corner details varied with a 25 mm radius and a 12 mm radius, respectively. Specimen 9.5dT8, which had a 12 mm radius corner, exhibited larger strains near the corner of the hole when compared with specimen 9.5dT3. The longitudinal distribution at the corners of specimen 9.5dT7 (Figures 5.18 and 5.19), which had a square corner, were fairly linear. Near the edge of the hole, the strains were not as large as the strains in specimens 9.5dT3 and 9.5dT8. The reason is that the tension fracture line, which occurred at the tension corners of the hole, and the compression crushing line, which occurred at the compression corners of the hole, did not run across the gage length of the demec gage. The strain distribution in specimens 9.5dT3 and 9.5dT8 curved near the edge of the hole because the tension crack line or the compression crushing line initiated at the corners of the hole and grew in length and width towards the flanges of the beam. The demec gage not only measured the linear deformations due to stresses across the gage length, but also measured the growth of a tension crack line or a compression crushing line. The tension cracking or compression crushing explains why such large deformations over 12 000 microstrains can be reached by some specimens.

The effect of increasing the shear span is shown in Figure 5.8. Specimens 9.5dT3 and 9.5dT6 had the same hole geometry except the shear span was increased from 1000 mm to 1500 mm, respectively. Figures 5.12, 5.13, 5.16, and 5.17 show the shifting of the longitudinal strain distribution due to the increased bending stresses from the increased moment arm. The bending stresses cause the longitudinal strains at the left corner of the hole to increase while the longitudinal strains at the right corners of the hole decrease. The increase in bending stresses results in a shear strength increase of 19% from 6.7 kN to 8.0 kN.

5.4 Indications of Failure Modes

5.4.1 Overall Behaviour

All beams with web openings deformed similarly. Initially, the web hole is rectangular. Under load, the web hole deforms into a parallelogram. The obtuse angle corners of the hole, always the top right and bottom left corners, undergo tensile strains while the acute angle corners, the top left and bottom right corners, undergo compressive strains. However, although all web openings deformed similarly, the way in which each beam failed was classified into three categories based on the visual observations of the failure. The categories were the web/flange connection failed, the corners overstrained, and the web buckled. The reference beams with no holes failed in a variety of ways including a bearing/stiffener failure, a tension chord fracture, a web splice fracture, lateral-torsional buckling, and compression chord crushing. Tables 5.1, 5.2, and 5.3 summarize the observed failures for each beam tested.

Table 5.1. 610 mm beam test results

specimen	max. shear, V_{max}, (kN)	max. shear, $\%V_o$	visual indications of failure
24dT1	15.8	52.8	corners of hole failed
24dT2	22.9	76.6	bearing failure at load point
24dT3	28.8	96.3	web buckled and corners failed
24dT4	21.9	73.2	lateral torsional buckling (no hole)
24dT5	14.0	46.8	corners of hole failed
24dT6	6.3	21.1	web pulled out of flange
24dT7	29.9	100	compression chord crushed (no hole)

Note: shear span = 1808 mm (3d) and V_o = max. shear of reference beam 24dT7

Table 5.2. 241 mm beam test results

specimen	max. shear, V_{max}, (kN)	max. shear, $\%V_o$*	visual indications of failure
9.5dT1	10.4	74	corners of hole failed
9.5dT2	14.0	100	fracture at web splice (no hole)
9.5dT3	6.7	48	corners of hole failed
9.5dT4	5.1	36	corners of hole failed
9.5dT5	3.8	27	web pulled out of flange
9.5dT6	8.0	57	corners of hole failed
9.5dT7	6.3	45	corners of hole failed
9.5dT8	6.3	45	corners of hole failed

Note: all shear spans = 1000 mm (4.1d) except specimen 9.5dT6 has a shear span = 1500 mm (6.2d)

* specimen 9.5dT2 is used as a reference for maximum shear, V_o

Table 5.3. 406 mm beam test results

specimen	max. shear, V_{max}, (kN)	max. shear, $\%V_o$	visual indications of failure
16dT1	11.8	57.6	corners of hole failed
16dT2	7.9	38.5	corners of hole failed
16dT3	20.5	100	tension chord fractured (no hole)

Note: shear span = 1250 mm (3.1d) and V_o = max. shear of reference beam 16dT3

5.4.2 Web/Flange Connection

The tensile forces were easily seen in action at the top right and bottom left "tension corners" of the hole when the height of the hole equaled the full height of the web. Specimens 9.5dT5 and 24dT6 had this hole geometry. As the beam was loaded, the tension corners of the hole developed high tensile strains perpendicular to the flanges of the wood I-beam. The beam deformed to a point where OSB web strands, embedded and glued into the flange lumber, failed in shear next to the web/flange glueline. The web slowly pulled out of the flange as the beam neared its maximum shear strength. Figures 5.1 and 5.3 show how the stiffness of the beam was reduced as the web pulled out of the flange until failure occurred. Figure 5.31 shows the web pulling out of the flange.

Figure 5.31. Web/flange connection failure in specimen 9.5dT5

5.4.3 Corners Overstrained

Another indication of failure was OSB fibers breaking at the corners of the hole. In Figures 5.32 and 5.33, the shear versus 45° reading (deformation) curve of each hole corner was plotted together according to the location of the corner. Almost all of the demec readings included the crack line formed at the tension corners and the crushing line formed at the compression corners. The development of crack growth or crushing can be seen on the shear versus deformation curves. Crack growth initiated when the shear versus deformation curve became non-linear. In the tension corners, cracking started at approximately 3000 to 4000 microstrains. In the compression corners, crushing also occurred at approximately 3000 o 4000 microstrains. Tension cracking and compression crushing of the OSB fibers can be seen in specimen 16dT1 in Figures 5.34 and 5.35

The longitudinal deformations through the cross section of the beam at the ends of the hole also confirmed that large strains due to fibers breaking occurred at the corners of the hole. Figures 5.12 and 5.13 show the longitudinal strain distribution through the depth of the beam of specimen 9.5dT3. These corner deformations indicated that when the wood fibers at the corners reach a certain value of strain, failure occurred. The almost linear longitudinal strain distribution suggested that a Vierendeel analysis could be used to predict the failure stress. Therefore, if the strain corresponding to a stress can be predicted at the corners of the hole, the maximum shear strength can be predicted as well.

Also, Figure 5.36 shows the overall profile of three test specimens as they deflect downward under a load causing a transverse shear force of 5.1 kN. Two of the specimens have a hole width of 305 mm and the third specimen does not have a hole. As the height of the hole increased the vertical displacement increased from one end of the hole to the other end. Similar behaviour occurred when the length of the hole increased. The deflected shape of the prismatic "T" sections of the beam above and below the hole were similar in shape to a Vierendeel frame where the "T" sections transfer shear forces from one end to another. Vierendeel action can be seen in Figure 5.37 which shows the deflected shape of specimen 9.5dT6.

However, the 45° demec readings of specimens 24dT1 and 24dT3 remained linear and did not exhibit breaking of fibers. Specimen 24dT1 reached a maximum shear of 15.5 kN and the last demec reading was taken at 14.5 kN. Only the top left corner shear versus deformation curve became non-linear, thus indicating fibers breaking. The top right and bottom left corner demecs did not include the tensile fractures which explains the absence of deformation on the shear versus deformation curves. The bottom right corner demec included the crushing line of OSB strands, but the shear versus deformation curve does not behave non-linearly. This means that failure was not initiated at the bottom right corner of the hole. Specimen 24dT3 shear versus 45° corner deformation curves also did not exhibit non-linear behaviour. The last demec reading taken was at 22 kN because web buckling occurred and failure was thought to be imminent. However, the beam failed at 28.8 kN. The demec readings at the bottom left and right corners did not exhibit fibers breaking even after the deformations reached 4500 and 5000 microstrains, respectively. Specimens 24dT1 and 24dT3 suggested a failure mode different from that initiated by Vierendeel truss action. Figure 5.29 shows the longitudinal deformations in specimen 24dT3. The nonlinear strain distribution indicated that Vierendeel truss action was not predominate in the hole geometry.

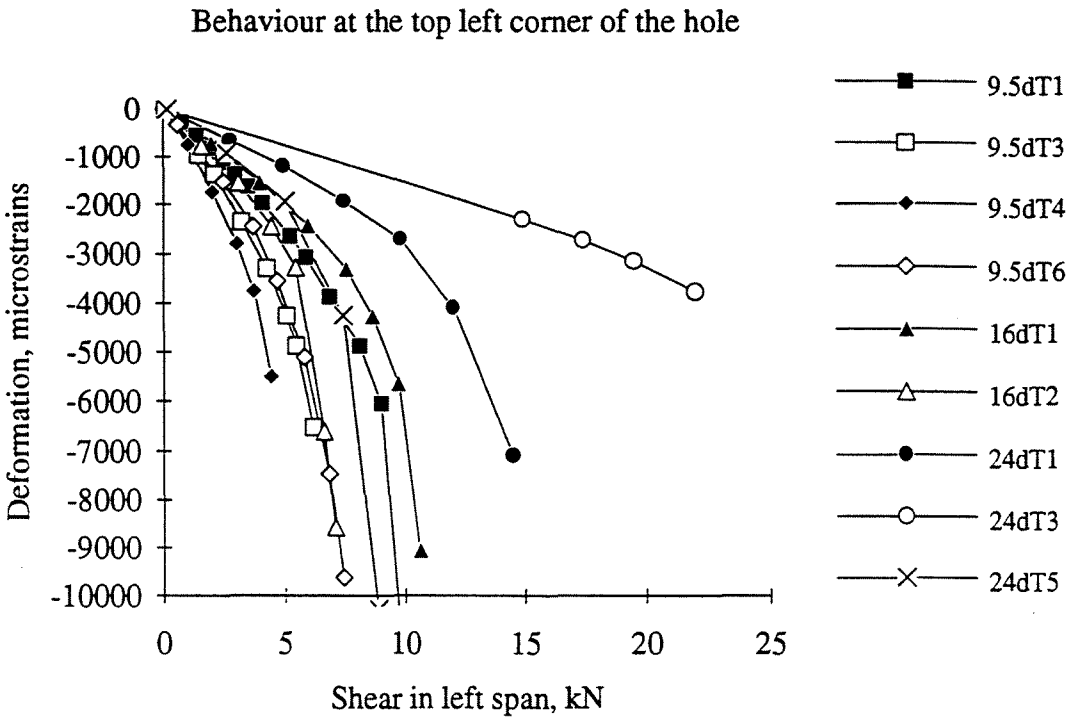

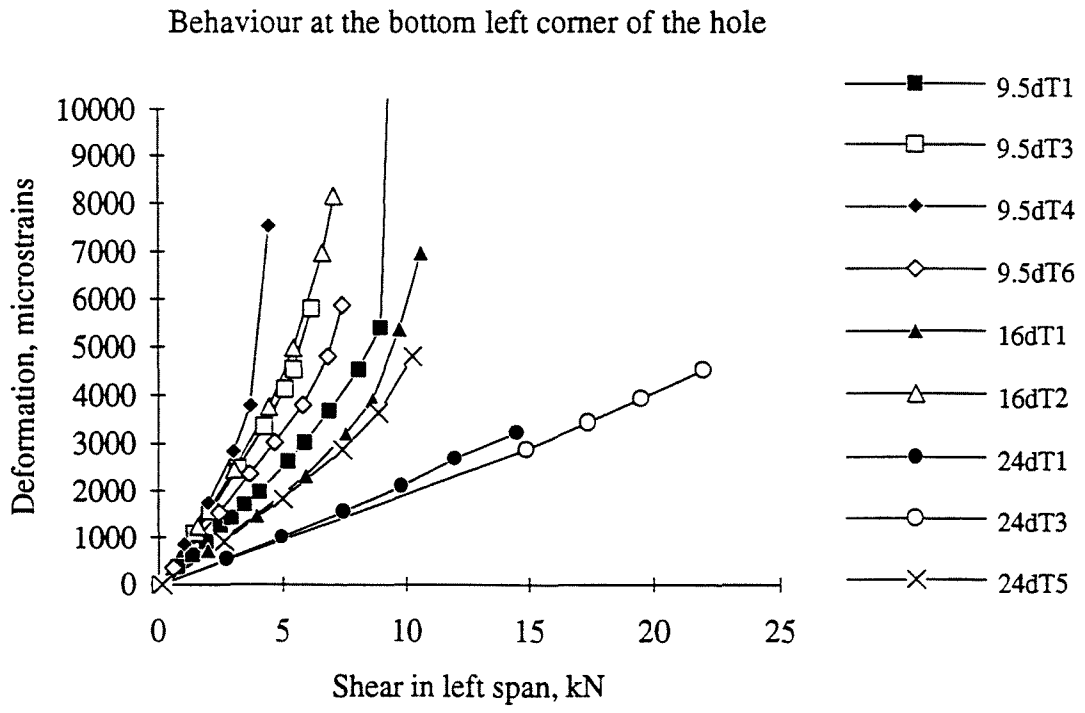

Figure 5.32. 45°demec readings at the left corners of the hole

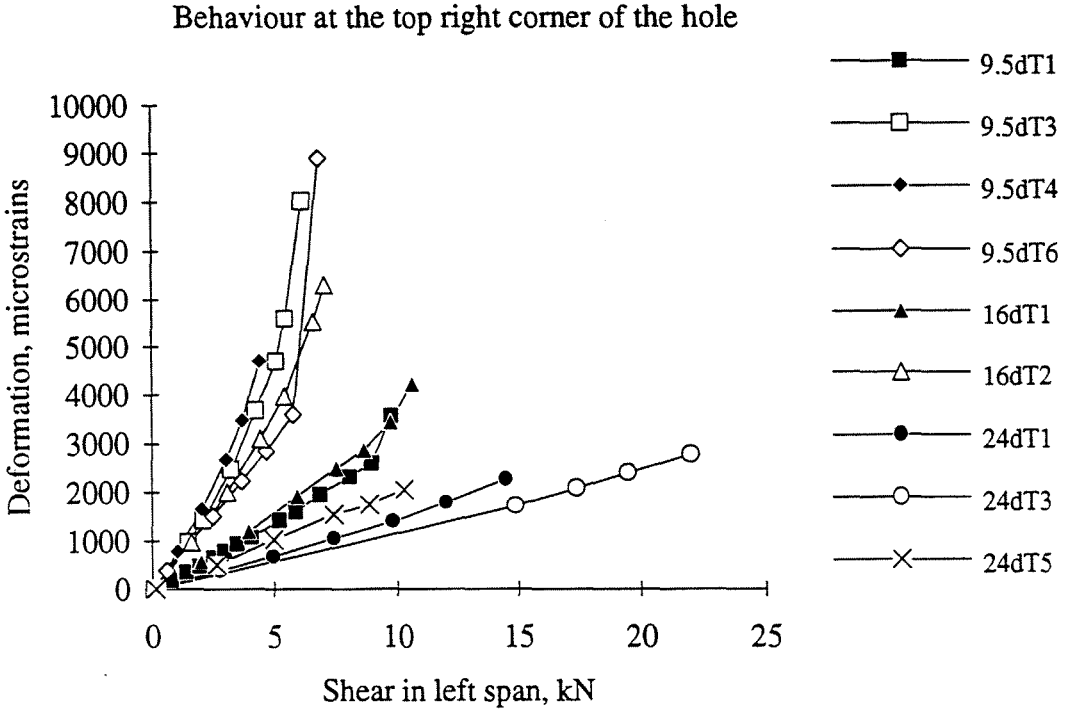

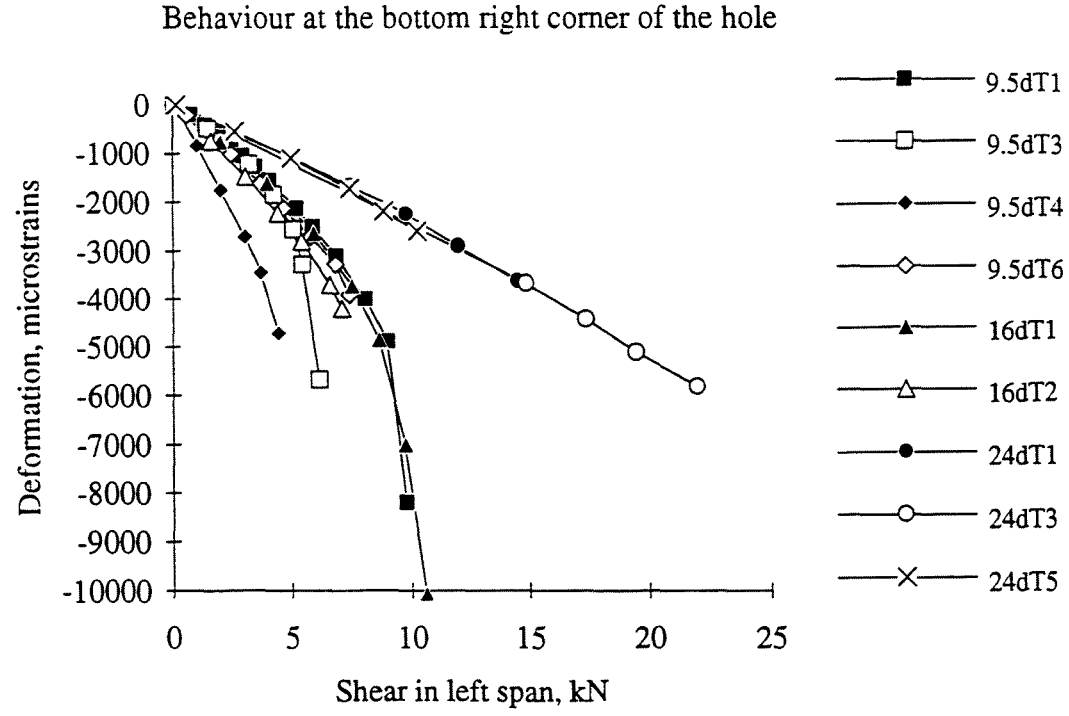

Figure 5.33. 45° demec readings at the right corners of the hole

Figure 5.34 Left corner failures in spec imen 16dT1

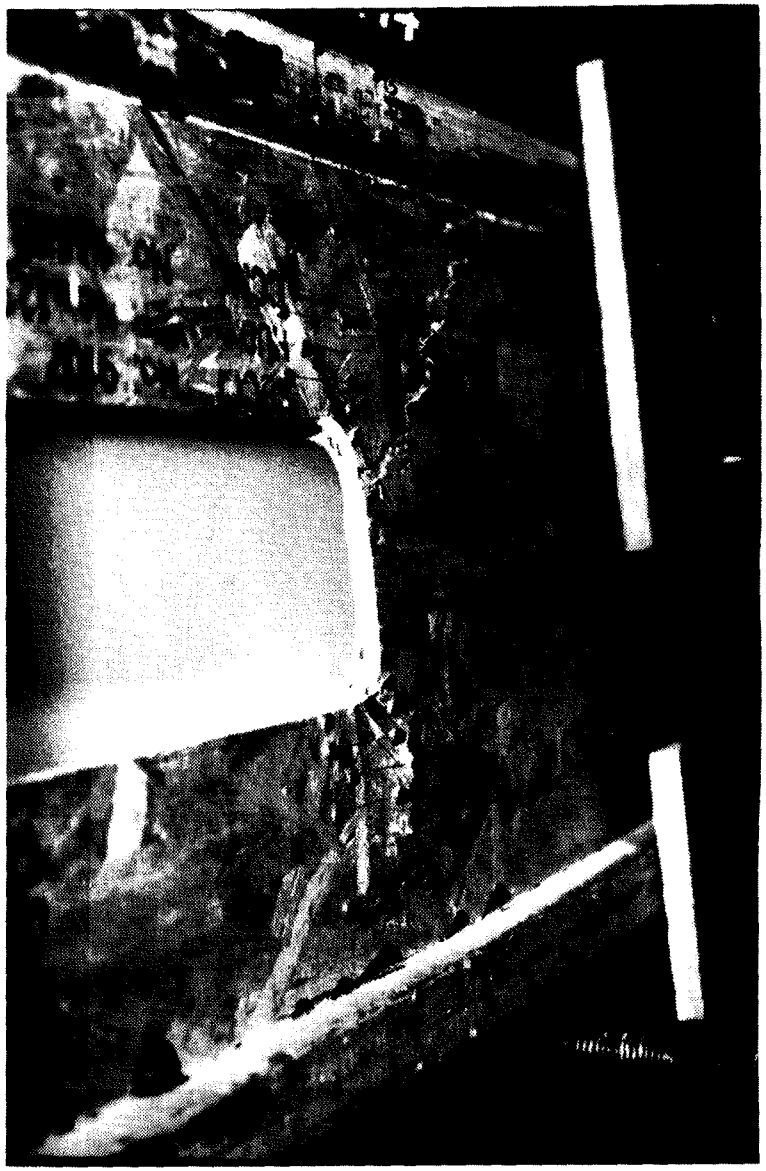

Figure 5.35 Right corner failures in specimen 16dT1

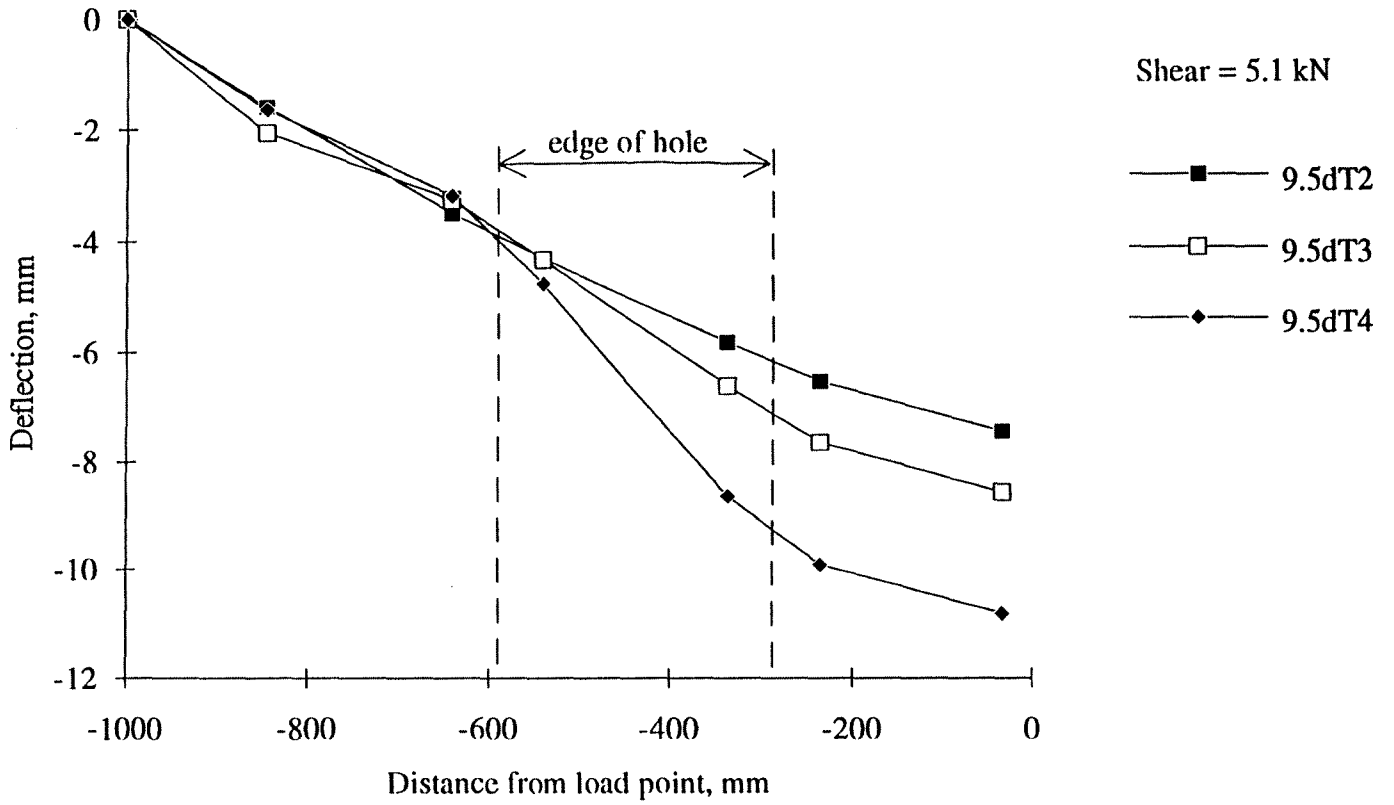

Figure 5.36. Profile of deflected shape of specimens 9.5dT2, 3, and 4

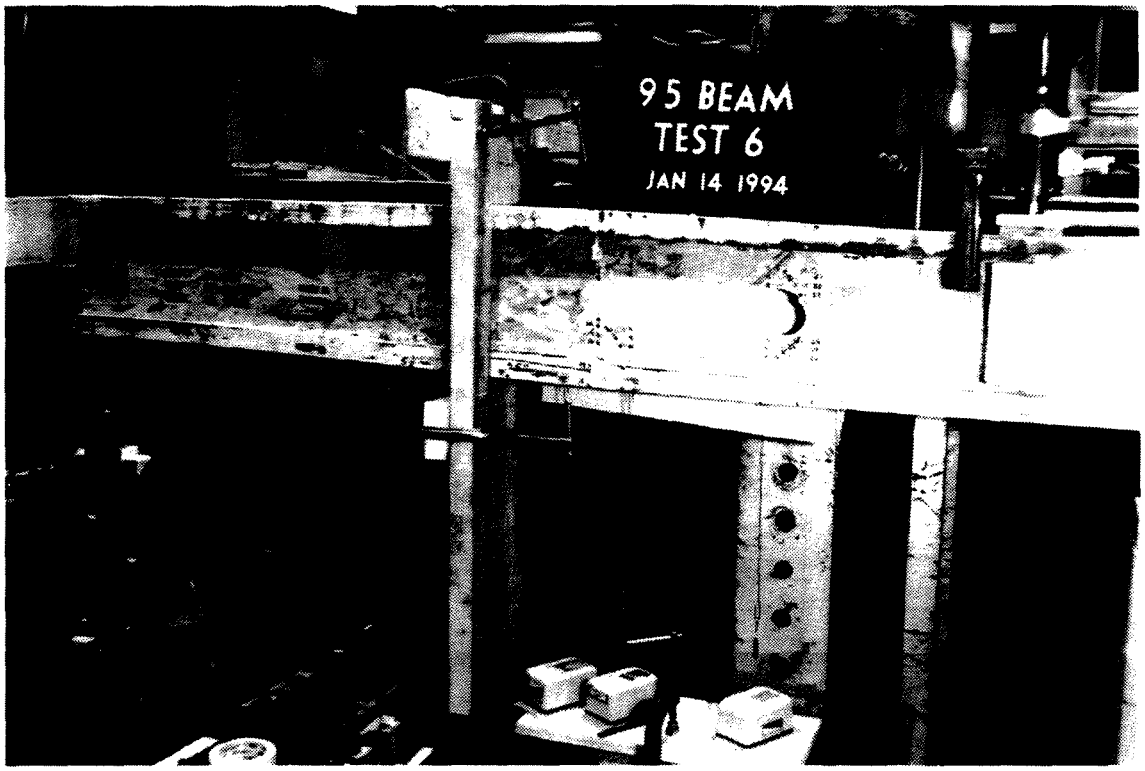

Figure 5.37 Vierendeel truss action exhibited in specimen 9.5dT6

5.4.4 Web Buckling

In specimens 24dT3 and 24dT5, buckling was observed around the holes. Figure 5.38 shows the overall buckling of the web after a tensile fracture occurred in specimen 24dT3. The web buckled in the load increment after the 22 kN shear load increment. The web buckled more and more as the beam was loaded until failure occurred. Figure 5.39 shows the local buckling at the bottom right corner of the hole in specimen 24dT5. The buckling occurred at the 10.4 kN to 14.0 kN shear load increment. It is uncertain whether the local buckle helped to cause the failure or whether the buckle occurred after failure of the beam was initiated at the top left corner where deformations reached over 18 400 microstrains in compression.

5.4.5 Other Failures

Specimen 24dT2 failed in bearing under the single point load because the OSB stiffeners provided were inadequate. Therefore, 2 x 4 lumber was used as stiffeners for all of the subsequent test specimens. Test parameters in specimen 24dT2 were repeated in specimen 24dT3. Specimen 24dT4 was the reference beam for the 610 mm deep beams. This beam failed in lateral-torsional buckling. Therefore, test 24dT4 was repeated with test 24dT7. Specimen 24dT7 failed with an in-plane compression failure at the top flange. Specimen 9.5dT2 failed with a web splice fracture and specimen 16dT3 failed with the tension flange fracturing.

Figure 5.38 Overall web buckling in specimen 24dT3

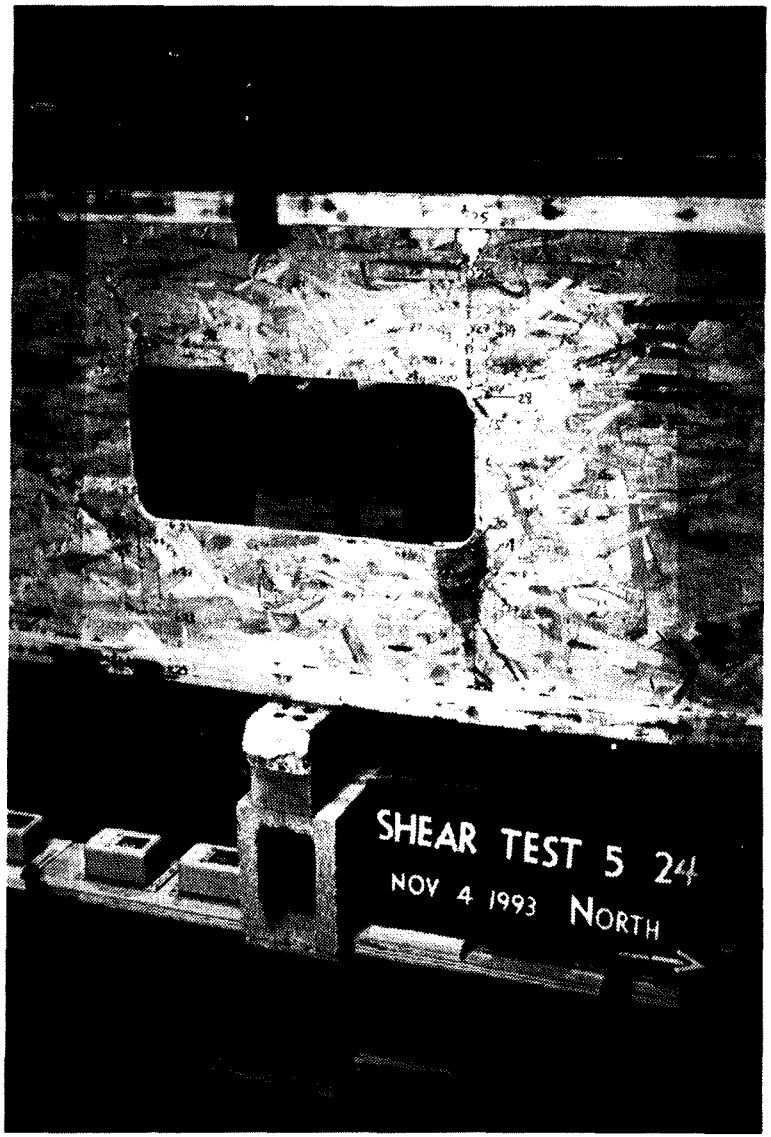

Figure 5.39 Local web buckling in specimen 24dT5

6. ANALYSIS AND DISCUSSION

6.1 General

Based on the test results, four possible failure modes have been identified. Web/flange connection failures occurred when the height of the hole equaled the height of the web. Because the web/flange connection was proprietary, this mode of failure was beyond the scope of this research. The Vierendeel failure was also clearly identified. However, some hole geometries did not fall in either of these failure modes. To account for this behaviour a cross section strength check was developed. Lastly, web buckling occurred when the stem of the "T" section above and below the hole becomes long. Failure was not initiated by web buckling alone, but it contributed to the failure of the beam.

6.2 Vierendeel Analysis Applied to OSB Wood Composite I-beams

Wood and wood composite materials may be described as an orthotropic material or in other words wood has unique and independent mechanical properties in the directions of three mutually perpendicular axes. Wood can also be modeled as a linear and elastic material.

The OSB webbed I-beams were made from two orthotropic materials, namely sawn lumber flanges and an OSB web. In order to apply the Vierendeel analysis to wood I-beams, the material properties parallel to the long axis of the beam must be used. From material tests, the M.O.E. of lumber was 13 600 MPa in tension and 12 100 MPa in compression. Since the tension and compression M.O.E. of the lumber were so close, the average M.O.E. of 12 850 MPa was used in the analysis. The M.O.E. of OSB in tension was 4840 MPa and in compression was 5170 MPa. The average value of 5005 MPa was used as the M.O.E. for OSB. The compression value for OSB was based on the tests with the strain readings on the edge side of the specimen. This value was used because the strain readings on the face strand side of the specimen were more variable than the edge side readings. In order to apply the elastic flexure formula, the cross section consisting of two different M.O.E. must be transformed into a section with one M.O.E.. This procedure is identical to transforming sections in reinforced concrete. The Vierendeel analysis can now be applied to the beam.

Using material properties from material tests, the maximum tension or compression stress of OSB was used as the maximum longitudinal stress the beam could experience before failure. The longitudinal stresses were then calculated based on elementary beam theory and the stress concentrations around the corners of the hole were ignored. It is important to note that the secondary bending moment M_T, was calculated using a moment arm measured from the middle of the hole to the nearest tangent point at the corner of the hole. The calculations showed that one corner would reach a maximum stress before the other corners. Based on test results from specimen 24dT5, one corner reaching maximum stress does not mean that failure is imminent. The analysis showed that when a second corner reached a maximum stress, the third corner was also close to failing as well. Therefore, the failure criteria due to Vierendeel truss action was that failure will occur when two of the four corners of the hole have reached their maximum stress. The stresses can be tension or compression or both. The maximum compression stress from material tests was 18.8 MPa. The face strands of the compression coupon were parallel to the load. The maximum tension stress from material tests was 14.1 MPa. The results of the analysis were compared to the test shear strengths in Table 6.1.

Table 6.1 Comparison of test strengths with predicted shear strengths

specimen	test kN	predicted failure		test/predicted ratio
		Vierendeel kN	cross section kN	
9.5dT1	10.4	16.0	9.0	1.16
9.5dT3	6.7	6.4	9.0	1.05
9.5dT4	5.1	5.3	4.5	1.14
9.5dT5	3.8	---	---	pullout failure
9.5dT6	8.0	6.8	9.0	1.18
9.5dT7	6.3	5.8	9.0	1.09
9.5dT8	6.3	5.3	9.0	1.19
16dT1	11.8	14.2	18.0	0.83
16dT2	7.9	6.6	9.0	1.21
24dT1	15.8	25.1	14.5	1.09
24dT3	28.8	42.1	29.0	0.99
24dT5	14.0	19.2	29.0	0.73
24dT6	6.3	---	---	pullout failure

Excluding web pullout failures, the Vierendeel analysis predicts the failure of the beam with reasonable accuracy with the exception of specimens 9.5dT1, 24dT1, and 24dT3. These three specimens all have a short hole width dimension of 152 mm. From beam theory, the longer the "T" section the greater the effect of Vierendeel truss action. In these specimens, the length of the "T" section was short enough that Vierendeel truss action was not significant enough to fully cause failure.

6.3 Cross Section Shear Strength

In Bower's (1968) research on the ultimate strength of steel I-beams, the shear stress as well as the bending stresses were used to determine the ultimate strength of the beam. Due to the ability of the beam to form plastic hinges at the corners of the hole, the web was fully yielded before failure occurred. The yielding, based on Von Mises yield criterion, was due to a combination of shear and bending stresses. In Bower's analysis, the shear stresses across the beam were assumed to be uniform across the web of the beam at the corners of the hole. Similarly, the shear stress distribution may be approximated by a uniform shear stress distribution across the web of the beam at the hole location. By assuming this shear stress distribution, the cross section shear strength of the OSB I-beam can be determined easily. The edgewise shear strength of OSB was determined by the two-rail shear test to be 8.0 MPa. The cross section shear strength is then given by

$$V_{CS} = A_n \tau_u \qquad [7]$$

in which A_n = the net area of the web remaining after the hole is cut and τ_u = 8 MPa, the maximum shear stress. The results of this strength check are tabulated in Table 6.1. They indicate that specimens 9.5dT1, 24dT1, and 24dT3 are governed by the cross section shear strength rather than the Vierendeel truss action.

6.4 Web Buckling

Web buckling occurred in specimens 24dT3 and 24dT5. In specimen 24dT3, the effect of overall buckling of the web did not effect the cross section shear strength significantly. However, in specimen 24dT5 the local buckling of the web may have reduced the shear strength of the beam resulting in a lower shear strength than expected. The influence of buckling may be significant in hole geometries where the stem of the "T" section is long compared to the thickness of the web. Future research should investigate the effects of web buckling.

6.5 Shear Span Effects

The shear strength increased when the shear span increased. Specimens 9.5dT3 and 9.5dT6 had the same hole geometry, but specimen 9.5dT6 had a 500 mm longer shear span. Longitudinal strain diagrams in Figures 5.12, 5.13, 5.16, and 5.17 show that the deformations at the left side of the hole increased slightly near the flanges, but remained the same near the hole. However, the longitudinal strains on the right side of the hole decreased. The increase in moment due to the longer shear span shifted the neutral axis away from the flanges of the beam. This reduced the strain at the corners of the hole, thus, allowing the beam to carry a higher load.

6.6 Corner Radius Effects

OSB has wafers oriented on the face layers of the board. However, there is still a randomness in the arrangement of the wafers which allows the wafers to interlock together in different directions. Test specimens 9.5dT3, 9.5dT7, and 9.5dT8 all had the same hole dimensions except the holes had 25 mm radius, 12 mm radius, and square corners, respectively. From Figure 5.7, the shear strength varied only slightly between the tests. Specimen 9.5dT3 carried only 6% more shear than the other two specimens. The radius of the corner had little effect on the overall shear strength of the beam. The random interlocking of the wafers at the corners allowed cracks to form by breaking some fibers, but tension forces were transferred through other fibers which remained intact. The tension cracks formed are jagged through the thickness of the web and the cracks zig zag from the tension corners of the hole to the nearest flange. At the compression corners, the shear capacity is more a function of the amount of material available to transfer load than the shape of the corner of the hole.

6.7 Deflection of the Reference Beams

The deflection of the three reference beams 9.5dT2, 16dT3, and 24dT7 were calculated and compared with the actual deflections. The calculated deflections were based on an approach used by Ghali and Neville (1989). The essence of the method is described below.

Using the method of virtual work and applying it to elastic systems, the deflection at coordinate 1 (load point) shown in Figure 6.1 is

$$D_1 = \int \frac{M_{u1} \cdot M}{E \cdot I} d\ell + \int \frac{V_{u1} \cdot V}{G \cdot a_r} d\ell \qquad [8]$$

where

E = the elastic modulus of the I-beam.

I = the moment of inertia.

G = modulus of rigidity or shear modulus.

a_r = the reduced area of the cross section taken as the area equal to the thickness of the web times the full height of the beam.

V_{u1} and M_{u1} are the values of the shear and bending moment internal forces at any section due to a unit virtual force applied at coordinate 1 where the displacement is required.

V and M are the shear and bending moment stress resultants at any section due to the actual applied loads.

Figure 6.1 shows the concepts of V_{u1} and M_{u1}.

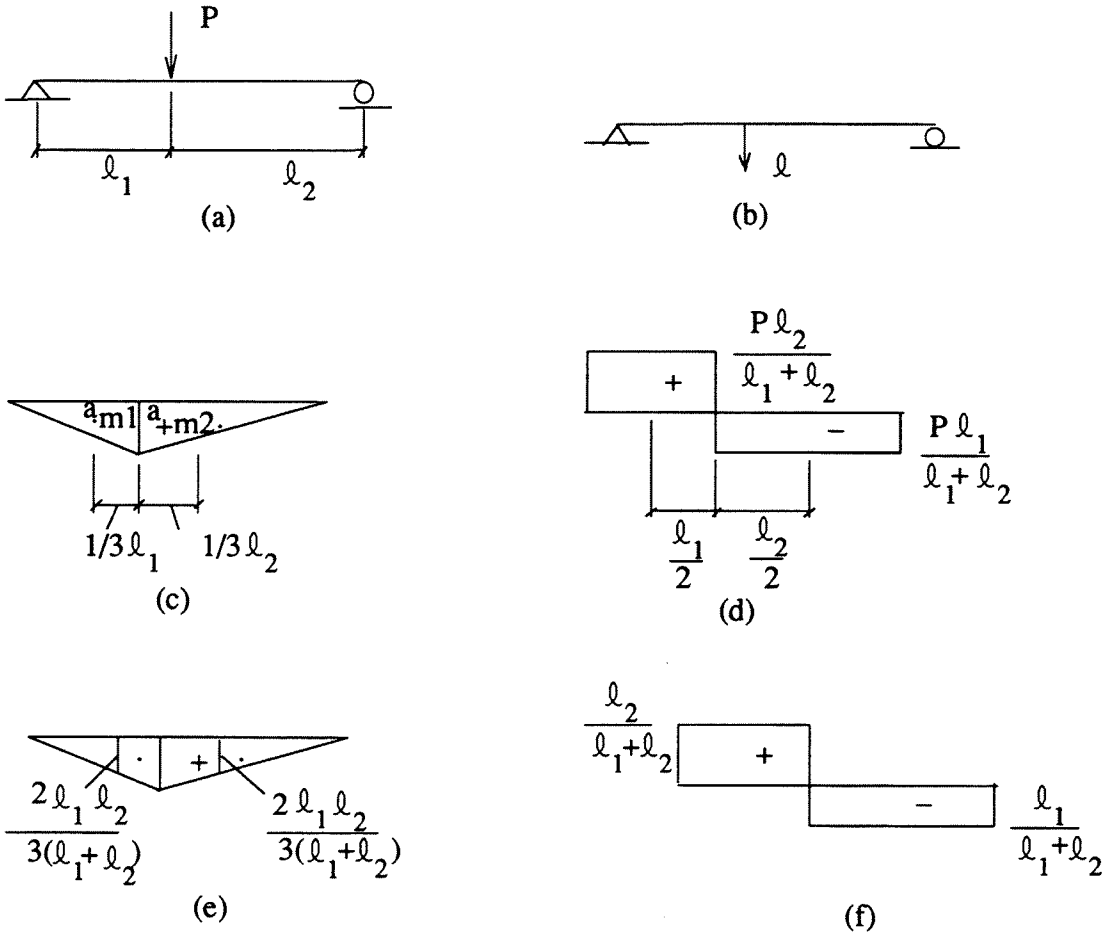

Figure 6.1. Loading on reference beam, (a) Beam (b) Coordinate system (c) M diagram (d) V diagram (e) M_{u1} diagram (f) V_{u1} diagram

The integration of equation [8] can be carried out by

$$\int \frac{M_{ul} \cdot M}{E \cdot I} d\ell = \Sigma\, a_m \cdot \overline{M}_{ul} \qquad [9]$$

where

a_m = the area in a section of the bending moment diagram divided by EI.

$\overline{M}_{ul}$ = the value of the M_{ul} diagram at the section where the centroid of the area, a_m, is located.

$$\int \frac{V_{ul} \cdot V}{G \cdot a_r} d\ell = \Sigma\, a_v \cdot \overline{V}_{ul} \qquad [10]$$

where

a_v = the area in a section of the shear force diagram divided by Ga_r.

$\overline{V}_{ul}$ = the value of the V_{ul} diagram at the section where the centroid of the area, a_v, is located.

The first part of equation [8] accounts for bending deformations while the second part accounts for shear deformations. The values for E and G were 12 850 MPa and 1640 MPa, respectively. The calculations show that the shear deformations were a significant part of the total deflection. The results of the calculated deflection, shown in Figure 6.2, are conservative and over predict the deflections. However, this method gives a good approximation of the actual deflection.

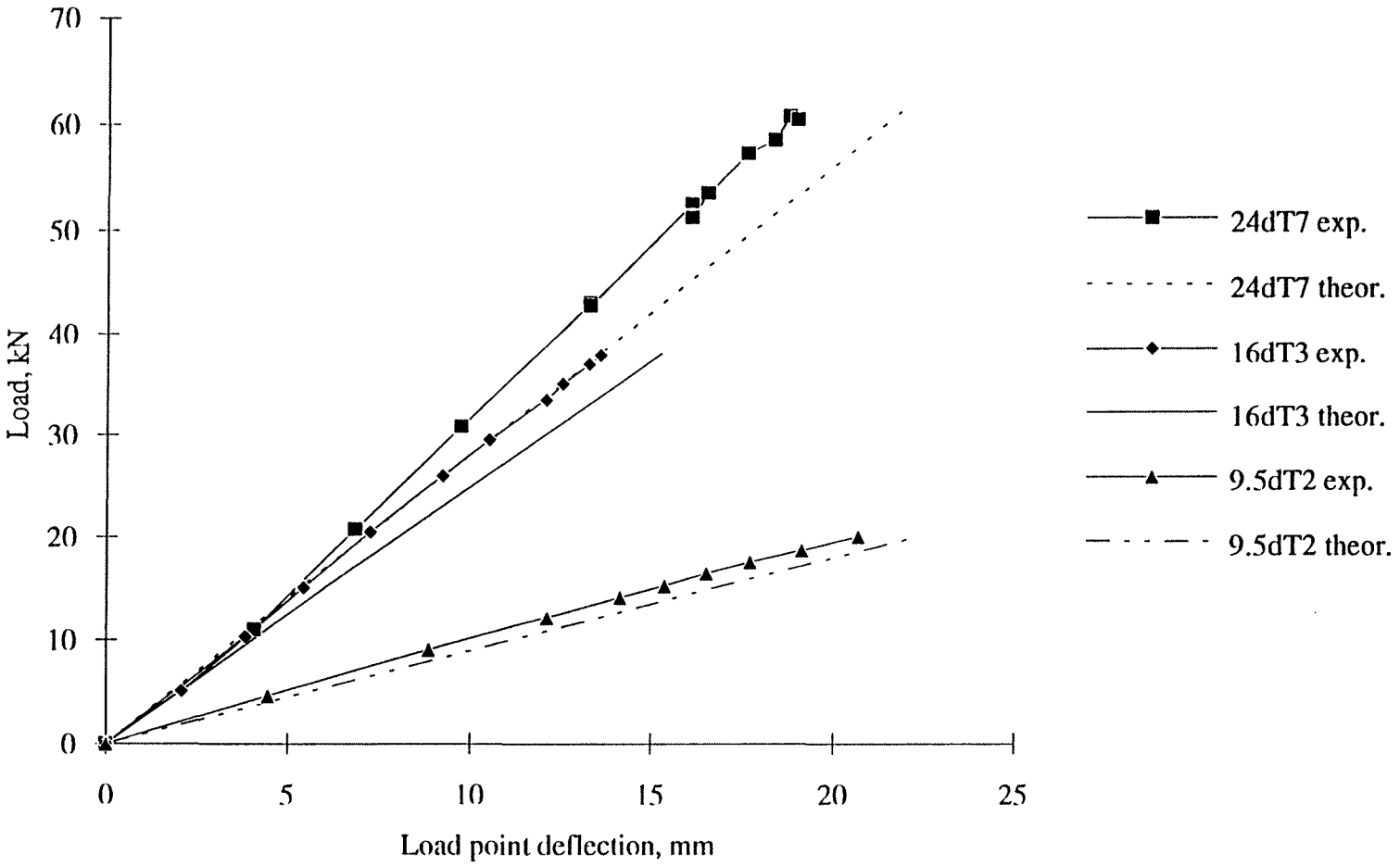

Figure 6.2. Predicted vs. experimental load point deflections for reference beams

7. Conclusion and Recommendations

7.1 Conclusion

The short term shear behaviour of OSB webbed I-beams was experimentally investigated by testing 18 I-beams which included three depths of beams with different hole geometries. Material properties of the I-beam components were determined from material tests and were used in the theoretical phase of this research. The results of both the experimental and theoretical phases of this research are summarized as conclusions.

1. Four mechanisms which contribute to shear failure were identified.

   a. Beams with web opening heights equal to the full height of the web failed in shear at the web/flange connection. This shear failure allowed the web to pull out of the flange.

   b. Beams with sufficient web material above and below the hole exhibited a Vierendeel failure if the web hole was sufficiently wide enough to allow large deformations and corresponding large longitudinal stresses to develop at the corners of the hole.

   c. If the hole was short in width, the beam failed due to the shear strength of the cross section being exceeded.

   d. Web buckling was observed in deeper beams (610 mm) with or without holes.

2. Specimens with web openings failed without warning.

3. Tests show that the effects of varying the radius of the corner of the hole were not significant. When the corner detail of the hole was reduced from a 25 mm radius to a square corner, there was only a 6% loss in shear strength.

4. Longer shear spans corresponding to greater bending moments at the location of the hole resulted in an increase in shear strength.

5. The load point deflection of the beam was predicted with reasonable accuracy by using the principle of virtual work and including bending and shear deformations. The shear deflection was a large part of the total deflection.

6. The compression strength and M.O.E. of OSB were determined in two perpendicular directions from material tests. The tension strength and M.O.E. of OSB were also determined in two perpendicular directions from material tests. The edgewise shear strength and shear modulus of OSB were determined experimentally.

7.2 Recommendations

A design procedure using a Vierendeel analysis and a cross section check was used to predict the shear strength of OSB I-beams with a rectangular opening. This procedure gave a good estimate of the shear strength of the OSB I-beams and resulted in a test/predicted ratio varying between 0.73 and 1.21. This simple design procedure is recommended and will be described below with certain cautions which the designer should keep in mind.

Shear strength design procedure for OSB I-beams with a rectangular hole

1. Calculate the shear strength based on the Vierendeel analysis using equation [6] which is

$$\sigma_x = \frac{V \cdot x \cdot y_T}{I_T} + \frac{M \cdot y}{I_n}$$

The value of "x" must be measured along the edge of the hole from the centre of the hole to the nearest tangent point at the corner if the hole has rounded corners. When σ_X exceeds the maximum compression or tension stress of OSB at one corner, that corner has failed. When any two of the four corners have failed, the beam has reached its maximum shear strength, V_v.

2. Calculate the cross section shear strength using equation [7] which is

$$V_{CS} = A_n \tau_u$$

3. The ultimate shear strength, $V_{u,}$, is equal to the lesser of V_v or V_{CS}.

Assumptions:

- The OSB and flange lumber material were linear elastic until failure occurred.
- The absolute values of the compression and tension M.O.E. of the OSB in the direction of the longitudinal axis of the beam were close enough that the average value was used.
- Similarly, the absolute values of the compression and tension M.O.E. of the flange lumber were close enough that the average value was used.
- The beam was restricted to in-plane movement only. Therefore, sufficient bracing must be provided so that lateral-torsional buckling does not occur. Also, web buckling was not included in the design procedure so web buckling must not occur or it must be shown that its effects are negligible.
- Bearing failures were excluded by providing the necessary web stiffeners and ensuring the bearing area was sufficient to avoid local crushing of the flange.
- Bending failures were excluded by using elementary beam theory to estimate the bending stresses in the flanges and ensuring that the flange material was strong enough.

Future research should investigate the following topics:

1. The long term behaviour of OSB I-beams with web openings.
2. Web hole reinforcement.
3. Lateral-torsional buckling of OSB I-beams with openings.
4. Web buckling and web stiffener design.

8. REFERENCES

ASTM D 198. 1984. Standard methods of static tests of timbers in structural sizes. American Society for Testing and Materials, Philadelphia, PA.

ASTM D 2719. 1989. Standard test methods for structural panels in shear through-the-thickness. American Society for Testing and Materials, Philadelphia, PA.

ASTM D 3044. 1976. Standard test method for shear modulus of plywood. American Society for Testing and Materials, Philadelphia, PA.

ASTM D 3500. 1990. Standard test methods for structural panels in tension. American Society for Testing and Materials, Philadelphia, PA.

ASTM D 3501. 1976. Standard methods of testing plywood in compression. American Society for Testing and Materials, Philadelphia, PA.

ASTM D 5055. 1990. Standard specification for establishing and monitoring structural capacities of prefabricated wood I-joists. American Society for Testing and Materials, Philadelphia, PA.

Bower, J.E. 1966. Experimental stresses in wide-flange beams with holes. Journal of the Structural Division. Proceedings of the ASCE. 92(ST5):167-186.

Bower, J.E. 1968. Ultimate strength of beams with rectangular holes. Journal of the Structural Division. Proceedings of the ASCE. 94(ST6):1315-1337.

CAN/CSA O437.0. 1993. Strandboard and waferboard. Canadian Standards Association. Rexdale (Toronto), Ontario, Canada.

Fergus, D.A. 1979. Effect of web voids and stiffeners on structural performance of composite I-beams. Ph.D. dissertation, Purdue University, West Lafayette, IN. 255 pp.

Ghali, A.; Neville, A.M. 1989. Structural analysis. A unified classical and matrix approach. 3rd. ed. New York: Chapman and Hall.

Hilson, B.O.; Rodd, P.D. 1984. The effect of web holes on the behavior and ultimate shearing strength of timber I-beams with hardboard webs. Struct. Eng. 62B(4):69-79, 90.

Johannesson, B. 1977. Holes in plywood beams and glued laminated timber beams. Chalmers Tekniska Hogskola, Inst. for konstruktionsteknik. Stal- och Trabyggnad, Publ. S77:4, Goteborg.

Leichti, R.J.; Falk, R.H.; Laufenberg, T.L. 1990a. Prefabricated wood I-joists: an industry overview. Forest Products Journal. 40(3):15-20.

Leichti, R.J.; Falk, R.H.; Laufenberg, T.L. 1990b. Prefabricated wood composite I-beams: a literature review. Wood and Fiber Science. 22(1):62-79.

Maley, J.D. 1987. Wood I-joists: a closer look. Proceedings of Structures Congress/87, Building Structures. American Society of Civil Engineers, New York, 221-235.

Nelson, S.A. 1975. Prefabricated wood joists, wood structures: a design guide and commentary. ASCE Structural Division, New York, 213-215.

Structural Board Association. 1993. OSB and waferboard in wood frame construction. Canadian edition. (booklet)

Tang, R.C.; Leichti, R.J. 1984. Manufacturing composite wood I-beams by using small diameter trees and its engineering performance. Symposium of Utilization of Medium and Small Diameter Trees. Taichung, Taiwan, Republic of China (in Chinese), 70-78.

APPENDIX A

16dT1, rosette at 520 mm from the right reaction at mid-height

Shear in right span	Demec readings in rosette, microstrains			
kN	V	S\	H	S/
0.00	0	0	0	0
1.61	50	-125	-25	150
3.24	75	-275	-75	350
4.89	100	-450	-75	500
6.21	100	-575	-100	675
7.12	125	-700	-125	775
8.05	100	-775	-125	900
8.80	125	-875	-150	975

16dT2, rosette at 775 mm from the right reaction at mid-height

Shear in right span	Demec readings in rosette, microstrains			
kN	V	S\	H	S/
0.00	0	0	0	0
1.26	-25	-175	-25	75
2.47	-50	-350	-75	200
3.60	-100	-475	-100	300
4.43	-100	-600	-125	400
5.40	-100	-750	-150	475

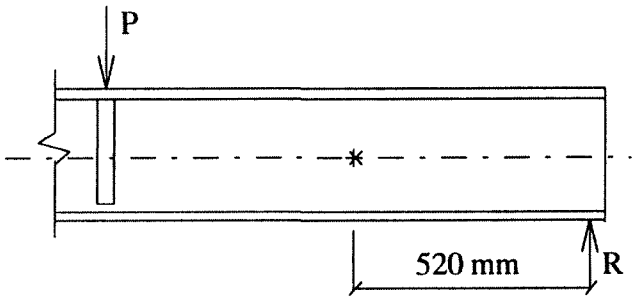

Position of demec gages on all rosette

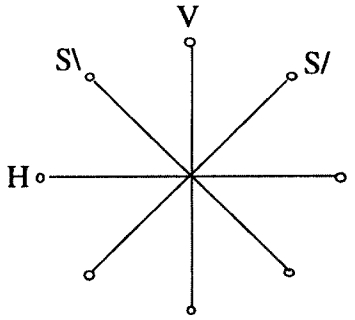

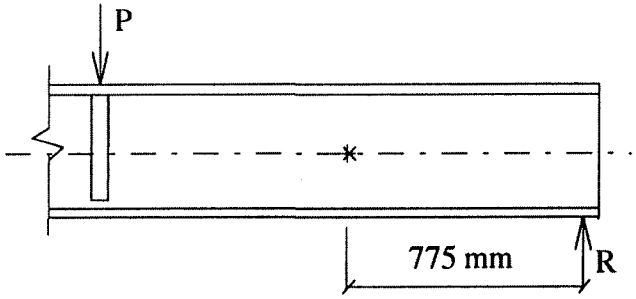

9.5dT2, rosette at 435 mm from the left reaction at mid-height

Shear in left span	Demec readings in rosette, microstrains			
kN	V	S\	H	S/
0.00	0	0	0	0
2.95	-175	350	-125	-550
5.87	-350	525	-225	-1050
7.91	-450	875	-325	-1350
9.14	-550	950	-375	-1650
9.90	-575	1075	-425	-1825
10.59	-650	1150	-475	-1950
11.33	-675	1225	-500	-2050
12.08	-775	1300	-550	-2200
12.91	-875	1375	-600	-2400

9.5dT2, rosette at 689 mm from left reaction at mid-height

Shear in left span	Demec readings in rosette, microstrains			
kN	V	S\	H	S/
0.00	0	0	0	0
2.95	-75	350	-150	-500
5.87	-25	825	-350	-1075
7.91	25	1200	-500	-1400
9.14	50	1400	-600	-1675
9.90	125	1750	-650	-1800
10.59	175	1900	-700	-1950
11.33	225	2050	-750	-2075
12.08	325	2225	-800	-2200
12.91	500	2450	-825	-2275

9.5dT3, rosette at 1377 mm from the right reaction at mid-height

Shear in right span	Demec readings in rosette, microstrains			
kN	V	S\	H	S/
0.00	0	0	0	0
0.70	25	-75	-50	100
0.99	0	-150	-75	200
1.54	50	-225	-25	325
2.06	75	-325	0	400
2.47	0	-350	0	475
2.66	25	-425	-75	525
3.01	25	-475	-25	575

9.5dT6, rosette at 642 mm from left reaction at mid-height

Shear in left span	Demec readings in rosette, microstrains			
kN	V	S\	H	S/
0.00	0	0	0	0
0.50	50	125	-25	-175
2.39	100	475	-25	-500
3.60	-75	675	-25	-675
4.59	25	825	-50	-850
5.71	100	1025	-25	-1100
6.74	50	1225	0	-1275
7.32	100	1350	25	-1425

24dT1, Top rosette

Shear in right span	Demec readings in rosette, microstrains			
kN	V	S\	H	S/
0.00	0	0	0	0
2.67	75	-100	-50	125
4.90	200	-175	-150	250
7.42	275	-250	-150	350
9.80	375	-300	-200	475
12.05	450	-375	-250	575
14.57	550	-425	-275	700

24dT1, Mid-height rosette

Shear in right span	Demec readings in rosette, microstrains			
kN	V	S\	H	S/
0.00	0	0	0	0
2.67	-50	-150	0	175
4.90	-125	-325	0	200
7.42	-225	-575	50	300
9.80	-250	-725	50	325
12.05	-375	-925	50	475
14.57	-525	-1175	100	525

24dT1, Bottom rosette

Shear in right span	Demec readings in rosette, microstrains			
kN	V	S\	H	S/
0.00	0	0	0	0
2.67	-100	-125	200	225
4.90	-175	-250	375	425
7.42	-275	-350	550	650
9.80	-375	-525	675	825
12.05	-425	-700	850	1025
14.57	-625	-800	1000	1250

Position of top, mid-height and bottom rosettes in specimen 24dT1

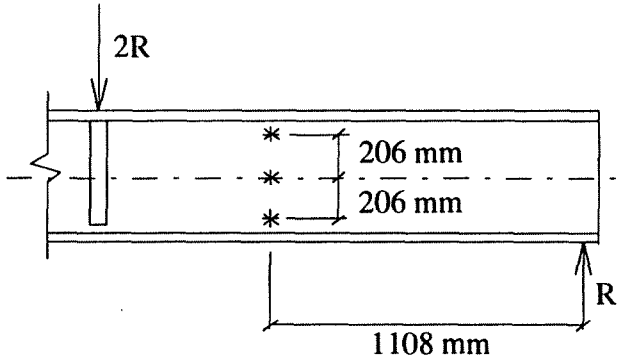

Position of corner rosettes with respect to the hole
for specimens 24dT1, 3, and 5

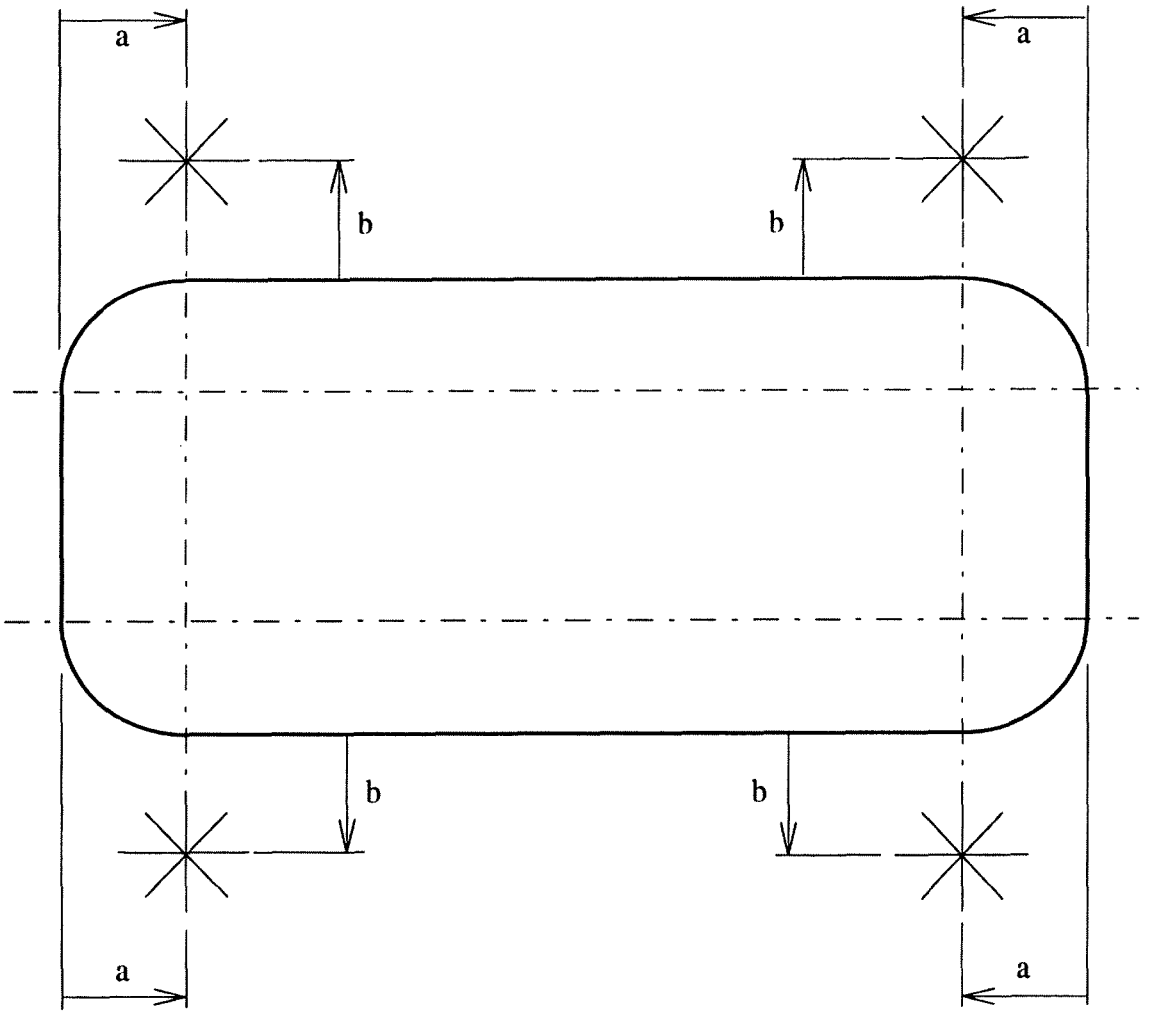

24dT1, Rosette at the top left corner of the hole

Shear in left span	Demec readings in rosette, microstrains			
kN	V	S\	H	S/
0	0	0	0	0
2.63	-100	125	-225	-650
4.83	-150	250	-350	-1200
7.33	-250	375	-525	-1925
9.69	-250	475	-725	-2700
11.91	-275	375	-1125	-4100
14.39	-450	525	-1625	-7100

24dT1, Rosette at the top right corner of the hole

Shear in left span	Demec readings in rosette, microstrains			
kN	V	S\	H	S/
0	0	0	0	0
2.63	75	375	-100	-300
4.83	150	675	-175	-525
7.33	250	1050	-275	-750
9.69	350	1400	-325	-975
11.91	400	1800	-275	-1075
14.39	450	2275	-150	-1175

24dT1, Rosette at the bottom left corner of the hole

Shear in left span	Demec readings in rosette, microstrains			
kN	V	S\	H	S/
0	0	0	0	0
2.63	225	525	225	-200
4.83	400	1000	400	-325
7.33	600	1550	575	-550
9.69	775	2100	825	-650
11.91	950	2675	1025	-775
14.39	725	3225	1425	-1000

24dT1, Rosette at the bottom right corner of the hole

Shear in left span	Demec readings in rosette, microstrains			
kN	V	S\	H	S/
0	0	0	0	0
2.63	-375	225	75	-600
4.83	-700	475	150	-1075
7.33	-1050	675	250	-1675
9.69	-1400	900	300	-2250
11.91	-1775	1150	300	-2900
14.39	-2100	1400	175	-3625

Note: The positions of the corner rosettes are located by the dimensions a = 25.4 mm and b = 28.6 mm.

24dT3, Rosette at the top left corner of the hole

Shear in left span	Demec readings in rosette, microstrains			
kN	V	S\	H	S/
0	0	0	0	0
14.79	-825	-125	-300	-1125
17.28	-950	-125	-275	-1325
19.39	-1100	-150	-325	-1500
21.88	-1325	-250	-375	-1800

24dT3, Rosette at the top right corner of the hole

Shear in left span	Demec readings in rosette, microstrains			
kN	V	S\	H	S/
0	0	0	0	0
14.79	950	875	-200	-525
17.28	1100	1075	-175	-625
19.39	1175	1200	-150	-725
21.88	1275	1350	-75	-800

24dT3, Rosette at the bottom left corner of the hole

Shear in left span	Demec readings in rosette, microstrains			
kN	V	S\	H	S/
0	0	0	0	0
14.79	1125	1700	775	25
17.28	1325	1975	950	50
19.39	1475	2275	1100	75
21.88	1700	2575	1200	100

24dT3, Rosette at the bottom right corner of the hole

Shear in left span	Demec readings in rosette, microstrains			
kN	V	S\	H	S/
0	0	0	0	0
14.79	-1200	500	-400	-1775
17.28	-1425	625	-500	-2150
19.39	-1650	675	-550	-2450
21.88	-1925	700	-625	-2750

Note: The positions of the corner rosettes are located by the dimensions a = 0 and b = 28.6 mm.

24dT5, Rosette at the top left corner of the hole

Shear in left span	Demec readings in rosette, microstrains			
kN	V	S\	H	S/
0	0	0	0	0
2.49	-300	-200	-450	-650
4.84	-625	-400	-975	-1375
7.26	-1475	-1125	-2100	-2875
8.7	-3775	-4250	-5350	-6625
10.13	-6750	-6700	-10000	-13150

24dT5, Rosette at the top right corner of the hole

Shear in left span	Demec readings in rosette, microstrains			
kN	V	S\	H	S/
0	0	0	0	0
2.49	0	350	125	-50
4.84	250	650	300	-100
7.26	375	975	525	-150
8.7	275	1200	725	-175
10.13	275	1475	1025	-200

24dT5, Rosette at the bottom left corner of the hole

Shear in left span	Demec readings in rosette, microstrains			
kN	V	S\	H	S/
0	0	0	0	0
2.49	325	425	350	50
4.84	625	1100	675	125
7.26	1050	1725	925	200
8.7	1500	2175	1050	250
10.13	2050	2825	1275	275

24dT5, Rosette at the bottom right corner of the hole

Shear in left span	Demec readings in rosette, microstrains			
kN	V	S\	H	S/
0	0	0	0	0
2.49	-175	-50	-250	-275
4.84	-300	-150	-450	-575
7.26	-450	-275	-700	-850
8.7	-625	-375	-900	-1125
10.13	-725	-550	-1050	-1150

Note: The positions of the corner rosettes are located by the dimensions a = 0 and b = 28.6 mm.

APPENDIX B

LVDT position #1

Load, 2R	Out-of-plane deflection, mm			
kN	a	b	c	d
0	0	0	0	0
8.1	-0.12	-0.16	-0.14	-0.09
18	-0.15	-0.07	0.01	0.06
27.5	0.05	0.58	0.84	0.75
36.8	0.40	3.72	4.81	3.46
40.8	0.57	6.79	8.80	6.33

LVDT position #2

Load, 2R	Out-of-plane deflection, mm			
kN	a	b	c	d
0	0.00	0.00	0.00	0.00
8.1	-0.24	-0.26	-0.17	-0.15
18	-0.47	-0.38	-0.19	-0.06
27.5	-1.15	-0.74	-0.11	0.17
36.8	-3.98	-1.06	1.70	2.21
40.8	-7.56	-1.60	3.74	4.56

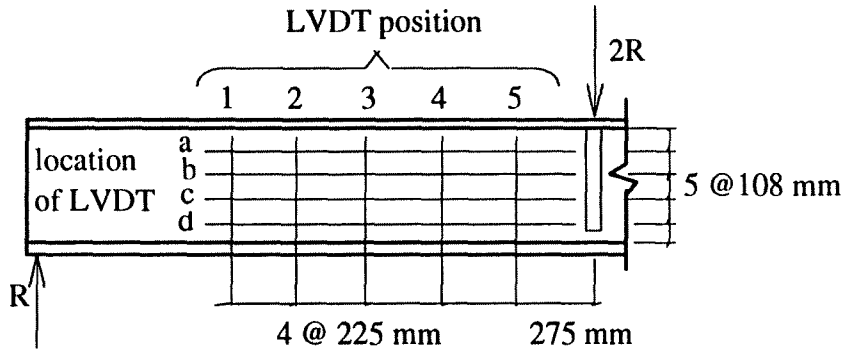

The out-of-plane buckled shape of the web for specimen 24dT4 was recorded using a vertical column of four LVDT's (a, b, c, and d) mounted on a brace which moved freely along the length of the beam. Readings were taken at five LVDT positions for each load step.

LVDT position #3

Load, 2R	Out-of-plane deflection, mm			
kN	a	b	c	d
0	0	0	0	0
8.1	-0.07	-0.04	0.05	0.12
18	-0.43	-0.35	-0.13	0.14
27.5	-1.61	-1.46	-0.78	-0.06
36.8	-7.49	-6.28	-2.82	-0.13
40.8	-14.33	-11.23	-4.46	0.22

LVDT position #4

Load, 2R	Out-of-plane deflection, mm			
kN	a	b	c	d
0	0	0	0	0
8.1	0.33	0.40	0.44	0.43
18	0.15	0.22	0.36	0.44
27.5	-1.01	-1.25	1.32	3.86
36.8	-7.49	-8.74	1.32	0.96
40.8	-14.99	-16.56	-10.39	-4.34

LVDT position #5

Load, 2R	Out-of-plane deflection, mm			
kN	a	b	c	d
0	0	0	0	0
8.1	0.45	0.43	0.33	0.19
18	0.77	0.70	0.48	0.27
27.5	0.78	0.39	0.07	0.00
36.8	-2.00	-4.62	-4.59	-2.58
40.8	-5.10	-9.92	-9.33	-5.30

GLOSSARY

a_m	area in a section of the bending moment diagram divided by EI
a_v	area in a section of the shear force diagram divided by Ga_r
A_n	net area of web remaining after the hole is cut
a_r	the reduced area of the cross section taken as the area equal to the thickness of the web times the full height of the beam
d	full depth of beam
E	elastic modulus of the I-beam, MPa
G	modulus of rigidity or shear modulus, MPa
h	full height of web
h_o	width of hole
I	moment of inertia
I_T	moment of inertia of "T" section
I_n	moment of inertia of the net cross section of the beam about its centroidal axis
L	length of beam from support to support
l_S	length of the left shear span which included a hole
ℓ_1	left shear span of reference beam
ℓ_2	right shear span of reference beam
M	bending moment
M_T	secondary bending moment applied to "T" section above and below the hole
M_{u1}	bending moment at any section due to a unit virtual force applied at coordinate 1 where the displacement is required
$\overline{M}_{u1}$	value of the M_{u1} diagram at the section where the centroid of the area, a_m, is located
M(u)	bending moment at a distance "u" from the left reaction
P	point load, kN
R	reaction force, kN
u	distance from left reaction to centre of hole
V	shear force, kN
V_{CS}	cross section shear strength, kN
V_{max}	maximum shear force in left shear span before failure, kN
V_o	maximum shear force in left shear span of reference beam, kN
V_u	ultimate shear strength, kN
V_{u1}	shear at any section due to a unit virtual force applied at coordinate 1 where the displacement is required
$\overline{V}_{u1}$	value of the V_{u1} diagram at the section where the centroid of the area, a_v, is located
V_v	Vierendeel shear strength, kN
w_o	height of hole
x	horizontal distance from centre of hole
x_o	position of the right edge of the hole from the load point
y	vertical distance from centre of hole
y_T	vertical distance from centroid of "T" section
σ_{XT}	secondary bending stress caused by M_T, MPa
σ_P	primary bending stress caused by M, MPa
σ_X	total bending stress, MPa
τ_u	maximum edgewise shear strength of OSB, MPa